PROTON TRANSFER, ELECTRICAL RESISTIVITY, AND MAGNETIC SUSCEPTIBILITY IN THE TANTALUM-HYDROGEN AND TITANIUM-HYDROGEN SYSTEMS

by
William Bruno Hillig

A dissertation submitted in partial fulfillment
of the requirements for the degree of
Doctor of Philosophy in the
University of Michigan
1953

Committee in charge:

Professor Kasimir Fajans, Chairman
Associate Professor Ernst Katz
Assistant Professor Clifford C. Meloche
Assistant Professor Robert W. Parry
Assistant Professor Peter A. S. Smith

To

BETH

ACKNOWLEDGEMENTS

The author is sincerely grateful for the opportunity of conducting his research under the inspiring direction of Professor Kasimir Fajans, whose personal guidance throughout the work and help in formulating this dissertation, are especially appreciated. The author also hopes that he may have acquired some of the capacity for independent thinking and the scientific enthusiasm always displayed by Professor Fajans.

Special thanks are extended to the School of Dentistry for the use of the hand rolling mill, to the Department of Mineralogy for the use of X-Ray Diffraction facilities, and to the Department of Physics for the loan of the Wheatstone bridge.

The assistance of my wife, Doctor Beth Cook Hillig, in the preparation of this dissertation, especially of the illustrations, is greatly appreciated.

The writer gratefully acknowledges the financial aid received from the Paul F. Bagley Fellowship, and the James E. Harris Scholarship held during the first and second semesters of 1952-1953, respectively.

TABLE OF CONTENTS

LIST OF TABLES

LIST OF ILLUSTRATIONS

I. Introduction

A. General Characteristics of Binary Hydrogen Systems.

Hydrogen has the ability to enter into combination with almost every element, although stoichiometric compounds are not always formed. The following discussion surveys briefly those general characteristics of binary hydrogen systems which are indicative of their atomic configuration and electronic structure.

There is some latitude in the meaning of the term "hydride". In this presentation the word will be used in its broadest sense to indicate any binary hydrogen system, and will not necessarily imply stoichiometry.

It is appropriate to divide the binary hydrides into two natural classes, depending on whether or not they are derived from transition elements. In general, the non-transition element hydrides are true stoichiometric compounds, whereas the hydrides of the transition metals are mostly non-stoichiometric.

1. Hydrides of Non-Transition Elements. The hydrides of the alkali and alkaline earth metals are crystallographic and electronic analogs of the corresponding halides, and are therefore commonly referred to as the "saline" hydrides. The remaining non-transition elements form compounds which exist under normal conditions as gases, liquids, or soft solids, and are often termed the "volatile" or covalent hydrides. An extensive review of the chemistry of the

hydrides of the non-transition elements is contained in the book by Hurd[1].

2. Hydrides of the Transition Metals. Most of the transition metals in massive form occlude elemental hydrogen, forming products which retain much of the luster and electrical conductivity of the parent metal. For uranium hydride only the stoichiometric composition UH_3 is known. The hydrides of Ti, Th, and Zr have variable compositions, among which stoichiometric phases containing two hydrogen atoms per metal atom have been reported[2,3].

The composition of all non-stoichiometric hydrides is dependent upon temperature and pressure, and often upon the form and history of the substance; hence the term "solution-type hydrides" is often applied to these systems. The metals forming the solution-type hydrides can in turn be classified as endothermic or exothermic occluders. Among the exothermic occluders are those rare earths and transition elements of Groups IV and V which have been investigated, as well as Pd, Th, and U.

a. Endothermic Occluders. The "solubility" of hydrogen in the endothermic occluders ranges from a few tenths to several volumes of hydrogen gas per volume of metal, an amount small relative to that absorbed by the exothermic occluders. The amount increases with increasing temperature, and appreciable absorption usually occurs only at elevated temperature, often near the melting point of the

metal. At a given temperature, the concentration of absorbed hydrogen is proportional to the square root of the pressure (Sieverts' law), as first found by Hoitsema[4] in the case of Pd, but later extended by Sieverts to many other systems. This dependence indicates that occlusion involves the process $H_2 \longrightarrow 2H$. Hence, these systems are frequently considered to be solid solutions of atomic hydrogen in the metals. They have received little study indicative of their electronic structure because the concentration of hydrogen under ordinary conditions is so small.

b. Exothermic Occluders. Hydrogen solubility in the exothermic occluders decreases with increasing temperature, and at room temperature amounts to hundreds of volumes of hydrogen per volume of metal. Titanium, the best occluder, absorbs over 1800 volumes of hydrogen per volume of metal. Up to 42 kcal. (in the case of Ce) are released per mole of hydrogen occluded. In massive metals, temperatures of 300-800° are usually required to initiate absorption, which continues in most cases at temperatures as low as 20°.

Up to about ten atom per cent of hydrogen, the absorption isotherms of these systems, in general, obey Sieverts' law, but then depart from it markedly. At low temperatures and sufficiently high hydrogen concentrations, the dissociation pressure is usually almost constant over a wide range of compositions; i.e. the isotherm has a nearly horizontal plateau. At still larger concentrations the isotherm rises

abruptly. The existence of the plateau and the fact that it is not quite horizontal are generally interpreted as being due to the coexistence of two solid hydride phases which are not in true (thermodynamic) equilibrium[5]. With increasing temperature the concentration range of the plateau narrows, and the slope gradually becomes larger until the plateau disappears at a critical temperature. Further evidence for the absence of a true thermodynamic equilibrium in the metal-hydrogen system is the fact that dissociation pressures observed during the occlusion of hydrogen differ from those observed during its evolution. Such dependence of a property upon the path by which a given composition is attained is termed hysteresis.

Palladium and tantalum absorb hydrogen readily, not only from the gas phase but also when made the cathode in the electrolysis of water.

(i) Electrical Resistance and Transport. The dependence of electrical resistance upon hydrogen concentration has been reported only for the Pd-H and Ta-H systems. Below 100° the resistance of Pd increases as hydrogen is absorbed, reaching a maximum value 1.7 times that of the original metal at about $PdH_{0.77}$[6,7]. At higher temperatures, the resistance vs. composition curve for the Pd-H system shows hysteresis as well as discontinuities in slope[5]. The temperature coefficient of resistivity for Pd-H is sensitive to both temperature and composition, and is negative when the atomic ratio

H/Pd is greater than 0.35.

The Ta-H system has been investigated by Sieverts and Brüning[8], who found that the resistance increases proportionally to the atomic ratio H/Ta, and is 7% larger at $TaH_{0.1}$ than that of the metal.

The electrical transport of hydrogen in transition-metal hydrides has been studied only in the Pd-H system. Coehn et al.[9-13] concluded that the hydrogen acts as a positive carrier, with a transport number of 10^{-6}. These results were confirmed by other investigators[14-16].

(ii) Magnetic Susceptibility. Numerous investigations[17-20] have shown that, as hydrogen is added to paramagnetic Pd metal, the magnetic susceptibility decreases linearly with increasing H/Pd ratio until $PdH_{0.55-65}$ is reached. At still higher hydrogen concentrations, the susceptibility remains practically constant and, according to several investigators, is either weakly paramagnetic or diamagnetic.

At compositions up to $ZrH_{2.2}$, the susceptibility showed a non-linear decrease up to 30% from the paramagnetism of the parent Zr[21]. The susceptibility of $TiH_{1.2}$ was found to be 18% greater than that of the original paramagnetic Ti[21]. It has been reported that ThH_2[3] is diamagnetic, and that UH_3[22] is more strongly paramagnetic than the metal.

(iii) Crystal Structure. Only a few of the transition-metal hydrides have been investigated by X-ray or the more appropriate neutron diffraction techniques. The

latter has been applied to the stoichiometric UH_3[22], ThH_2[3], and ZrH_2[3]. X-ray diffraction cannot detect hydrogen, but the influence of the latter on the metal atom matrix can be followed. In general, as hydrogen is first absorbed the lattice type of the transition metal does not change, but the unit cell expands continuously. At higher hydrogen concentrations new phases appear.

The results of numerous studies on the Pd-H system have been collected in the book by D. P. Smith[23], p. 110, hereafter given as "Smith p.110". Electrolytic hydrogen is absorbed in Pd without change of phase up to the composition $PdH_{0.03}$. Then the face centered cubic α phase is gradually replaced by a β phase, which differs from the former one merely by a 10% increase in the specific volume. The two phase $\alpha \rightleftharpoons \beta$ region extends up to $PdH_{0.7}$. Upon evolution of hydrogen from Pd, the process $\beta \rightarrow \alpha$ takes place; however, the two-phase region now extends between a somewhat different set of compositions. Figure 1, which represents a projection of the "quasi-constitutional diagram" for the Pd-H system upon an isobaric plane, shows this behavior as a function of temperature. The solid curve and dashed curve indicate the transition points during hydrogen absorption and evolution respectively.

Several other systems have been investigated less thoroughly, although over wide ranges of composition: Ta-H, Ti-H, V-H, and Zr-H by Hägg[24]; Th-H by Rundle, Shull and Wollen[3]; Nb-H and Ta-H by Horn and Ziegler[25]. Determinations at only

one or a few concentrations have been reported for Ti-H and Zr-H by Fitzwilliam, Kaufmann and Squire[21]; Ti-H by Gibb and Kruschwitz[2]; La-H by Dreyfus-Alain[26,27]; and La-H, Ce-H and Pr-H by Rossi[28].

The X-ray studies and absorption isotherms for the Ti-H system indicate two non-stoichiometric hydride phases[2,29]. In Ta-H Hägg found three phases, Horn and Ziegler only one. For Zr-H Hägg reports five phases, but the absorption isotherm studies by Sieverts and Roell[30] as well as by Hall, Martin and Rees[31] indicate only two.

B. Electronic State of Hydrogen in Binary Hydrides.

Electrolysis of the molten saline hydrides, as well as their crystal structure, shows that hydrogen is present as the H^- ion[1]. According to the quanticule viewpoint, hydrogen in some of the volatile hydrides, e.g. B_2H_6, is present as strongly deformed H^- [32], while in others, e.g. HCl, the hydrogen is present as a proton which penetrates and deforms the anion[33].

Very little is known about the electronic structure of the transition-metal hydrides. The large heats of absorption observed for most of the exothermic occluders do not support Hägg's view that these hydrides consist of hydrogen atoms, presumably in their ground state, distributed among the "interstices" in the metal lattice[34]. Furthermore, on the basis of the Langevin relationship, the presence of atomic hydrogen at 20° would increase the paramagnetic susceptibility

of Pd by 100% at the composition $PdH_{0.5}$, whereas a decrease to practically zero was observed.

Therefore, the magnetic measurements on Pd-H have been interpreted by Oxley[35,36] as indicating the formation of a diamagnetic "pseudo-atom" (PdH), or by Vogt[37,38] of a diamagnetic complex ion $(PdH)^+$. On the basis of the band theory of metallic structure, Mott and Jones[39] propose that the hydrogen is completely dissociated into protons and electrons. These would just fill the d band, rendering the system diamagnetic, when the composition $PdH_{0.55}$ was reached.

From the experimentally determined diffusion constant and the mobility, the effective charge of hydrogen in Pd has been calculated by Duhm[15] to be +1/25 elementary charge, and by Wagner and Heller[16] to be +(0.40-0.55) elementary charge. This has been interpreted to mean either that only 4-55% of the hydrogen atoms are ionized, or that the electron "gas" of the metal shields the protons and decreases their mobility, in analogy to the considerations of Debye and Hückel regarding the lowering of ionic mobilities in aqueous solutions[40].

Since the high occlusive capacity of palladium is unique among the group VIII metals and among the neighboring elements of the fifth period of the periodic system, it is questionable to generalize the results of the transport studies on Pd-H, in spite of the similarities between this and other hydride systems. For instance, it is conceivable that in some of

the transition-metal hydrides the electronic state of the hydrogen may be represented by the H^- configuration.

C. Purpose and Main Results of the Present Investigation.

This study represents an effort to aid in the clarification of the electronic structure of hydrides of transition metals. The systems Pd-H, Ta-H and Ti-H were investigated. The Pd-H system was chosen for preliminary transport experiments to test, with a previously studied material, the adequacy of the method intended for the investigation of the other two systems. The previous results were confirmed with respect to the direction of the transport, as well as to the order of magnitude of the transport number and mobility.

The selection of the Ta-H and Ti-H systems was based on several factors: availability of high purity metal in suitably fabricated form; resistance of metal and hydride to atmospheric attack under ordinary conditions; ease of preparation and mechanical strength of the hydride; stability of the hydride with respect to dissociation, and its suitability for magnetic measurements.

The following investigations were performed on the Ta-H and Ti-H systems:

(1) The direction of transport was ascertained by measuring the change in resistance of anodic and cathodic sections and by determining the resistance vs. composition dependence. In both systems, hydrogen was found to be transported toward the cathode, showing that at least part of the

hydrogen is protonic. The transport number and mobility of the hydrogen, as well as the dependence of the temperature coefficient of resistivity on the hydrogen concentration, were obtained for various compositions.

(2) Measurements of magnetic susceptibility were made for various compositions. The molar susceptibility of $TaH_{0.5}$ was found to be 77% of that of the paramagnetic metal. The paramagnetism of the Ti-H system first decreases slightly as hydrogen is added, reaching a minimum for $TiH_{0.2}$. It then increases to a value 1.19 times larger than that of the metal for the composition $TiH_{1.7}$. It will be concluded from these results that only a small fraction of the hydrogen, if any, is present in the state of un-ionized atoms.

(3) X-ray powder diffraction photographs were made of the samples used for the magnetic susceptibility measurements.

II. Electrical Conductivity and Transport in the Palladium-Hydrogen, Tantalum-Hydrogen, and Titanium-Hydrogen Systems

A. Experimental, General.

1. Previous Measurements. (a) Proton Transfer. The only previous observations of hydrogen transport in a transition-metal hydride under the influence of an electric field have been made on the Pd-H system. Various methods were used to follow the transport. Coehn et al.[9-13] used the following technique. In order to dissolve electrolytic hydrogen in a U-shaped loop of palladium wire, the latter was partially immersed in dilute sulfuric acid and made the cathode. Platinum leads welded to eachend and to the middle of the loop, divided the wire into two segments. The change in hydrogen distribution due to the passage of a direct current through the wire was studied by three methods: (1) The two segments were made the arms of a Wheatstone bridge, and the change in the ratio of their resistances, together with the resistance vs. concentration dependence, showed the direction of the transport. (2) The electrode potential at fixed points along the wire in contact with the dilute acid was measured and compared with its known dependence on composition. (3) The hydrogen peroxide, formed in the reaction of the hydride with atmospheric oxygen, produced a blackening of a photographic plate, which was used to detect the distribution of hydrogen in the palladium at any given time.

Hydrogen was always observed to migrate toward the cathode.

Duhm[14] followed the diffusion and electrical transport in electrolytically hydrogenated palladium wire by cutting it into short pieces and determining their hydrogen content. Wagner and Heller[16] determined by an ingenious method the volume of hydrogen evolved at the cathode of a hydrogenated palladium wire after a direct current was passed through it at 182° and 240°.

(b) Hysteresis in the Resistance vs. Composition Dependence. The resistance vs. composition dependence ("R vs. C dependence") in the Pd-H system has been studied by numerous investigators. Since the results show many of the complicating features which also appeared in the systems presently investigated, they will be reviewed here briefly.

Below 100°, Pd can be hydrogenated electrolytically to compositions up to $PdH_{0.9}$. The ratio of the resistance of the resulting hydride to that of the metal ("resistance ratio") is plotted vs. the atomic ratio H/Pd in Figure 2. In the (α+ß) phase region (see Figure 1) the resistance increase is nearly linear as expected. In the ß region the resistance drops sharply with increasing H/Pd ratio, but when the electrolytic current is interrupted, hydrogen is liberated and the resistance increases with time to a constant value[41]. The differences between the curves given for the ß region by various observers can be attributed to differences in procedure: Coehn and Jürgens[12] measured the resistance during the

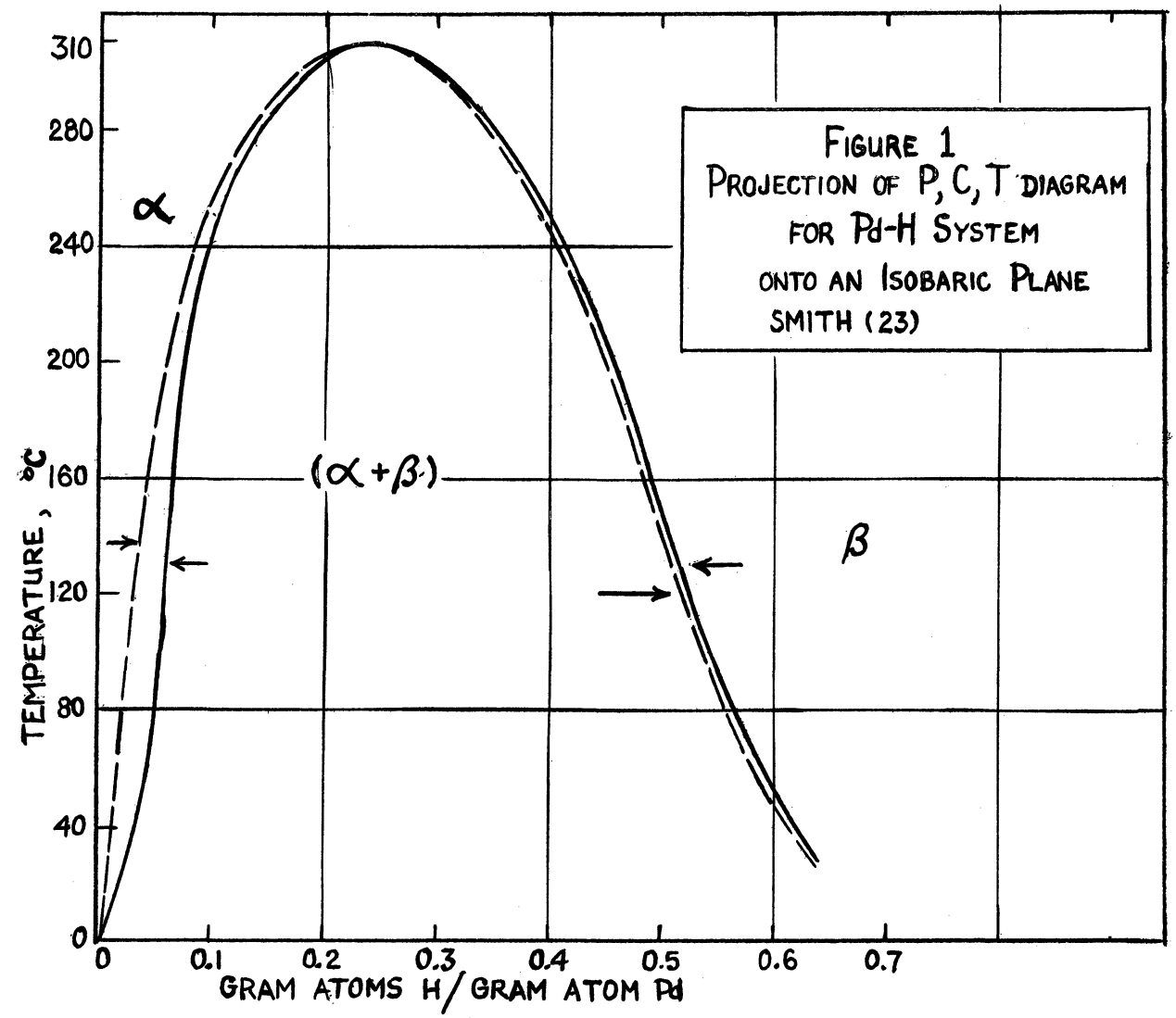

FIGURE 1
PROJECTION OF P, C, T DIAGRAM FOR Pd-H SYSTEM ONTO AN ISOBARIC PLANE
SMITH (23)

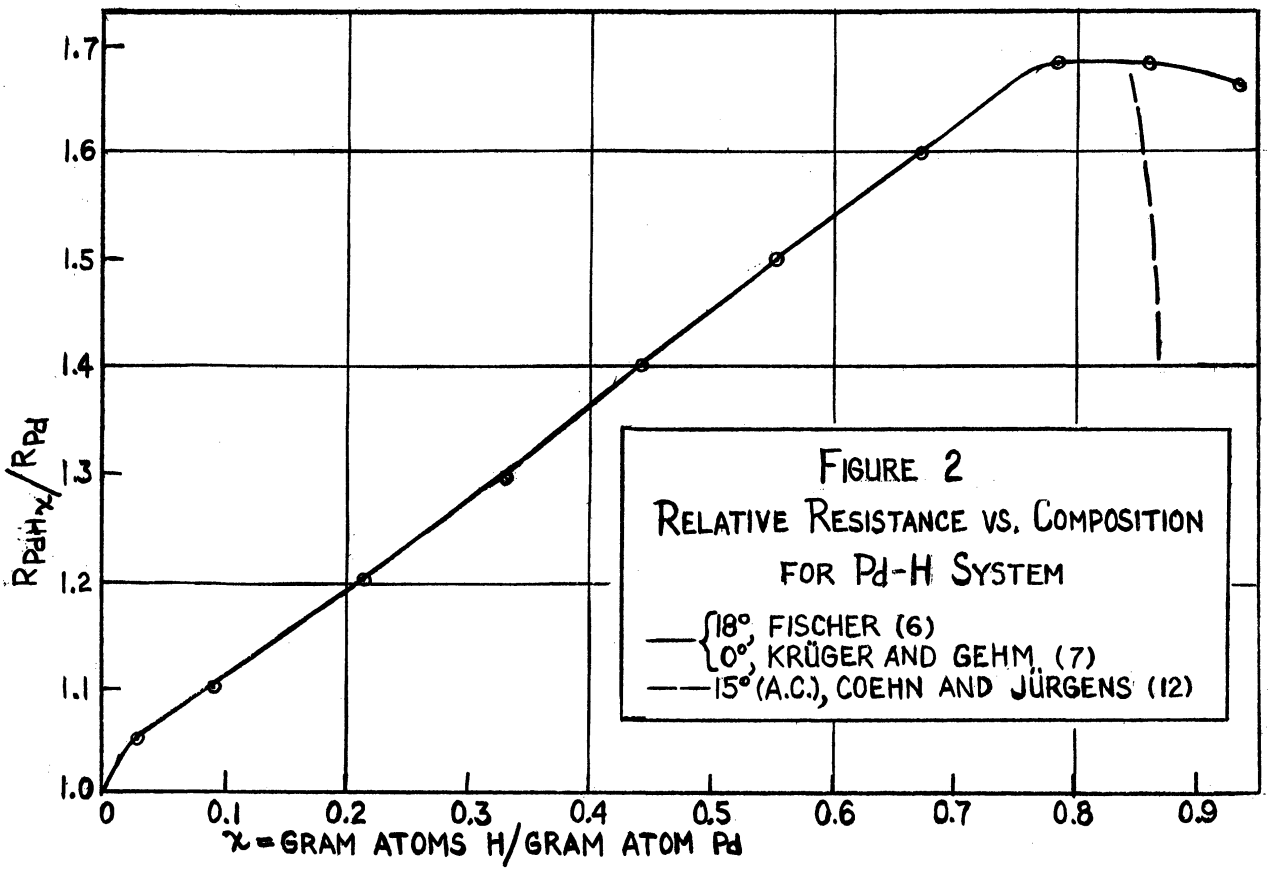

FIGURE 2
RELATIVE RESISTANCE VS. COMPOSITION FOR Pd-H SYSTEM
—{18°, FISCHER (6)
{0°, KRÜGER AND GEHM, (7)
– – 15° (A.C.), COEHN AND JÜRGENS (12)

passage of the electrolytic current; Krüger and Gehm[7] interrupted this current for the measurement. The much lower values observed by the former investigators "represent resistances depressed by the large co-conductions due to the presence of supersaturation hydrogen" (Smith, p. 124).

Brüning and Sieverts[5] measured simultaneously the resistance and dissociation pressure of Pd treated with gaseous hydrogen between 160° and 310° as functions of composition. Hysteresis occurs for both dependencies, as shown at 180° in Figures 3 and 4. The solid curves correspond to continuous absorption and subsequent evolution of hydrogen, while the dashed curves are hysteresis loops obtained when a small concentration range was retraced; the arrows indicate the direction of concentration change.

Over the $\alpha+\beta$ phase regions, the dissociation pressure and R vs. C curves show nearly linear branches during both increase and decrease of hydrogen concentration. The R vs. C dependence has a positive slope except when hydrogen is evolved above $PdH_{0.45}$. At temperatures below 180°, the region of positive slope, i.e., the (α+b) range, extends to higher concentrations.

Smith (p. 133) cites convincing evidence for rift formation in both endothermic and exothermic occluders due to changes of hydrogen concentration, and concludes that the hysteresis of the resistance is due to "the presence . . . and the ionized state of the rift hydrogen". On the other

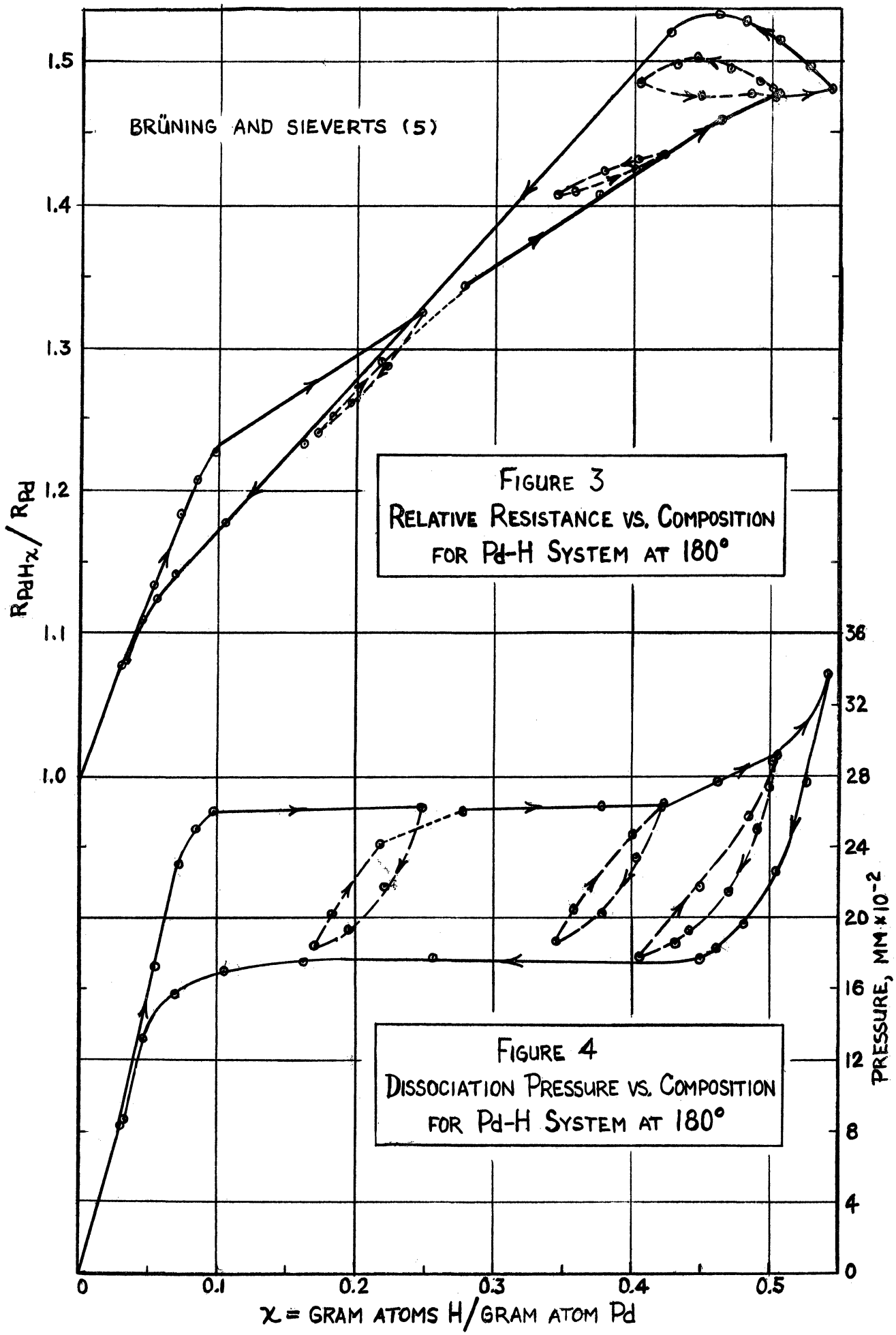

FIGURE 3
RELATIVE RESISTANCE VS. COMPOSITION FOR Pd-H SYSTEM AT 180°

FIGURE 4
DISSOCIATION PRESSURE VS. COMPOSITION FOR Pd-H SYSTEM AT 180°

hand, Brüning and Sieverts[5] attribute the hysteresis to mechanical stresses. The Pd-Pd distance increases discontinuously by about 3% at the diffusion front of the critical concentration at which the $\alpha \longrightarrow \beta$ transformation occurs. Therefore, at that boundary severe mechanical stresses are produced in the crystal, and this occurs also on removal of hydrogen. Since the formation of rifts cannot relieve all stresses, it is probable that hysteresis is due to both rifts and stresses.

Sieverts and Brüning[8] followed the resistance of Ta as hydrogen was absorbed at 500° and 600° up to the saturation level at one atmosphere, and was then evolved. The R vs. C dependence, while much simpler than that for the Pd-H system, also displayed hysteresis. Measurements at 400° were incomplete because the wire broke, apparently due to the rifts and stresses produced during hydrogenation.

One can expect for any exothermic occluder (e.g. Ta and Ti), that when enough hydrogen is absorbed to cause a phase transformation, distorting forces will appear at the critical diffusion boundary. Depending on the relative change in volume for the particular system, and the plastic and tensile properties of the two phases, rifts will be formed and/or severe cold-working will occur.

2. Method of Present Investigation. In the present investigation, hydrogen was occluded by the metal from the gas phase. This permitted a direct determination of the amount

absorbed, as well as of the R vs. C dependence over a wide temperature range.

The technique of following the hydrogen transport was similar to method (1) of Coehn. However, while Coehn measured the ratio of the resistances of the two segments of a Pd wire, in this study the absolute resistance of a ribbon and of each of its two segments was observed for the Pd-H, Ta-H, and Ti-H systems.

The very precise resistance measurements were chosen to determine the hydrogen concentration. In the following discussion, absorbed hydrogen will be assumed to be transported from one segment to another when a direct current is sent through the ribbon. In the ideal case where resistance is a single-valued linear function of composition, the resistance of one of the equal segments decreases during hydrogen transport as much as that of the other increases, while the total resistance remains constant.

In general, resistance is not a single-valued function of composition. Since stresses are produced during hydrogenation and require time to be relieved, the total resistance is time dependent. However, if the relief occurs uniformly throughout the specimen, this or any other uniform effect can be corrected for by using the ratio of the resistance of one segment to that of the total sample (resistance ratio). The appropriateness of this quantity can be seen especially clearly by comparing curves C and D in Figure 23. Curve C

is the observed absolute resistance of the left ribbon segment, while the much smoother curve D is the resistance ratio for the same segment.

If the R vs. C curve displays hysteresis such that the observed slope is discontinuous whenever the direction of the hydrogen concentration change is reversed (see Figure 3), then this discontinuity will contribute to the slope of the curve representing the total resistance vs. amp.-hrs. To show how the latter and the resistance ratio will be affected by the discontinuity in slope, the following designations are chosen:

R_1, R_2, R = resistances of segments 1 and 2 and of the total ribbon at the start of the transport
R_1', R_2', R' = corresponding resistances at the end of the transport
r_1, r_2, r = resistance changes in segments 1 and 2 and in the total ribbon due to relief of stresses during time of transport
M_1, M_2, M = gram atoms of metal in segments 1 and 2 and in the total ribbon
m_i, m_d = slopes of the relative resistance vs, composition curve for increasing and decreasing hydrogen concentration respectively
δx = gram atoms of hydrogen transported from one segment to the other

The following simplifying assumptions are made:

(1) The ribbon has a uniform cross-section and, before transport occurs, a uniform composition.

(2) Segments 1 and 2 have equal length.

It follows that:

$$M_1 = M_2 = M/2 ,$$

$$R_1 = R_2 = R/2 , \text{ and}$$

$$r_1 = r_2 = r/2 .$$

When δx is transported, the hydrogen to metal ratio for the segments decreases and increases by $2\delta x/M$, and the values for the segment resistances become, when transport is in the direction $2 \longrightarrow 1$,

$$R_1' = \frac{R}{2} + \frac{r}{2} + 2m_i \frac{\delta x}{M}, \text{ and} \qquad \text{Eq. (1a)}$$

$$R_2' = \frac{R}{2} + \frac{r}{2} - 2m_d \frac{\delta x}{M} . \qquad \text{Eq. (1b)}$$

When the transport direction is $1 \longrightarrow 2$,

$$R_1' = \frac{R}{2} + \frac{r}{2} - 2m_d \frac{\delta x}{M}, \text{ and} \qquad \text{Eq. (2a)}$$

$$R_2' = \frac{R}{2} + \frac{r}{2} + 2m_i \frac{\delta x}{M} . \qquad \text{Eq. (2b)}$$

Therefore, independent of the direction of transport,

$$R' = R_1' + R_2' = R + r + 2(m_i - m_d) \frac{\delta x}{M} . \qquad \text{Eq. (3)}$$

The expression for the resistance ratio for segment 1, after transport in the direction $2 \longrightarrow 1$, is obtained by dividing Eq. (1a) by Eq. (3) and rearranging:

$$\frac{R_1'}{R'} = \frac{1}{2} + \frac{m_i + m_d}{MR'} \cdot \delta x. \qquad \text{Eq. (4a)}$$

Similarly, after transport in the direction $1 \longrightarrow 2$, the resistance ratio for segment 1 is

$$\frac{R_1'}{R'} = \frac{1}{2} - \frac{m_i + m_d}{MR'} \cdot \delta x. \qquad \text{Eq. (4b)}$$

Determining the direction of hydrogen transport involves ascertaining which of the two equations, (4a) or (4b), is

obeyed for a given transport current direction. This can be inferred from the sign of m_i, which is known from the R vs. C studies and from the sign of the slope of the resistance ratio vs. amp.-hr. dependence as follows.

The quantities M, R', and δx are positive, and the sign of m_i is known. Although m_d has not been determined in this study it is reasonable to assume that it has the same sign as m_i. As an example, consider that m_i is positive. If the resistance ratio $\frac{R_1'}{R'}$ increases during transport, then Eq. (4a) applies, indicating that hydrogen is transported into segment 1. If $\frac{R_1'}{R'}$ decreases, then according to Eq. (4b), the transport must be in the reverse direction. On the other hand, if m_i is negative and $\frac{R_1'}{R'}$ increases during transport, then Eq. (4b) is obeyed, and hydrogen is transported into segment 2; if $\frac{R_1'}{R'}$ decreases, the transport is into segment 1.

The above analysis is valid even if m_i and m_d are of opposite sign, provided that the hysteresis is not so extreme that $|m_d| > |m_i|$. Such extreme hysteresis has been observed by Sieverts in the Pd-H system at 180° near the composition $PdH_{0.5}$ (Figure 3), but it is very improbable that it occurred during hydrogen transport for the following reasons:

1. Hysteresis is a non-equilibrium phenomenon which has been observed only during gross changes in hydrogen concentration. It can be expected to be less pronounced when equilibrium conditions are approached, as they were during the transport experiments. The small concentration changes

occurred so slowly that any resulting stresses would have been relieved.

2. If m_i and m_d were of opposite sign, then the factor $(m_i - m_d)$ in Eq. (3) would have the same sign as m_i, and the sign of the time rate of change of the total ribbon resistance, $\frac{dR}{dt} = \frac{dr}{dt} + \frac{2}{M}(m_i - m_d)\cdot\frac{dx}{dt}$, would depend upon the sign and magnitude of $\frac{dr}{dt}$, relative to $\frac{2}{M}(m_i - m_d)\frac{dx}{dt}$.

Case 1: Consider that the sign of $\frac{dr}{dt}$ is the same as that of m_i, or if it is opposite, then $\left|\frac{dr}{dt}\right| < \left|\frac{4m_i}{M}\cdot\frac{dx}{dt}\right| < \frac{2}{M}(m_i - m_d)\frac{dx}{dt}$. Then the slopes of the R', R_1', and R_2' vs. amp.-hr. curves would all have the same sign as m_i [from Eqs. (1a) - (2b)], even when the transport direction is reversed. Such behavior has not been observed in this study. In one case, shown in Figure 17, the slopes of all three functions did have the same sign, but this did not persist after the current was reversed. Furthermore, the sign of the slopes was opposite to that of m_i.

Case 2: Consider that the sign of $\frac{dr}{dt}$ is opposite to that of m_i, and $\left|\frac{dr}{dt}\right| > \left|\frac{4m_i}{M}\cdot\frac{dx}{dt}\right|$. This would mean that the rate of relief of the stresses produced during hydrogenation is large, and that $\frac{dr}{dt}$ must be decreasing. Therefore, measurements have been considered reliable only when the change in total resistance of the ribbon was not larger than the changes produced in the segments by the transport. Thus the data in Figure 17, up to about half-way between the first and second current reversals, would not be considered reliable if taken by itself.

When two hydride phases are present, the total resistance will be also dependent on the thermal history during transport, since the specific resistances of the phases differ and their relative amounts depend on temperature. Assuming the temperature variation to be random, small irregularities will occur in the resistances. Furthermore, when a voltage is applied across the specimen, an increase or decrease in hydrogen concentration, i.e., polarization, will occur at the electrical contacts. Since the mobility of hydrogen is small in the solid hydrides (e.g., in Pd-H it is some 500 times smaller than in aqueous solution), an appreciable time is required to reach steady state conditions. Hence discontinuities will result in the slope of the dependence of both the total and segment resistances vs. total charge passed, whenever the current is reversed.

Variations of the total resistance as a function of passed charge (i.e., of time also) determined for the systems studied in the present investigation, illustrate the phenomena described above. For example, Curve A in Figure 14 for the Pd-H system indicates that stresses were gradually relieved and/or that hysteresis was gradually diminishing, whereas polarization played a negligible role. The scattering of the points is well beyond observational error, and can be attributed to temperature variations during transport.

On the other hand, curve A in Figure 19 shows a much more complicated behavior. The discontinuities in slope,

attributable to polarization, appear upon each reversal of current.

3. Materials. (a) Metals. Palladium, tantalum, and titanium wire were converted into ribbon by means of a small manual rolling mill. The enlargement of the surface and diminution of the thickness were expected to accelerate the hydrogen absorption and to make the hydrogen distribution throughout the material more uniform.

Palladium wire (No. 26) used for the preliminary transport study was supplied to this laboratory by Eimer and Amend more than twenty years ago, and no information was available regarding its purity. The wire was rolled without annealing into a ribbon of cross-section 1.0 mm x 0.06 mm.

Tantalum wire (0.050" dia.), having a specified purity of 99.5%, was obtained from the Fansteel Metallurgical Corporation of North Chicago, Illinois. It was rolled into ribbon of 2.5 mm x 0.054 mm cross-section. For some of the studies, the ribbon was cut in half lengthwise.

Two sample of titanium wire (0.030" and 0.050" dia.) were obtained from the Rem-Cru Corporation of Midland, Pennsylvania. No analyses of the wires were available; however, the composition of the cast Ti ingots from which other forms are fabricated is reported to be[42]: >98.8% Ti; 0.05-0.25% Fe; 0.01-0.05% N; 0.01-0.20% O; 0.20-1.00% C; <0.01% each of Mg, Cl, and H. In a recent Rem-Cru brochure, the most common composition of fabricated Ti is stated to be: >99.0% Ti; 0.2% Fe; O, N and other trace elements together, 0.8%.

The thinner Ti wire was annealed at about 700° prior to, during, and at the conclusion of the rolling process. The resulting ribbon (cross-section 2.0 mm. x 0.10 mm.) was cut in half lengthwise. Sections in which small longitudinal cracks had developed were discarded. As the thicker wire was converted to ribbon (cross-section 3.5 mm. x 0.12 mm.), cracking was avoided by vacuum annealing at 700° after each diminution of the cross-section by about 25%.

(b) Hydrogen. Commercial hydrogen was purified by passing over copper turnings at 400°, then through Drierite, and finally through a cold trap immersed in dry ice or liquid nitrogen. The "pure" hydrogen thus obtained was used for the hydrogenation of Pd and of some Ta and Ti specimens. For later experiments with Ta and Ti, "extra pure" hydrogen was produced by treatment of the "pure" hydrogen with Ti sponge in the apparatus shown in Figure 11. Eight grams of Ti sponge was heated in a Vycor tube to about 800° under high vacuum. "Pure" hydrogen was then admitted to the tube. The sponge absorbed 2.2 liters of gas when cooled slowly to room temperature. The system was evacuated to 10^{-6} mm., the sponge heated, and the hydrogen evolved and stored in a 2 liter flask. Any impurities of N_2, O_2, CO_2, CO, or organic vapors were fixed to the Ti sponge as refractory nitrides, oxides, or carbides.

4. Apparatus and Techniques. (a) Sample Assembly. A unit, consisting of the "sample" (the metal ribbon or its hydride), a glass tube into which the sample was sealed,

lead wires, insulators and supports, is termed "sample assembly". Three assembly designs were used in the various experiments. In each design, electrical contacts were made at the two ends and at the middle of the ribbon. Depending upon the form of the ribbon, these contacts are designated as top, middle, and bottom (T, M and B) as in Figures 5 and 6, or as left, middle, and right (L, M and R) (Figure 7).

Sample assembly I, used in the studies of Pd-H, is shown in Figure 5. About 2 mm of No. 26 Pd wire was spot welded to each end and to the middle of the 100 mm long Pd ribbon, using a spot welder especially built for this purpose. Silver leads were welded to the Pd leads. After placing the ribbon in the pyrex sample tube, seals around the lead wires were made with silver chloride covered with Apiezon wax. The silver chloride, which has a considerably higher melting point than the wax, prevented the latter from being sucked into the tube when the Pd ribbon was heated under vacuum.

The same design was used in early studied of Ta-H, with the substitution of Pt wire for the Pd contacts. The design was abandoned, however, because the Ta ribbon distorted during hydrogenation, resulting in breakage of the welded contacts or of the ribbon itself. This difficulty was eliminated in sample assembly II, Figure 6. A 167 mm long Ta ribbon was shaped into a helix having a diameter of 5 mm and a pitch of two turns per cm. To the helix were spot welded Pt contacts, and to these silver lead wires, a portion of which had

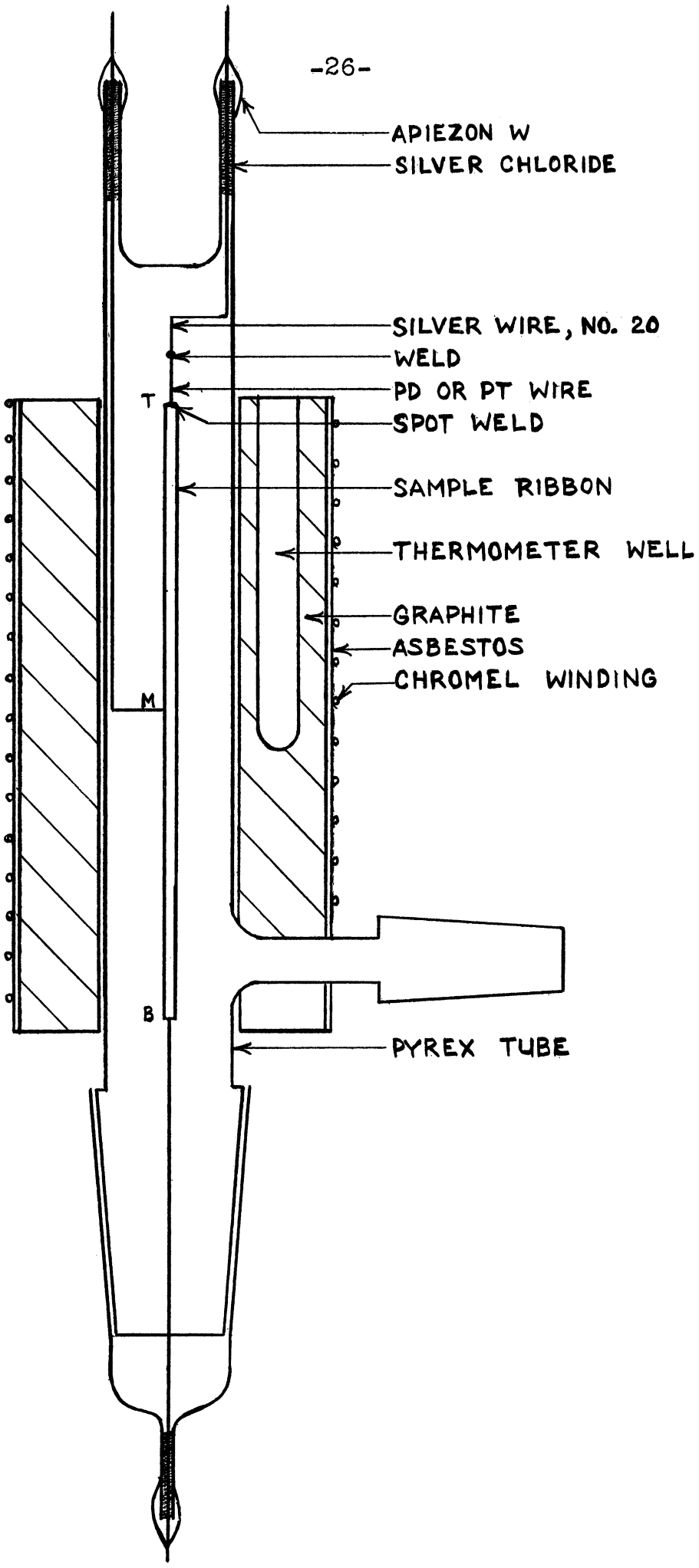

FIGURE 5. SAMPLE ASSEMBLY I

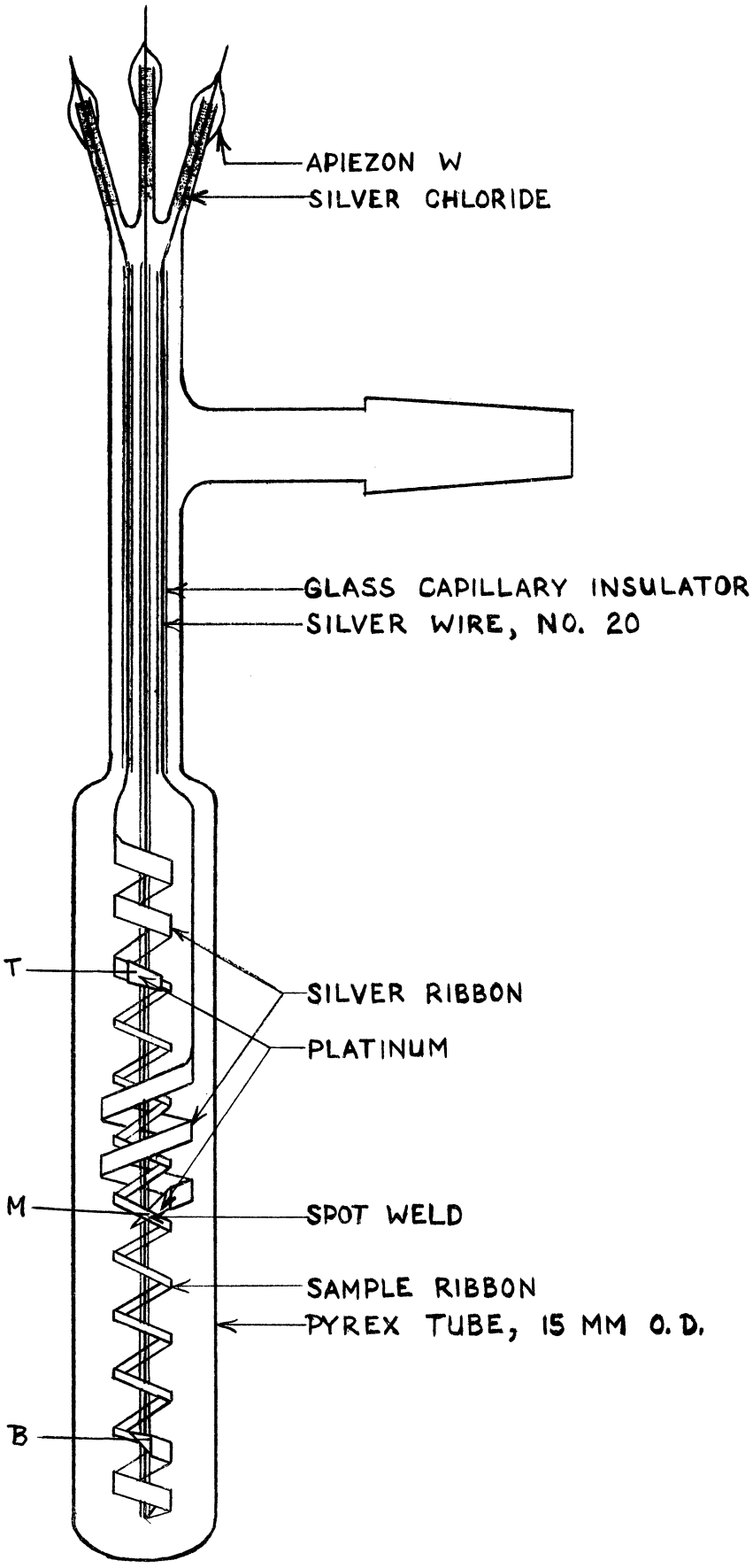

FIGURE 6. SAMPLE ASSEMBLY II

been flattened and bent into a spiral. This helical assembly permitted considerable distortion without exerting severe stress on either the Ta ribbon or the welded contacts.

In early measurements on Ti-H using sample assembly II, the Ti helix sagged when heated, the spot welded contacts failed, or the sample ribbon broke. The first of these difdiculties was overcome by the adoption of sample assembly III, shown in Figure 7. A 25 cm ribbon was bent into the form of a W and was held in shape by means of mica separators. These allowed the ribbon to expand, yet confined it sufficiently to prevent shorting and distortion at the welds. Another advantage of this design was its symmetry, which resulted in equal resistance changes due to temperature increase in each lead wire, and in compensation of thermal E.M.F. produced at the Ag-Ti contacts.

To improve the contact welds, a technique was developed for fusing the silver leads directly to the specimen. The end of a silver wire was melted to a ball, through which a slit was cut in the direction of the axis of the wire. The ribbon was inserted in the slit at least 1" from either end of the specimen, and the slit was squeezed shut. The ribbon was gripped at each end by a copper wire, as shown in Figure 8. After the assembly was evacuated, a current brought the ribbon to 900:, bonding it to the silver ball and producing a reliable contact without melting the silver wire. The hydrogenation was performed at higher temperatures than had

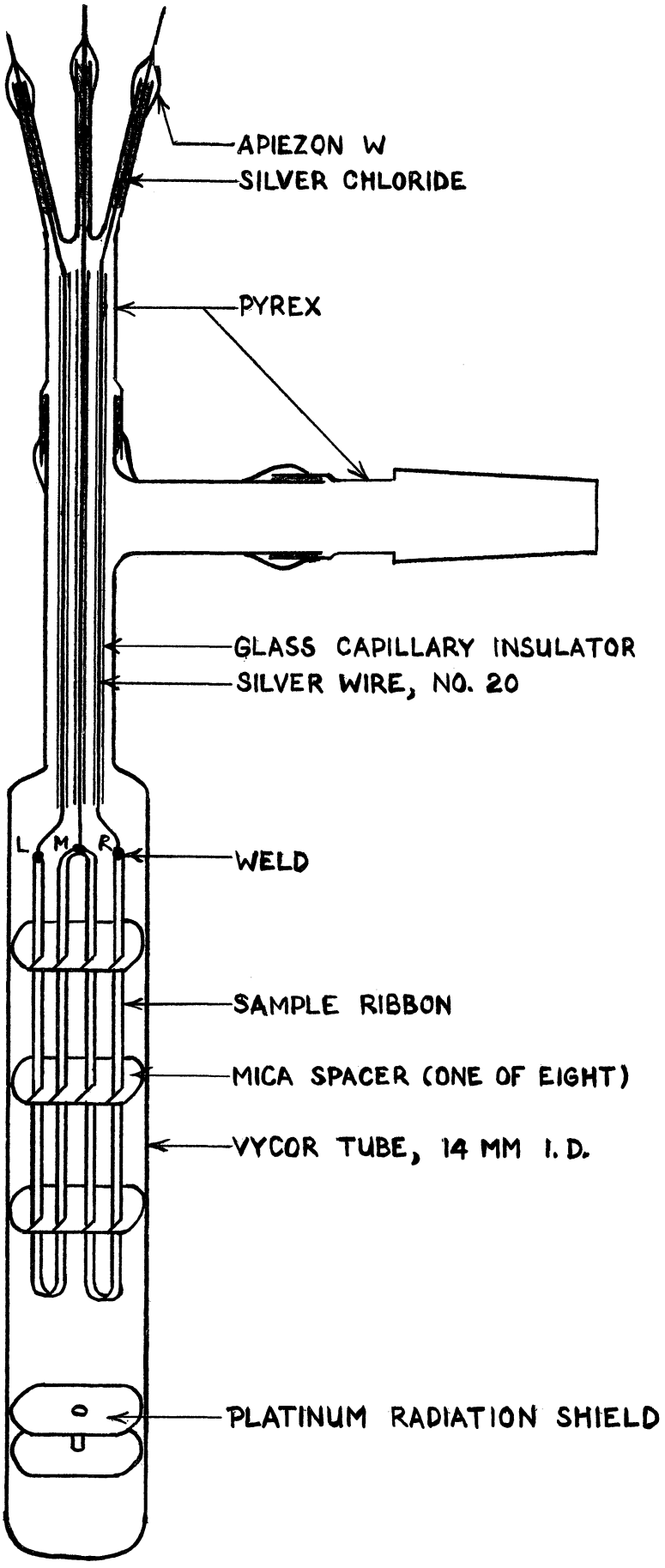

FIGURE 7. SAMPLE ASSEMBLY III

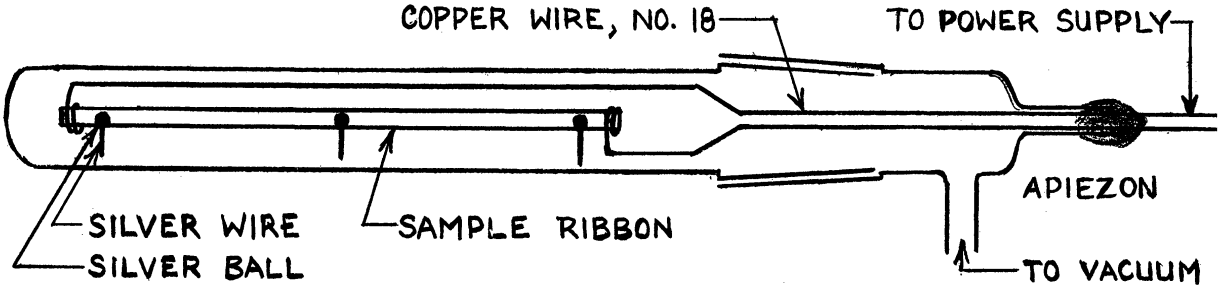

FIGURE 8. WELDING ASSEMBLY

been used previously, relieving stresses in the ribbon and preventing its breaking. The Vycor glass (96% silica) sample tube did not distort when maintained for a long time at temperatures of 400° or higher.

Sample assembly III was used for the R vs. C measurements of Ta-H at 400° and 100°.

(b) Hydrogenation and Thermal Control Apparatus.

(i) Preliminary Pd-H and Ta-H Studies. Design I of the hydrogenation train, shown in Figure 9, was used for the preliminary Pd-H and Ta-H investigations. In this train the sample tube was connected to a mercury manometer, a McLeod gauge, the apparatus for producing "pure" hydrogen (see section II, A, 3, b), and the vacuum line. This system, as well as its later modifications, was evacuated by an umbrella-type mercury diffusion pump, backed up by a "Hyvac" mechnical pump. The system was considered vacuum tight when the McLeod gauge indicated 10^{-6} mm with the system open to the diffusion pump.

The sample tube was heated by a small resistance furnace, the core of which was a graphite sleeve fitting snugly around the tube. A Variac regulated the furnace temperature to 72° ± 4°. This was observed on a thermometer which was inserted in a well in the graphite sleeve.

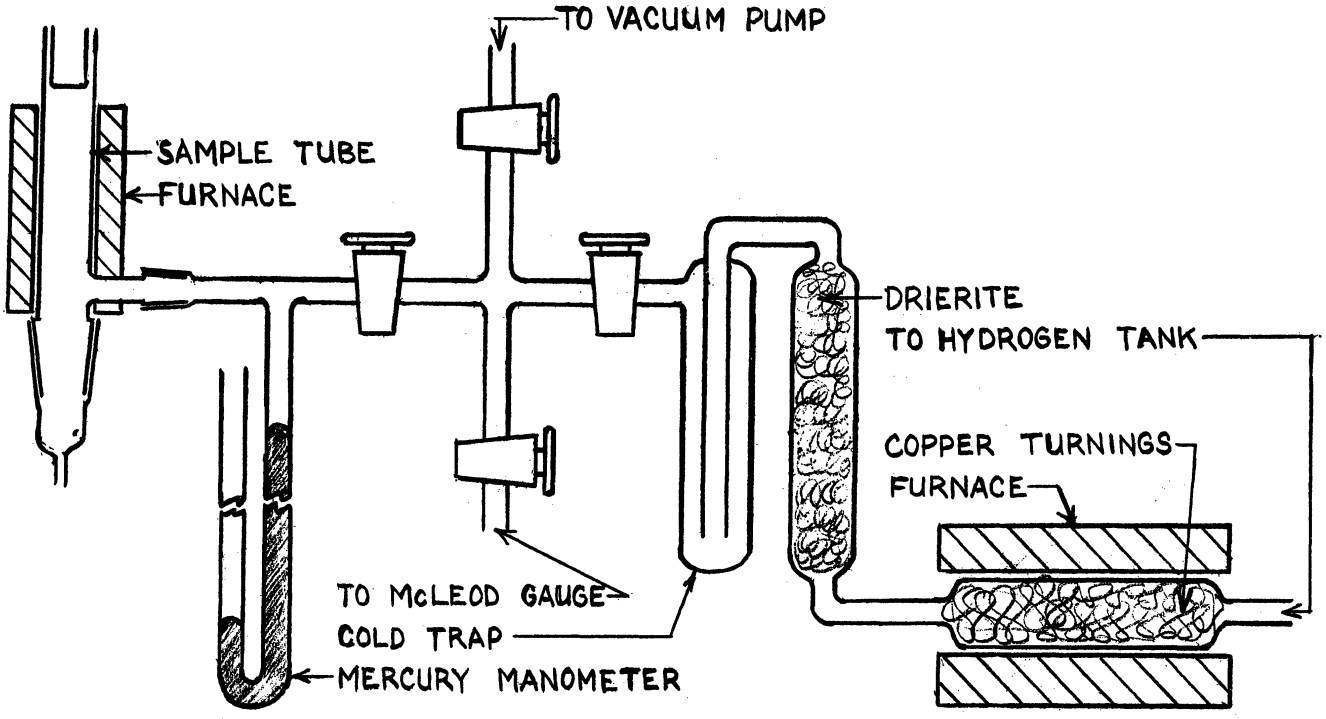

FIGURE 9. HYDROGENATION TRAIN I

The amount of hydrogen absorbed was obtained with sufficient approximation for these preliminary experiments from the decrease of hydrogen pressure, the estimated volume of the system, and the temperature.

(ii) Ta-H and Ti-H Studies at 76° and 100°.

For the study of the resistance vs. composition dependence of Ta-H at 76°, the hydrogenation train was redesigned to permit better control of the amount of hydrogen absorbed. As shown in Figure 10, the following features were incorporated in design II: a 10 ml burette for measuring the hydrogen delivered to the system; a Toepler pump used as a gas storage reservoir and for returning gas from the system to the burette; a cold trap to condense mercury vapor and to prevent contamination of the sample and amalgamation of the leads; a refluxing device to maintain the sample tube at the temperature of condensing carbon tetrachloride, fixed from

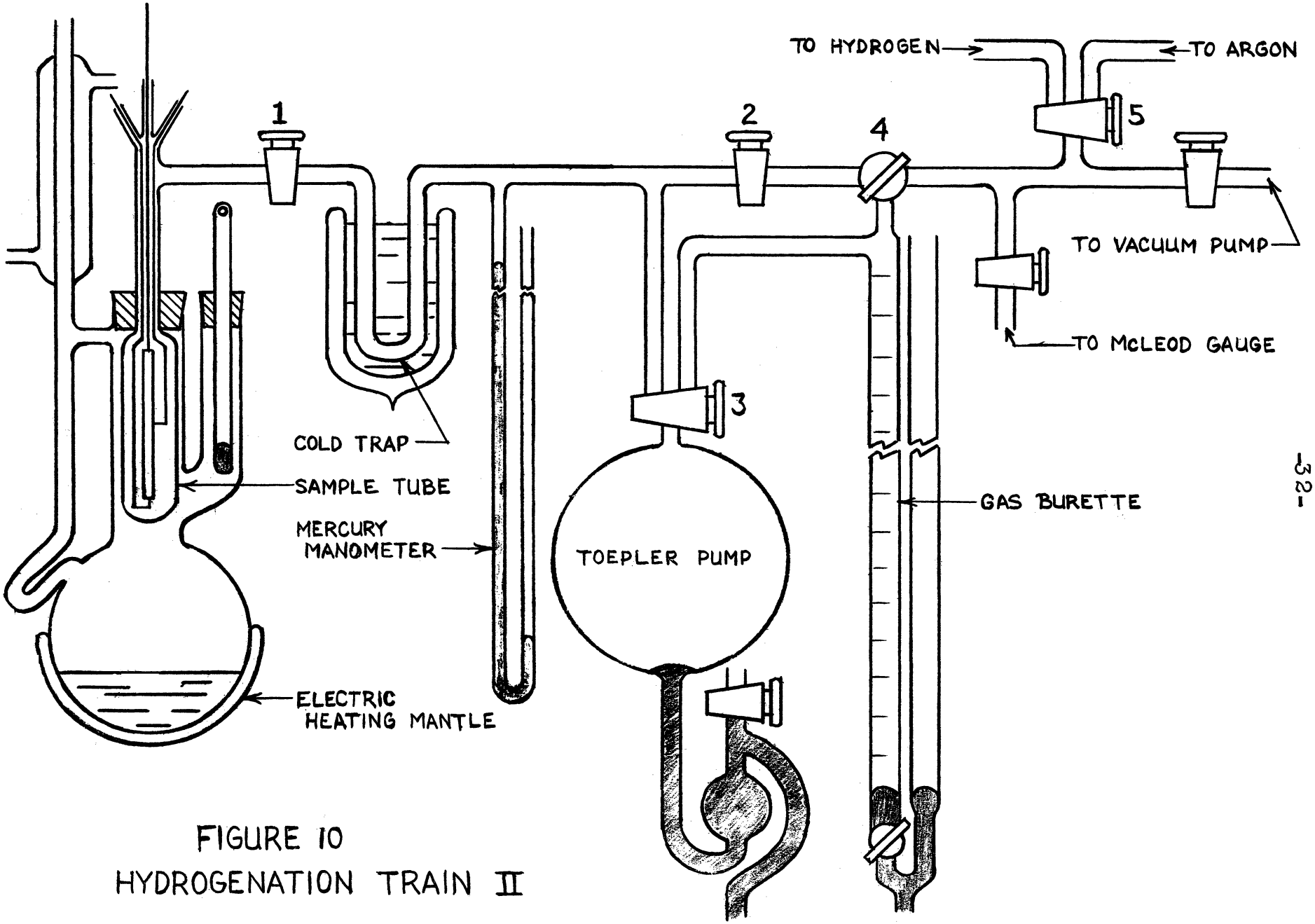

FIGURE 10
HYDROGENATION TRAIN II

the observed barometric pressure to within 0.1°.

Design II was slightly modified for the Ta-H and Ti-H studies at 99°. A Huygens-type oil manometer was added, which covered the pressure range up to 80 mm Hg and could be read to within ± 2 x 10^{-2} mm Hg. Boiling water was substituted for carbon tetrachloride.

Before the start of the hydrogenation, the system was evacuated to 10^{-6} mm Hg, and stopcocks 2 and 3 were closed. Stopcock 4 was then opened, and hydrogen was admitted to the burette through stopcock 5. After leveling the mercury in the two arms of the burette, hydrogen was admitted from the burette to the sample, the space between stopcocks 2 and 4 being used in the transfer of small increments. The quantity of hydrogen absorbed could be calculated from the initial and final burette readings, the barometric pressures, the hydrogen pressure remaining in the system, the volumes of the various parts of the system as obtained by calibration, and the temperatures of those parts. It was obviously very important to maintain a constant level of dry ice about the cold trap.

When the ribbon was heated internally to glowing, i.e., above about 550°, its temperature was estimated to about ± 100° from its color.

(iii) Ti-H and Ta-H Studies up to 500°.

(α) Hydrogenation Train. To insure sufficient purity of the hydrogen absorbed by Ti, hydrogenation train III, Figure 11, including an assembly for generating "extra pure" hydrogen

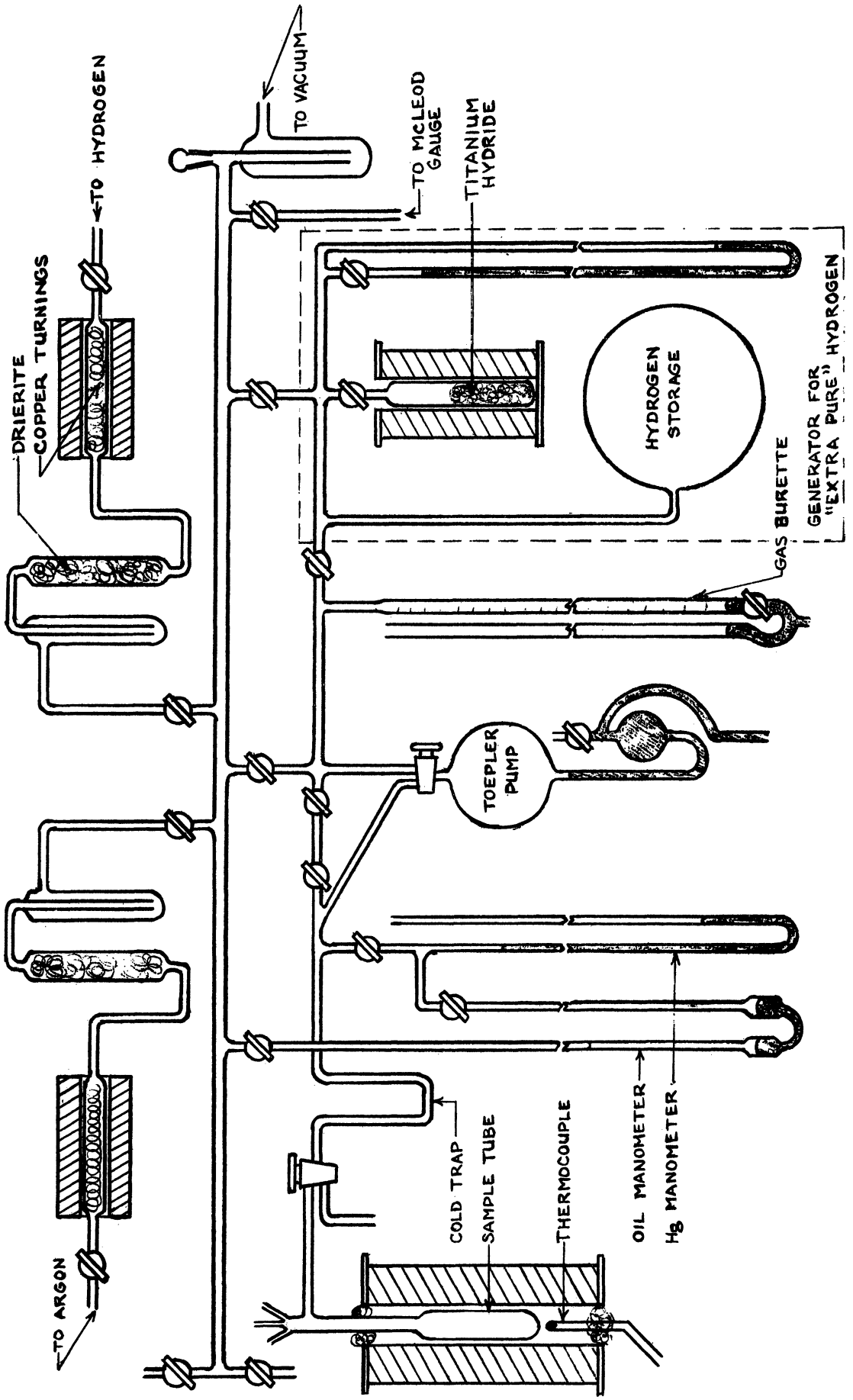

FIGURE 11. HYDROGENATION TRAIN III

(section II, A, 3, b), was employed. Precision-ground stopcocks were used wherever possible. For convenient measuring of large volumes, the 10 ml gas burette was replaced by a 50 ml burette.

(ß) Temperature Control and Measurement.

In order to reduce thermal shock and relieve mechanical stress, the Ti ribbon was heated externally to a sufficiently high temperature to effect absorption, and was kept at this temperature throughout the study. The electric furnace and temperature control circuit, shown in Figures 12 and 13, maintained the temperature between 20° and 500° to within ± 0.5°. A platinum winding in the furnace served as a resistance thermometer, and was made one arm of a Wheatstone bridge provided with a galvanometer relay instead of a galvanometer. When a decrease in temperature below the control value caused the resistance of this winding to decrease, the galvanometer relay closed, activating an electronic relay which in turn increased the current through the heater winding of the furnace.

The temperature of the ribbon was determined by means of a chromel-alumel thermocouple placed close to the sample tube. The potential difference between this junction and another kept at 0° was measured by a Leeds and Northrup Type K Potentiometer. Variations of 0.001 mV, corresponding to 0.025°, could be detected. The thermocouple was calibrated at 0°, 100°, and 419.45° (freezing point of zinc). Plugs of glass

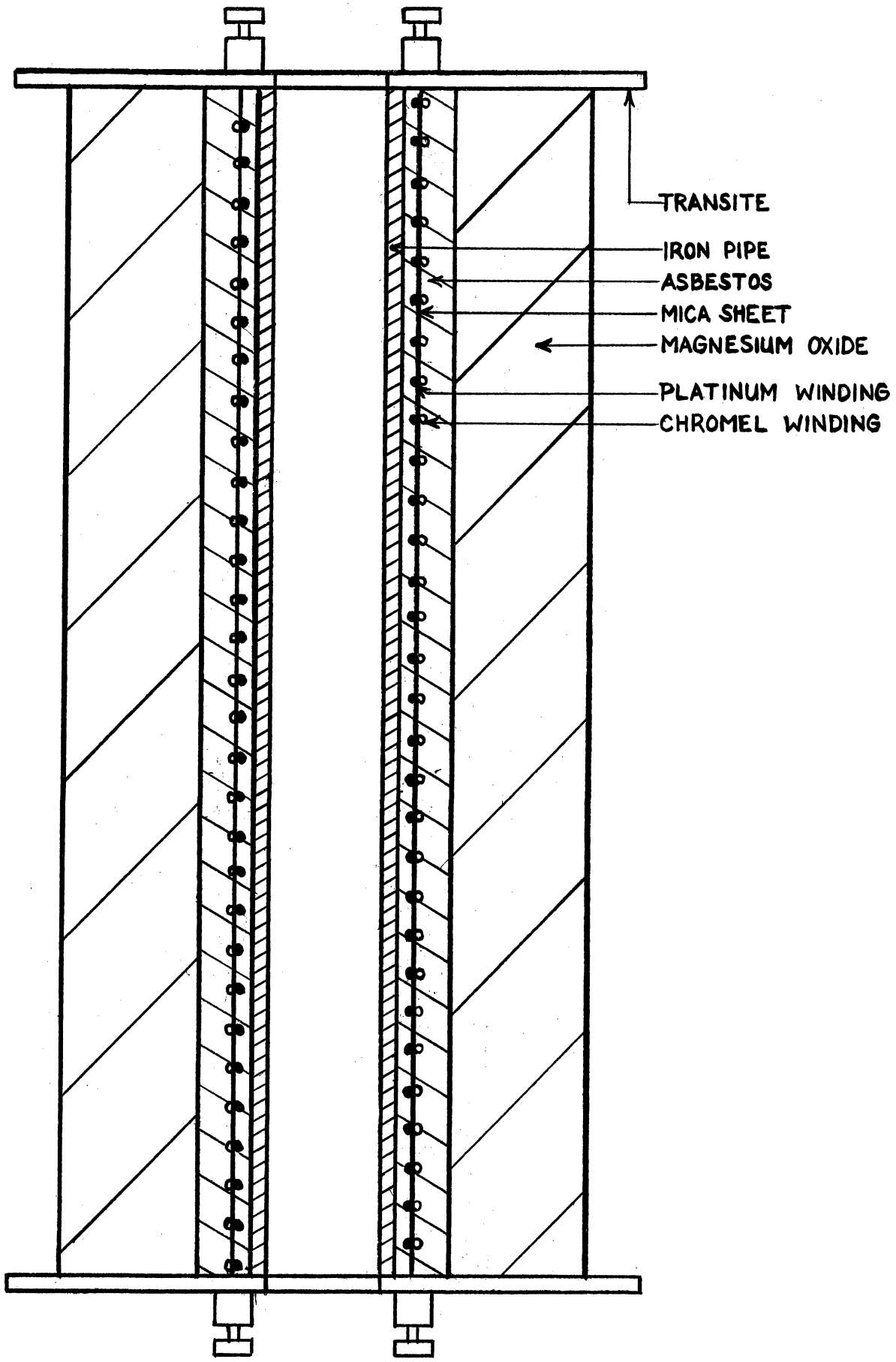

FIGURE 12. CONSTANT TEMPERATURE FURNACE

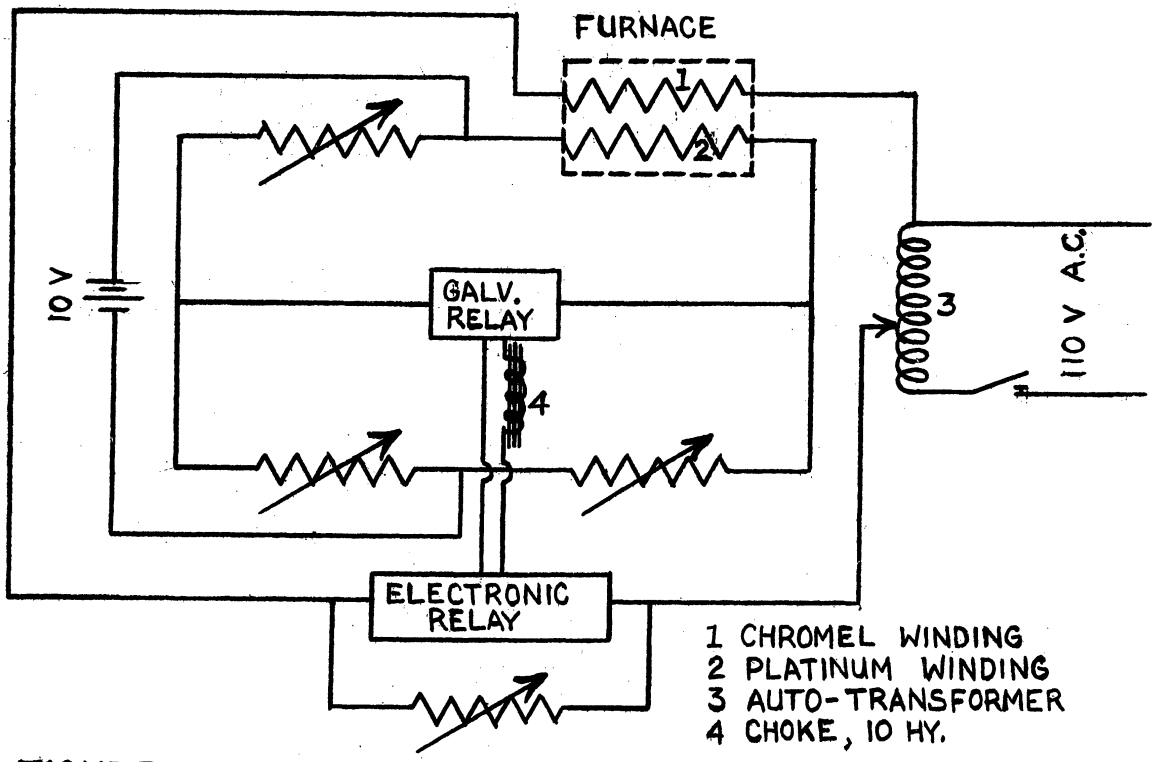

FIGURE 13. TEMPERATURE CONTROL CIRCUIT FOR ELECTRIC FURNACE

wool in the top and bottom furnace openings prevented thermal fluctuations due to convection.

(c) Resistance Measurements. Resistance was determined by means of a conventional four-decade Leeds and Northrup Wheatstone bridge, which read directly to the nearest 0.001 ohm. The fourth decimal place was estimated from the galvanometer deflection, which changed by about ten divisions when the bridge setting was changed by 0.001 ohm, with 1.5 volts across the bridge.

Electrical connections between the Wheatstone bridge and the metal specimen were made as follows. Three No. 18 or No. 20 silver wires 5-12" long were welded directly to the ends and middle of the ribbon, or were fused to short lengths of Pd or Pt which had been welded to it. The silver

wires were fused outside the sample tube to 3" of No. 18 copper wire. Each copper wire dipped into one arm of one of three U-shaped mercury wells. Two copper braids connected the terminals of the Wheatstone bridge with any two of the mercury wells. Amalgamation of the copper leads by the mercury eliminated contact resistances.

Since the ribbon resistance was of the order of tenths of an ohm and was determined to at least one part in a thousand, corrections had to be made for the lead resistance. The resistance of the copper braids was measured directly when they were short circuited by dipping the two free ends into the two arms of the same mercury well. The resistance of the leads between the mercury wells and the sample was calculated from their dimensions and specific resistivities.

The necessary corrections for variations in temperature were calculated from the experimentally determined temperature coefficient of the resistance of the metal ribbons.

5. Procedure for Absorption and Transport of Hydrogen. Prior to hydrogenation, the metal specimen was degassed at 600-1000° by passing alternating current at low voltage through it until the pressure was 10^{-5} mm. Hydrogen was then admitted and the sample usually slowly heated internally, sometimes to glowing, until a decrease in pressure indicated that absorption had started. Then hydrogenation usually proceeded without continued internal heating. One to twenty-four hours elapsed between the addition of hydrogen increments

to the system. If this interval was long, the sample often had to be reheated in order to start the absorption again. Sometimes the heating caused evolution of part of the hydrogen absorbed before. In the experiment with Ti at 400°, the absorption of "extra pure" hydrogen went spontaneously.

The hydrogen increments admitted to the sample to produce various compositions up to saturation at atmospheric pressure amounted to 0.4-20 ml. Just before each addition, resistance measurements were made of the whole ribbon and usually of its two segments.

The hydrides used for the transport studies were those produced during the course of the R vs. C investigations, except in the cases discussed in sections II, B, 1, and II, C, 1, a. Transport was accomplished by passing a direct current of 0.50 ± .05 or 1.00 ± .05 ampere through the ribbon. The current was interrupted once or twice each day and the ribbon allowed to reach thermal equilibrium with its environment. The resistance of the whole specimen and of its segments was then measured.

6. Treatment of Data: Calculations. (a) Composition. The total amount of hydrogen which had been absorbed by the metal was calculated, using the ideal gas law, from the following equation:

$$V = \frac{273.2^\circ}{760\ \text{mm}}\left[\sum \frac{V_b P_b}{T_b} - P\left(\frac{V_t}{T_t} + \frac{V_c}{T_c} + \frac{V_s - V_t + V_c + v(p)}{T_s}\right)\right] \quad \text{Eq. (5)}$$

with V = S.T.P. volume of hydrogen absorbed
V_b = individual hydrogen volume delivered from burette
Σ = summation over all burette additions
V_t = volume of sample tube
V_c = volume of cold trap
V_s = total volume of system
$v(p)$ = correction to volume of system for manometer levels
P_b = pressure in the burette = atmospheric pressure
P = hydrogen pressure in system
T_b = temperature of burette
T_t = temperature of sample trap
T_c = temperature of cold trap
T_s = temperature of remaining parts

The first term on the right side of Eq. (5) represents the total volume of hydrogen at S.T.P. delivered from the burette to the system. The term indicated by the parentheses represents the S.T.P. volume of hydrogen remaining in the system after absorption.

Since only one side of the oil and mercury manometers is included in the system, the volume of the latter is pressure dependent; hence, V_s is defined as the volume when $P = P_b$. The volume V_c was determined from the amounts of hydrogen required to bring the previously evacuated system to atmospheric pressure when the cold trap was at T_s and when it was at T_c. The volume V_t of the sample tube was determined similarly with the sample tube at T_s and at T_t. The function $v(p)$ was obtained by calibration. Measured volumes of hydrogen at known temperature and pressure were admitted to the system. The volume of the system after each addition was then calculated from its temperature and the measured internal pressure.

The oil manometer was calibrated in terms of mm Hg by admitting known amounts of hydrogen to the system and calculating the pressures from the ideal gas law.

The concentrations of hydrogen in the hydrides were finally expressed in terms of atomic ratios.

(b) Transport. For each transport experiment, the resistances of the whole ribbon and of its two segments are plotted vs. the total charge passed in ampere-hours (amp.-hr.). The "resistance ratio", i.e., the ratio of the resistance of one segment to that of the whole ribbon (see section II, A, 2), has been similarly plotted. In the figures, the curves are labeled as follows:

A = total resistance of the ribbon = R_{B-T} or R_{L-R}

B = resistance of top or right segment = R_{T-M} or R_{R-M}

C = resistance of bottom or left segment = R_{B-M} or R_{L-M}

D = ratio of the resistance of the bottom or left segment to that of the total ribbon

+ or - in connection with B, T, L, or R show that the segment was anodic or cathodic respectively

(c) Transport Numbers and Mobilities. (i) Transport Numbers. It will be shown that in an electric field hydrogen migrates toward the cathode, not only in the Pd-H but also in the Ta-H and Ti-H systems. The fraction of the total current carried by the hydrogen (protons) is expressed by $t_{H+}/(t_{H+} + t_{e-})$, where t_{H+} and t_{e-} are called the transport numbers of the protons and electrons respectively.

The transport number of the proton can be calculated from the R vs. C dependence and transport data by means of equation (8), derived as follows. Let

t_{H+} = number of gram atoms of hydrogen transported per Faraday
Q = amp.-hr. of conducted charge
F_y = 1 Faraday = 26.8 amp.-hr.
x = gram atoms of hydrogen per gram atom of metal
M = number of gram atoms of metal in the ribbon
R° = total resistance of the unhydrogenated metal
R = total resistance of the hydrogenated metal
$a_1 = \frac{d}{dQ}(R_1/R)$ = slope of the resistance ratio vs. amp.-hr. curve for segment 1
$m = \frac{d}{dx}(R/R^\circ)$ = slope of the relative resistance vs. composition curve

(A subscript 1 indicates that the quantity relates to segment 1.)

If the ribbon is uniform in cross-section and uniformly hydrogenated, then

$$\frac{R_1}{R} = \frac{R_1^\circ}{R^\circ}, \text{ and}$$

$$M_1 = \frac{R_1^\circ}{R^\circ} M.$$

Changes in R_1 are due to changes in composition of segment 1, as well as to other factors, e.g., stress relief, which affect the total resistance. That is,

$$R_1 = f(x_1, R), \text{ so that}$$

$$\frac{dR_1}{dQ} = \frac{\partial R_1}{\partial x_1} \cdot \frac{dx_1}{dQ} + \frac{\partial R_1}{\partial R} \cdot \frac{dR}{dQ} .$$

Therefore, the change in resistance of segment 1 per amp.-hr. due to transport of hydrogen only is

$$\left(\frac{\partial R_1}{\partial Q}\right)_R = \frac{\partial R_1}{\partial x_1} \cdot \frac{dx_1}{dQ} = \frac{dR_1}{dQ} - \frac{R_1}{R} \cdot \frac{dR}{dQ} = R \frac{d}{dQ}\left(\frac{R_1}{R}\right)$$

$$= R\, a_1 \qquad \text{Eq. (6)}$$

The corresponding change in relative resistance of segment 1

per Faraday is

$$\frac{\partial}{\partial F_y}\left(\frac{R_1}{R_1^\circ}\right) = \frac{26.8}{R_1^\circ}\cdot\frac{\partial R_1}{\partial Q} \qquad \text{Eq. (7)}$$

$$= 26.8\,\frac{R}{R_1^\circ}\cdot a_1 \quad \text{from Eq. (6)} .$$

The left side of Eq. 7 is

$$\frac{dx_1}{dF_y}\;\frac{\partial}{\partial x_1}\left(\frac{R_1}{R_1^\circ}\right) = m\cdot\frac{dx_1}{dF_y} .$$

$$\therefore \frac{dx_1}{dF_y} = 26.8\,\frac{R}{R_1^\circ}\,\frac{a_1}{m}, \text{ and}$$

$$t_{H+} = M_1\cdot\frac{dx_1}{dF_y} = 26.8\cdot M\cdot\frac{R}{R^\circ}\cdot\frac{a_1}{m} . \qquad \text{Eq. (8)}$$

A sample calculation of t_{H+} is given in Table I.

(ii) Mobilities. The mobility of Hydrogen is equal to its net velocity per unit field; i.e., m_{H+} = (cm/sec)/(volts/cm). In addition to the symbols used in the previous section, let

I = transport current (amperes)
E = field strength in ribbon (volts/cm)
L = length of ribbon (cm)
v = drift velocity of protons during transport (cm/sec)

Then $v = \dfrac{\text{g.-at. H/sec}}{\text{g.-at. H/cm}} = \dfrac{t_{H+}\cdot I}{9.65\cdot 10^4}\left(x\frac{M}{L}\right)$,

and $E = \dfrac{IR}{L}$.

Therefore,

$$m_{H+} = v/E = \frac{t_{H+}\cdot L^2}{9.65\cdot 10^4\cdot x\cdot M\cdot R}\ \text{cm}^2/\text{volt sec.} \qquad \text{Eq. (9)}$$

A sample calculation of m_{H+} is given in Table I.

Table I

Sample Calculation of the Transport Number and Mobility of Hydrogen in $TaH_{0.16}$ at 72°

Wt. of ribbon = 0.103 g., $\therefore M = \frac{0.103}{180.9} = 5.7 \times 10^{-4}$ g.-at.

Length of ribbon = 10.0 cm.

Composition of ribbon = $TaH_{0.16}$, $\therefore x = 0.16$

$m_{TaH_{0.16}}$ = 2.5 (g.-at. H/g.-at. Ta)$^{-1}$, from 76° curve of Figure 15

$\frac{R}{R_o}$ = 1.58, from same curve

R = 0.47, from curve A of Figure 17

a_{B-T} = slope of transport curve D of Figure 17

= -3.0×10^{-4} amp.-hr.$^{-1}$, for linear region between start of transport and first current reversal

= $+2.15 \times 10^{-4}$ " , for region between first and second reversals

= -3.15×10^{-4} " , for region between second and third reversals

= $+2.3 \times 10^{-4}$ " , for region beyond third reversal

Ave. $|a_{B-T}| = (2.7 \pm 0.4) \times 10^{-4}$ amp.-hr.$^{-1}$

To obtain Transport Number, substitute into Eq. (8):

$$t_{H+} = 26.8 \cdot M \cdot \frac{R}{R_o} \cdot \frac{a}{m}$$

$$= 26.8 \times 5.7 \times 10^{-4} \times 1.58 \times \frac{(2.7 \pm 0.4) \times 10^{-4}}{2.5}$$

$$= (2.6 \pm 0.4) \times 10^{-6}$$

To obtain Mobility, substitute into Eq. (9):

$$m_{H+} = \frac{t_{H+} \cdot L^2}{9.65 \cdot 10^4 \cdot x \cdot M \cdot R}$$

$$= \frac{(2.6 \pm 0.4) \times 10^{-6} \times (10.0)^2}{9.65 \times 10^4 \times 0.16 \times 5.7 \times 10^{-4} \times 0.47}$$

$$= (6 \pm 1) \times 10^{-5} \text{ cm}^2/\text{sec volt}$$

B. Transport in $PdH_{0.46}$ at 72°.

1. Hydrogenation and Determination of Composition. Sample assembly I and hydrogenation train I (Figures 5 and 9) were used for the Pd-H investigation. After admitting pure hydrogen up to about 1700 mm , the sample tube was heated overnight at 155 ± 5°. Then to absorb more gas, the tube was kept at 135° for four hours and cooled to room temperature.

The Pd ribbon and Pd leads, weighing 65 mg , absorbed 2.9 ± 0.15 ml (S.T.P.) of hydrogen, corresponding to the composition $PdH_{0.42}$. At the conclusion of the transport experiment, the total amount of hydrogen evolved upon heating indicated a composition of $PdH_{0.46}$. The composition of the hydride obtained from its resistance (1.450 times that of the metal) and the R vs. C dependence, was $PdH_{0.51}$. This hydride will be referred to as $PdH_{0.46}$.

2. Transport. Transport was effected at 72 ± 4° by a current of one ampere. After 46.5 hours the current was reversed and measurements were continued for an additional 90 hours.

The changes in resistance of the whole ribbon and of each segment are summarized in Figure 14. The total resistance (curve A) increased smoothly to a maximum which was 0.0025 ohm larger than the value at the start of the transport. This increase was apparently due to the relief of stress and/or the decrease of hysteresis in the R vs. C

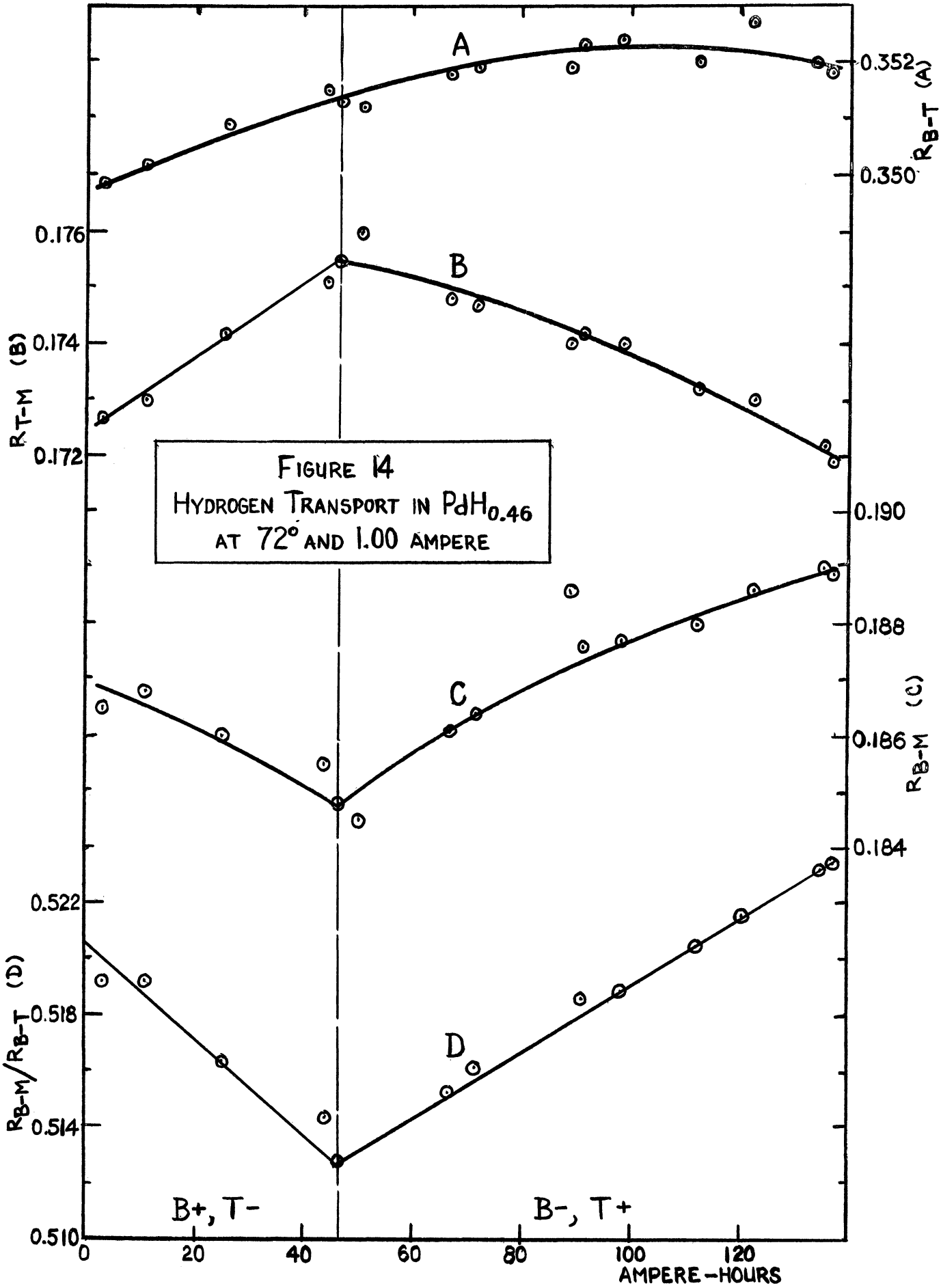

FIGURE 14
HYDROGEN TRANSPORT IN $PdH_{0.46}$
AT 72° AND 1.00 AMPERE

dependence.

The resistance changes of the top and bottom segments (curves B and C) were a function of the current direction and were approximately proportional to amp.-hr. The resistance of the cathodic segment always increased: during the first 46.5 amp.-hr. when the top segment was cathodic, its original resistance of 0.1725 increased by 0.0030 ohm; for the next 90 hours when the bottom segment was cathodic, its resistance increased by 0.0040 ohm over its value of 0.1848 ohm at the time of the current reversal. The anodic segment displayed the opposite behavior in each case.

The linearity of each branch of the resistance ratio (R_{B-M}/R_{B-T}) *vs.* amp.-hr. plot (curve D) shows that this function corrects the changes in resistance in the segments for the variations of the total resistance.

Measurements by Brüning and Sieverts[5] at 160° indicate that, although the R *vs.* C dependence is different when measured during absorption or evolution of hydrogen, the slope of the curve is positive in both cases in the composition range of the present study. Measurements at 0-18° (Figure 2) show the R *vs.* C dependence to have nearly constant positive slope up to $PdH_{0.75}$. Therefore, the observed increase in the resistance of the cathodic end of the ribbon shows that a positive charge is associated with the hydrogen. This result is in agreement with that described in section II, A, 1, a.

C. Tantalum-Hydrogen System.

1. Procedure and Measurements. (a) Transport in $TaH_{0.16}$ at 72°. Sample assembly I and hydrogenation train I were used in a preliminary transport investigation of $TaH_{0.16}$. Hydrogen was admitted to a pressure of 1150 mm , and the sample was internally heated to about 800°. It was then gradually cooled to room temperature over the course of an hour.

The composition of the resulting hydride was calculated to be $TaH_{0.155}$ on the basis of the changes in pressure which accompanied hydrogen absorption and its evolution at the conclusion of the experiment. The relative resistance at room temperature was 1.763 which indicates a composition of $TaH_{0.174}$, assuming the relative resistance vs, composition dependence to be that at 76° (see next section).

Transport was effected at 72 ± 4° by a current of one ampere. The current was reversed after the passage of 43-1/2, 85-1/2, and 130-1/2 amp.-hr.

(b) Resistance vs. Composition at 76°. A number of attempts were made to determine the R vs. C dependence for Ta-H at concentrations up to saturation at one atmosphere hydrogen pressure, using sample assembly I and hydrogenation train II (Figure 10). It was intended to use the resulting hydride for transport experiments under better controlled conditions than those for $TaH_{0.16}$. However, gross buckling of the hard, brittle, and fragile hydride caused parting of the contact welds or breaking of the ribbon before attainment

of the maximum concentration. These failures may have been due in part to stresses produced during hydrogenation, and in part to thermal shock incident to the internal heating and subsequent cooling of the ribbon.

Three series of measurements were made at 76° on two 100 mm Ta ribbons. Series A was terminated at the composition $TaH_{0.276}$ when sample ribbon A broke. In series B-1, ribbon B was hydrogenated to the composition $TaH_{0.084}$ when a condensate was observed in the cold trap. The ribbon was degassed at about 900° overnight, and another series of measurements (B-2) was made during hydrogenation up to $TaH_{0.0435}$, when the ribbon broke.

(c) Measurements at 99°. (i) Resistance vs. Composition. In order to avoid the difficulties previously encountered in the hydrogenation of Ta, sample assembly I was replaced by assembly II (Figure 6). An oil manometer was added to hydrogenation train II.

Four days were required to determine the R vs. C dependence over the range of equilibrium pressures up to 730 mm , corresponding to compositions up to $TaH_{0.209}$.

(ii) Transport in $TaH_{0.209}$ at 99°. A current of one ampere was passed through the sample of $TaH_{0.209}$ for 23.6 hours in one direction and then for 36.4 hours in the opposite direction. Erratic results were obtained, probably because of appreciable internal heating and its effect on the decomposition equilibrium. Satisfactory results were

obtained when one-half ampere was applied for a total of 148.5 amp.-hr., the current being reversed after 44.3 and 72.6 amp.-hr.

In order to demonstrate that the changes in resistance observed during the passage of direct current were due to transport, an alternating current of one-half ampere was passed for 46 hours, resistance measurements being made periodically.

(d) Resistance vs. Composition at 100° and 400°. Two series of measurements were carried out on the same specimen of Ta ribbon, using sample assembly III (Figure 7), hydrogenation train III (Figure 11), and "extra pure" hydrogen. Prior to starting series 1, the ribbon was degassed under high vacuum at 400° for one day. The most expeditious absorption of hydrogen in the metal involves a compromise between the rate of absorption, which is favored by heating, and the occlusive capacity, which decreases with increasing temperature. Therefore, the internal heating, required to initiate absorption after the addition of each hydrogen increment, was continued until the rate of absorption approached zero, and was then gradually reduced. Even with this procedure, the rate of absorption was only about one ml per day.

When absorption became very slow at 400°, the resistance was measured. The furnace temperature was then lowered to 100° and the resistance again measured. After the introduction of a new increment of hydrogen, the furnace temperature was readjusted to 400° and the process repeated. A leak in

the system halted this series at the composition $TaH_{0.112}$.

In order to extend this investigation, the absorbed hydrogen was expelled by heating to about 1100° under high vacuum overnight. Then series 2 of resistance measurements was made at 395° and 100° as hydrogen was reabsorbed. Internal heating of the ribbon was necessary only to initiate absorption at the start of this series. The series was terminated at the composition $TaH_{0.173}$ when, upon further addition of hydrogen, the sample ribbon disintegrated into pieces no longer than one-quarter inch.

2. Results. (a) Resistance vs. Composition. The relative resistance of hydrogenated tantalum at 76° and 99° is plotted against composition in Figure 15. The 76° curve has a positive slope and is nearly linear above $TaH_{0.10}$. The curve for 99° is parallel to the other up to the composition $TaH_{0.15}$. However, a marked resistance increase between points 11 and 12, corresponding to the compositions $TaH_{0.15}$ to $TaH_{0.19}$, occurred as hydrogen was being absorbed during the second overnight interval of 11-1/2 hours. No such increase was observed for the first and third overnight intervals between points 6 and 7 and between 13 and 14. When at 12 the ribbon was heated to initiate the absorption of a new increment of hydrogen, gas was evolved, so that point 13 was measured at a lower concentration. More hydrogen was subsequently absorbed.

These reversals of concentration change and the accompanying resistance behavior correspond to a hysteresis loop

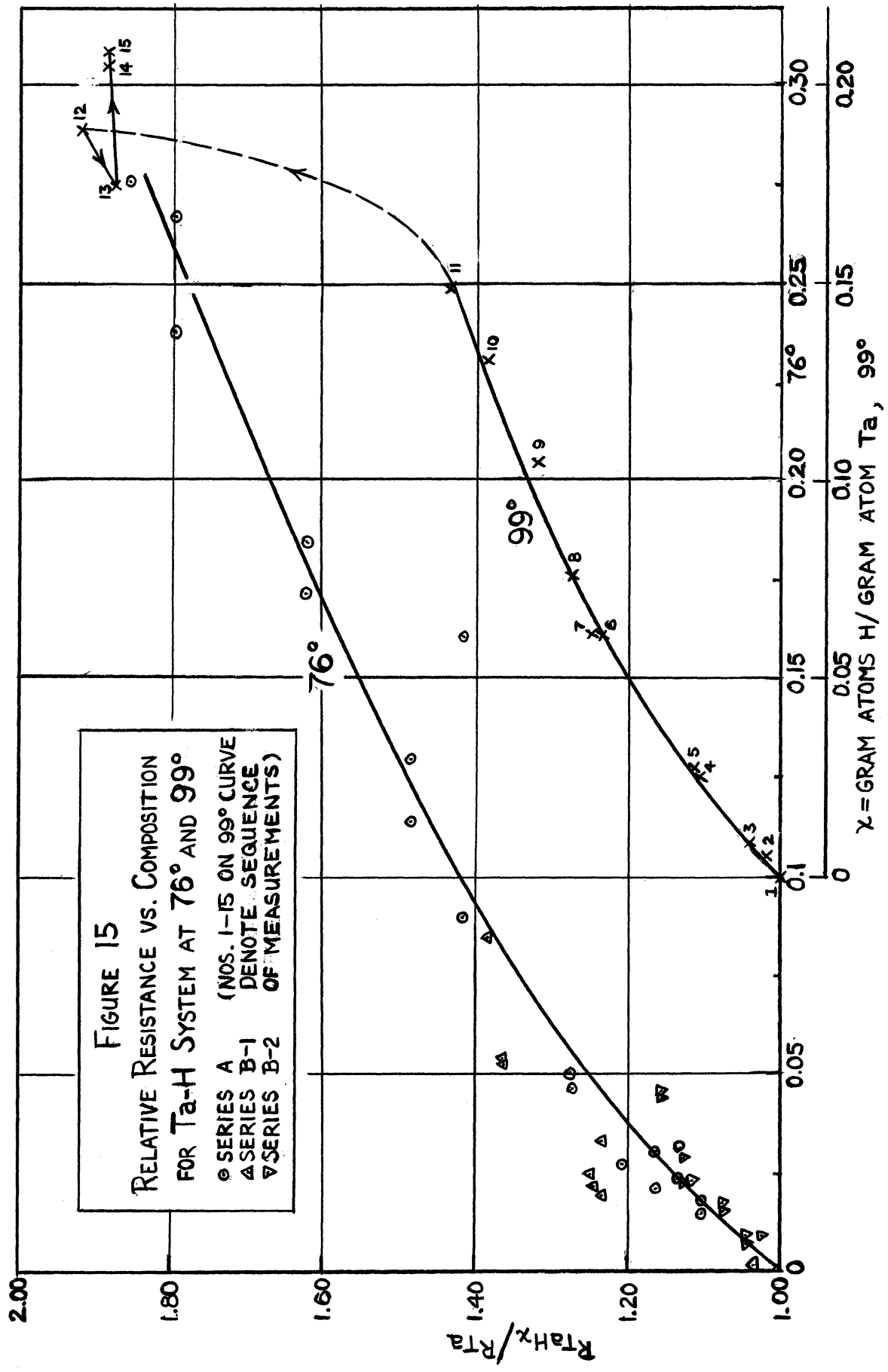
FIGURE 15
RELATIVE RESISTANCE VS. COMPOSITION FOR Ta-H SYSTEM AT 76° AND 99°
○ SERIES A (NOS. 1-15 ON 99° CURVE
△ SERIES B-1 DENOTE SEQUENCE
▽ SERIES B-2 OF MEASUREMENTS)
76°
99°
R_{TaH_x}/R_{Ta}
χ = GRAM ATOMS H/GRAM ATOM Ta, 99°
2.00
1.80
1.60
1.40
1.20
1.00
0
0.05
0.1
0.15
0.20
0.25
0.30
0.10
0.15
0.20
0.25
0.30
76°
99°

such as observed for palladium hydride (see Figure 3). The slope for decreasing hydrogen concentration (12 $\longrightarrow$ 13) is about 25% larger than that observed in the region $TaH_{0.05}$-$TaH_{0.15}$, while that observed during increasing concentration (13 $\longrightarrow$ 15) is 10% of the latter slope. As hysteresis diminishes, the slopes can be expected to approach an intermediate positive value. The R vs. C dependence at 76° shows positive slope even beyond this concentration range, as do the results of Sieverts and Brüning at 400° and 500°.

Since the transport study at $TaH_{0.209}$ was carried out in the region of the hysteresis loop in the R vs. C dependence, additional R vs. C measurements were made at 100° and 400°. Unfortunately, the ribbon broke before the composition $TaH_{0.209}$ had been attained.

Figure 16a shows the absolute resistance vs. composition dependence for series 1 at 400° and series 2 at 395° (see section II, C, 1, d). The curve for series 1 has initially a large positive slope and then, following an 18-1/2 hr. interval between readings, shows a discontinuity at $TaH_{0.032}$, where the resistance jumps from about 0.83 to 0.90 ohm. The errors in the resistance and composition measurements are negligible compared with the magnitude of the jump. No discontinuities were observed during subsequent 17-1/2 hour or longer intervals between measurements, and the curve continues with a constant slope which is about one-quarter of the initial one. The curve for series 2 is approximately

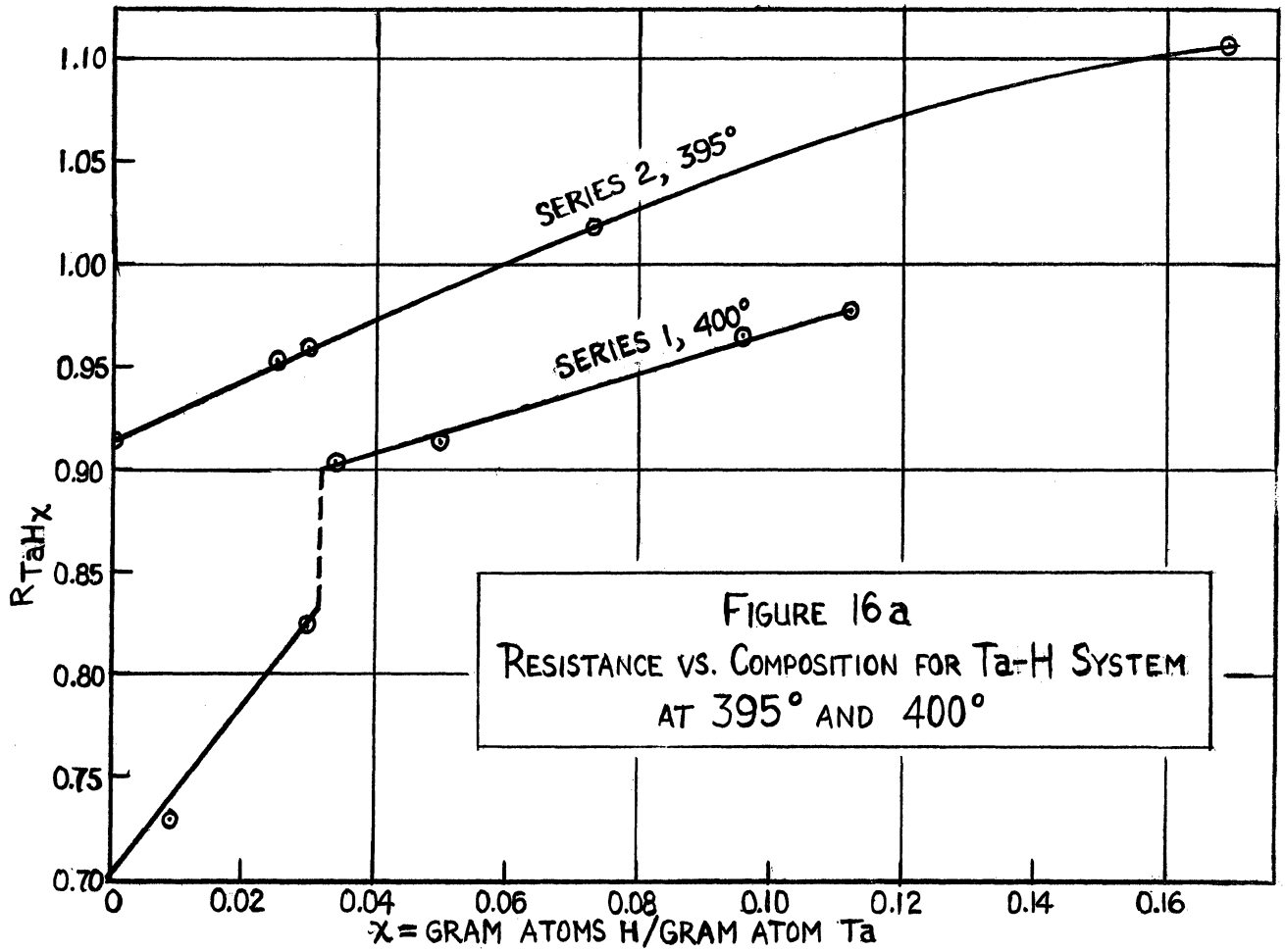

FIGURE 16a
RESISTANCE VS. COMPOSITION FOR Ta-H SYSTEM AT 395° AND 400°

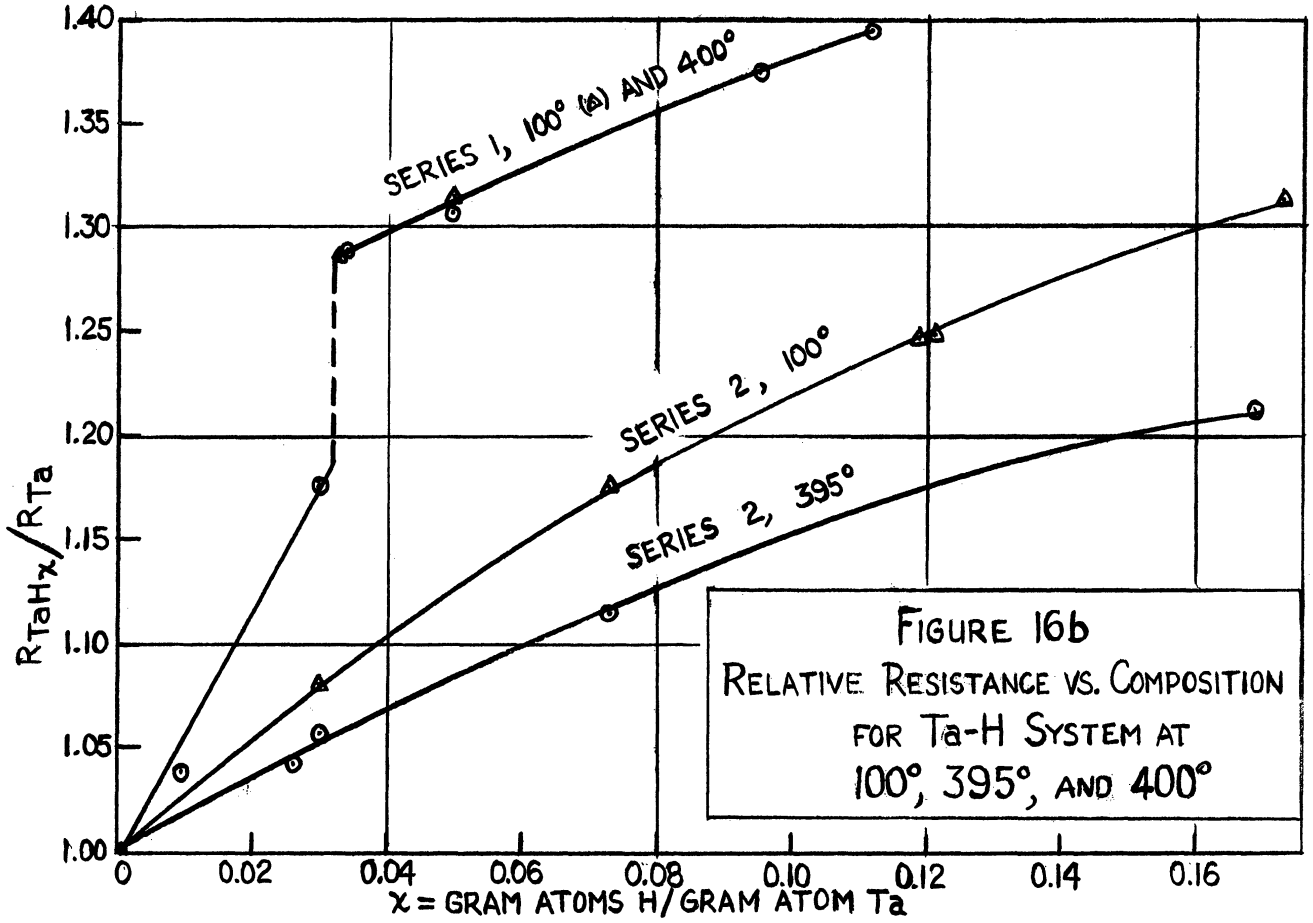

FIGURE 16b
RELATIVE RESISTANCE VS. COMPOSITION FOR Ta-H SYSTEM AT 100°, 395°, AND 400°

parallel to the leg of the other curve beyond the discontinuity. The differences in behavior between series 1 and 2 must be due in some way to the history of the tantalum specimen. Three possibilities are as follows.

First, since the original ribbon was not heated to glowing prior to absorption, it might be supposed that it was not annealed. However, it was heated to about 900° under high vacuum during the welding process, and was maintained at 400° for one day prior to beginning measurements. The Ta is also believed to have been stress-free at the start of the second series, since it was previously heated to about 1100° for twelve hours to evolve the hydrogen.

Second, it was found that after expulsion of the hydrogen at the end of series 1, the resistance at 400° was about 0.2 ohm larger than the original value of 0.7 ohm. This might suggest that the hydrogen had not been completely removed and that, according to the results of series 1, the composition of the ribbon at the beginning of series 2 was $TaH_{0.05}$. However, at the temperature of degassing, the solubility of hydrogen in tantalum at even one atmosphere pressure corresponds to the composition $TaH_{0.02}$. Therefore, the hydrogen concentration remaining in the sample was probably still smaller by a few orders of magnitude.

Finally, it is possible that some non-reversible change took place in the Ta ribbon. If the expansion accompanying hydrogenation causes the formation of rifts, then when hydrogen is withdrawn at low temperatures, they can be expected to

widen, due to the resulting contraction. The rifts reduce the effective cross-section of the sample, increasing its resistance. Since Ta is a highly refractory metal, it is possible that 1100° is not sufficient to heal the rifts. The data collected in Table II from other Ta-H experiments show that in every case the resistance of a degassed sample of previously hydrogenated Ta was higher than the original resistance.

Table II

Effect of Previous Hydrogenation on Resistance of Ta Metal

Sample*	Original Resistance	H/Ta before Degassing	Change in Resistance (ohms)	Temp., °C.	Remarks
P	0.1248	0.16	+0.0173	24	Ribbon may not have been completely degassed
Q	0.3748	0.08	+0.0774	76	Degassed at ca. 900° overnight
R	0.5971	0.005	+0.0150	99	Degassed at ca. 800° overnight
	"	"	+0.0330	"	Degassed at ca. 1100° for two more minutes
S	0.4925	0.112	+0.1483	100	Degassed at ca. 1100° overnight

*Samples P, Q, R and S were those used for experiments described in section II, C, 1, subsections a, b (ribbon B), c, and d respectively.

Rift formation could also be responsible for the discontinuity in Figure 16a (series 1) and the sharp rise in Figure 15. The rate of rift formation is expected to increase with temperature and hydrogen concentration gradient in the sample. In fact, in series 1 measured at 400°, the discontinuity at H/Ta = 0.03 occurred after an interruption of 18-1/2 hours, the three previous points having been obtained within six hours after the beginning of absorption. However, the discontinuity observed at 99° occurred at higher concentration (H/Ta = 0.25) and after several previous long interruptions between hydrogen additions. The absence of a resistance discontinuity in series 2 (Figure 16a) is also in agreement with the above hypothesis of rift formation since, once a network of rifts exists, this provides a means of relieving stresses produced during further hydrogenation.

The relative resistances at 100° and the higher temperatures for series 1 and 2, plotted in Figure 16b, show substantially the same behavior as the absolute resistances.

The results of the present measurements are in accord with those of Sieverts and Brüning[8]. The R vs. C dependence was found to have a positive slope over the range of temperatures and compositions studied with sufficient accuracy.

(b) Transport. During the preliminary transport experiment with $TaH_{0.16}$ at 72°, summarized in Figure 17, the total resistance (curve A) of the ribbon decreased from 0.4936 ohm to 0.4583 ohm in a complicated manner. The decrease indicates that stresses were being relieved and/or

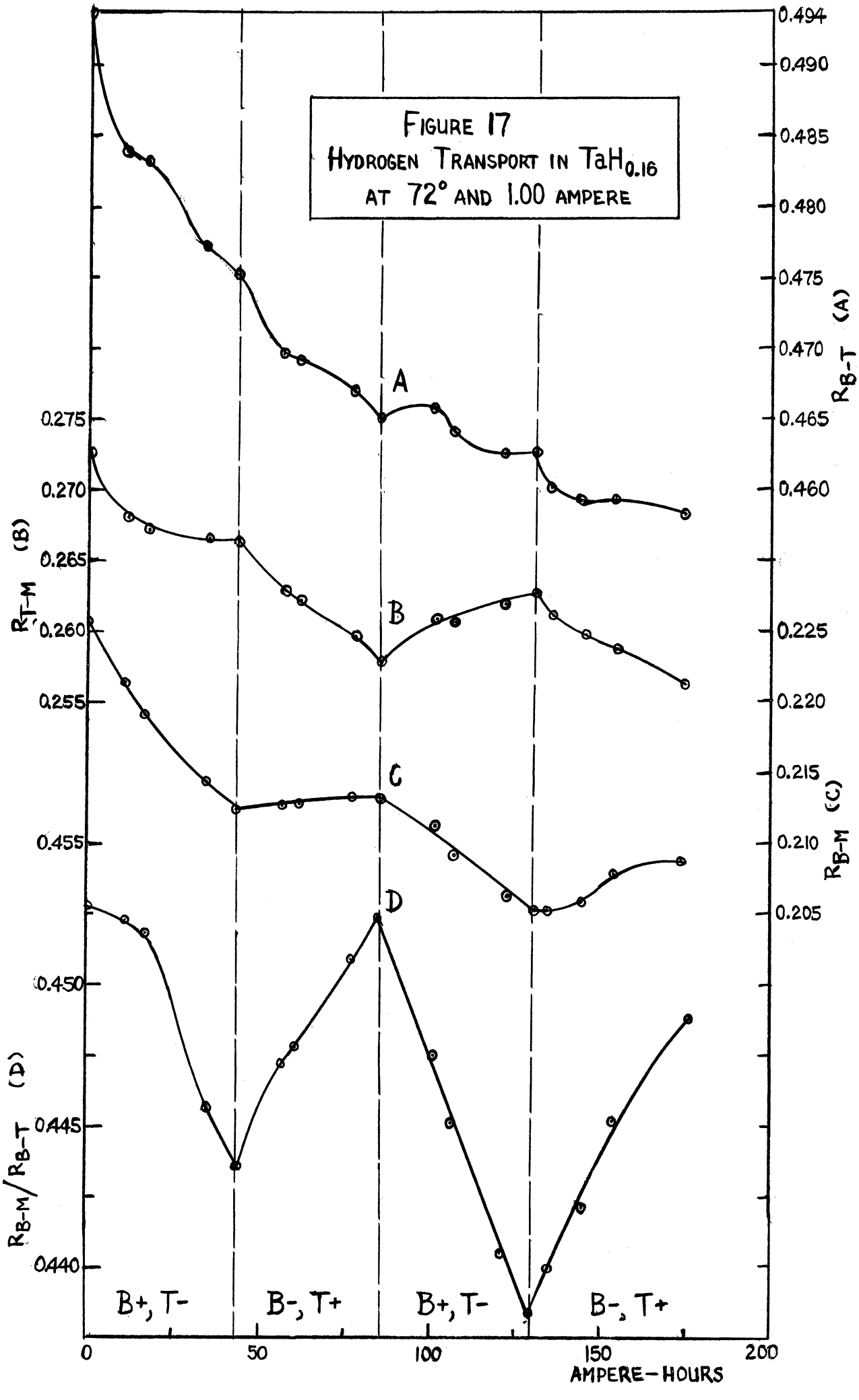
FIGURE 17
HYDROGEN TRANSPORT IN $TaH_{0.16}$
AT 72° AND 1.00 AMPERE
A
B
C
D
R_{T-M} (B)
R_{B-T} (A)
R_{B-M} (C)
R_{B-M}/R_{B-T} (D)
0.275
0.270
0.265
0.260
0.255
0.455
0.450
0.445
0.440
0.494
0.490
0.485
0.480
0.475
0.470
0.465
0.460
0.225
0.220
0.215
0.210
0.205
B+, T-
B-, T+
B+, T-
B-, T+
0
50
100
150
200
AMPERE-HOURS

that hysteresis was diminishing during the course of the transport. A new slope of short life-time appeared upon each current reversal and is characteristic of the polarization effect (section II, A, 2). However, curve B for the top and curve C for the bottom segments showed distinct discontinuities in slope upon current reversal, the sign of which persisted until the next current reversal. The slope always became more positive for either segment when it was made cathodic, and more negative when it was made anodic. Thus, the effect of the transport was to increase the resistance of the cathodic portion of the sample. This effect is shown especially clearly by the resistance ratio curve D.

The data for the transport in $TaH_{0.209}$ at 99° by a current of one ampere are shown in Figure 18. The slopes of the resistance ratio curve (D) are, for the same polarities, opposite in sign to those for $TaH_{0.16}$ in Figure 17, except in the interval between 50 and 60 amp.-hr. where the sign of the slope reverses without a change of the current direction. The trends of curves B and C also appear on the whole to be opposite to those observed previously, and show, as does curve A for the total resistance, unusually large variations, especially at 60 amp.-hr. where a more or less deep minimum appears in all four curves.

This irregular behavior is attributed, in part at least, to internal heating of the ribbon by the transport current. The temperature at any point will be greater, the smaller the

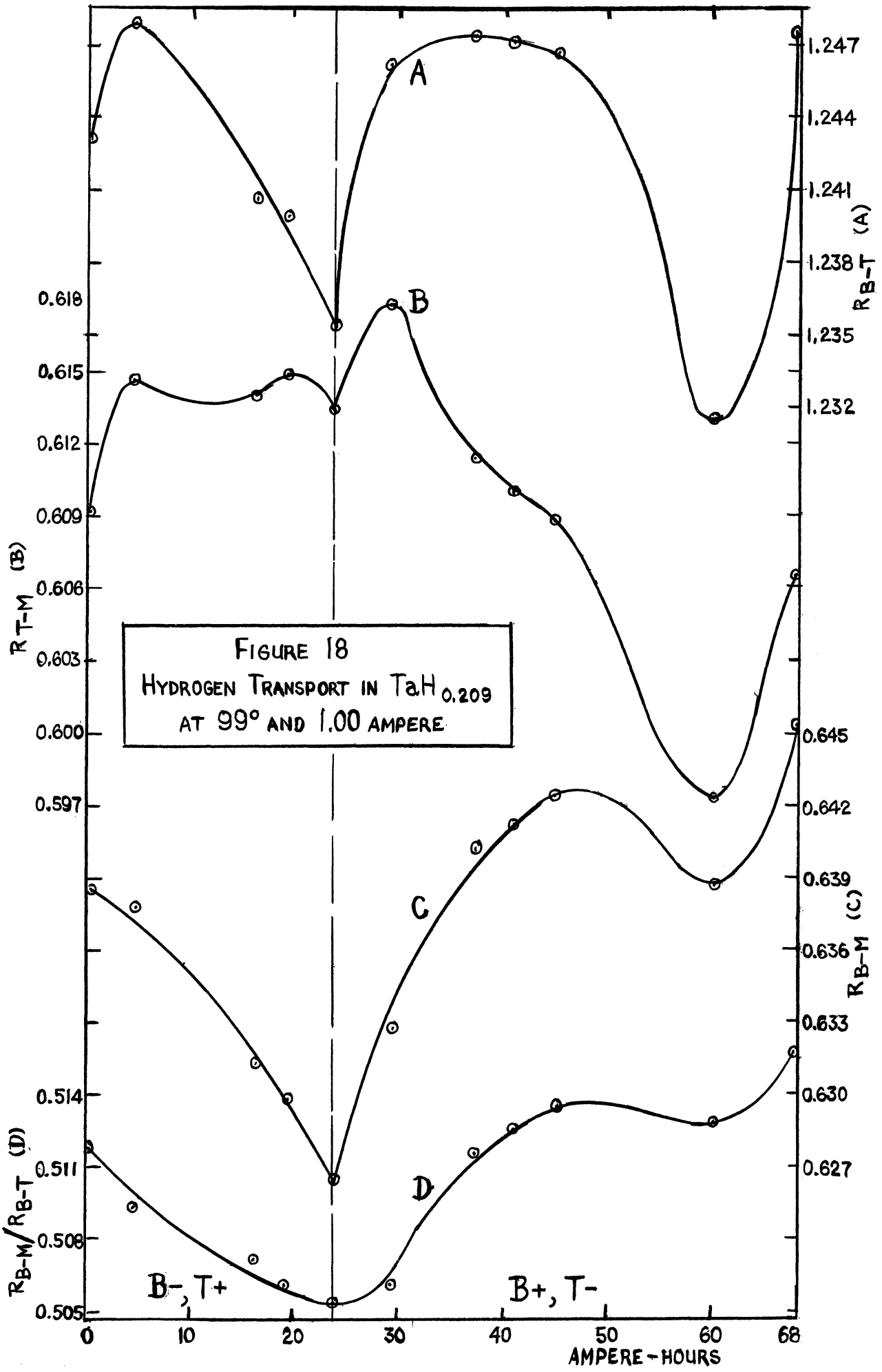

FIGURE 18
HYDROGEN TRANSPORT IN $TaH_{0.209}$
AT 99° AND 1.00 AMPERE

cross-section of the ribbon and the greater the hydrogen concentration at that point. Local temperature variations will produce redistribution of hydrogen since the dissociation equilibrium is temperature dependent. Therefore, no conclusion regarding the direction of transport can be drawn from these results and they are included here to illustrate the complications which arose during this study.

When the transport current in $TaH_{0.209}$ was reduced to one-half ampere, the curves reproduced in Figure 19 showed a much more regular behavior. The total resistance (curve A) of the sample increased sharply each time the current was reversed, and then gradually decreased, as is characteristic of a polarization effect. However, the curves for the individual segments and especially the resistance ratio (curve D) clearly show the dependence of the change in sign of the slope upon the direction of the current. The cathodic segment increased in resistance in each case, while the anodic segment decreased. Since the R vs. C dependence has a positive slope under the conditions of the transport in $TaH_{0.16}$ and $TaH_{0.209}$, positively charged hydrogen was transported toward the cathode in each case.

The reliability of the resistance measurements at one-half ampere is confirmed also by the results obtained when alternating current was sent through the sample, as seen on the right side of Figure 19. The total resistance and that of each segment increased monotonously with time. However, the resistance ratio (curve D) remained constant within

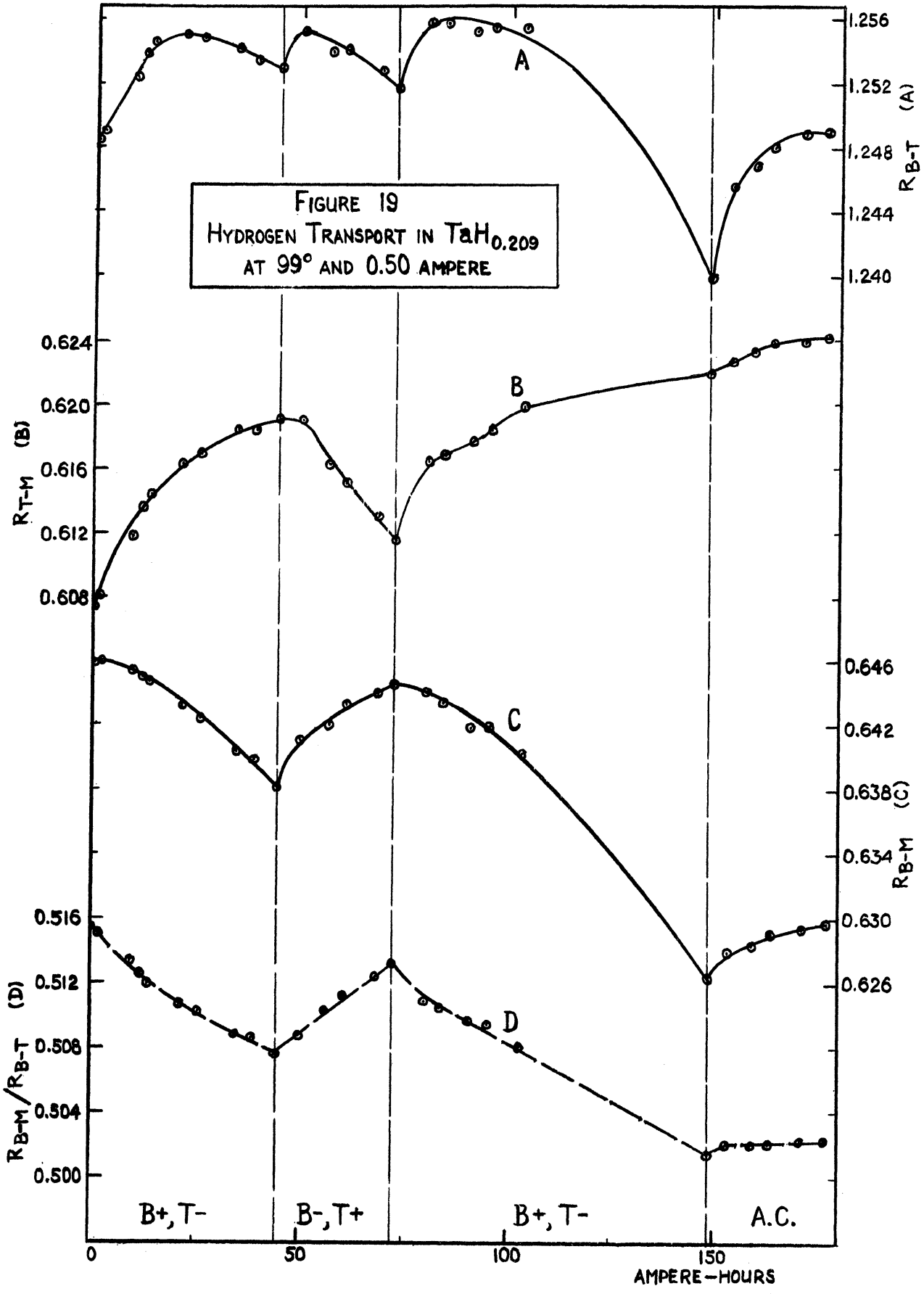

FIGURE 19
HYDROGEN TRANSPORT IN $TaH_{0.209}$
AT 99° AND 0.50 AMPERE

experimental error. Thus, there is no evidence of transport.

D. Titanium-Hydrogen System.

1. Procedure and Measurements. (a) Resistance vs. Composition at 99°. R vs. C measurements were made on two Ti ribbons at 99°, using sample assembly II and hydrogenation train II (Figures 6 and 10). Series A was terminated by the breaking of ribbon A at the composition $TiH_{0.955}$. Ribbon B was hydrogenated to $TiH_{0.438}$, degassed after a leak appeared in the system, rehydrogenated to $TiH_{0.207}$, degassed, and rehydrogenated to $TiH_{1.279}$, at which point the specimen broke. These three series will be referred to as B-1, B-2, and B-3 respectively. The absorption proceeded as a rule very slowly, apparently due to contamination of the Ti by impurities in the hydrogen or through leaks in the system. Because of these difficulties and those described in section II, A, 4, a, no transport measurements were made with this apparatus.

(b) Resistance vs. Composition at 400°. The R vs. C dependence was investigated on two Ti ribbons at 400°, using sample assembly III and hydrogenation train III (Figures 7 and 11). It was expected that the higher temperature would accelerate the attainment of the absorption equilibrium, and that the more uniform temperature distribution throughout the sample provided by external heating would make the composition more uniform.

The resistance of the one ribbon, C, was determined at

five compositions (series C-1) up to $TiH_{0.019}$, when a leak appeared in the hydrogenation train. After degassing the ribbon at about 800° under high vacuum and performimg a series of measurements (C-2) up to $TiH_{1.469}$, a leak occurred again and the ribbon broke. Up to the latter composition, absorption following the addition of each hydrogen increment was usually about 95% completed after only five minutes. After about one hour the manometer oil reached a constant level, indicating hydrogen dissociation pressures of zero up to $TiH_{0.55}$, and of less than 1 mm Hg up to $TiH_{1.5}$.

In series C-2, the resistance was time dependent over the range $TiH_{0.38}$-$TiH_{1.35}$. Resistance vs. pressure readings were taken during the first five minutes after each hydrogen addition and at least an hour later when absorption was actually completed.

The series D-1 was measured on another ribbon, D, up to the composition $TiH_{0.048}$, at which the transport was studied for about three weeks. Then the ribbon was heated to about 1050° under high vacuum for several hours to remove suspected contaminants. After cooling to room temperature, the resistance was found to be 4% higher than before hydrogenation; hence the ribbon was heated internally to about 1200° under high vacuum for ten minutes. After cooling, the resistance was 50% higher than originally. The appearance of a semi-transparent mirror on the wall of the sample tube indicated that some Ti had evaporated from the ribbon. Keeping the ribbon again at about 1200° for about five minutes resulted

in the evaporation of more Ti and in a further increase in resistance to a value 58% higher than the original one. After heating the sample assembly to 400°, the resistance of the ribbon was only 14.6% higher than originally at this temperature.

R vs. C observations (series D-2) were made as sample D was rehydrogenated to the composition $TiH_{0.54}$, at which a transport investigation was made.

At this stage, the ribbon was removed from the sample tube and weighed, and it was found that not more than 10% of the Ti had evaporated. Therefore, the probable explanation for the increase in the resistance of sample D upon degassing is that since this process was carried out at 1200°, considerably above the temperature (900°) of the $\alpha \longrightarrow \beta$ transformation from the hexagonal to the cubic close-packed forms, the subsequent resistance measurements at room temperature pertained to the sample mainly in the β modification. Heating to 400° would anneal the sample, so that in time it would recover its normal properties.

(c) Transport in $TiH_{0.048}$ and $TiH_{0.54}$ at 400°.

Transport was studied on ribbon D (see previous section) at compositions $TiH_{0.048}$ and $TiH_{0.54}$. The R vs. C curve at these two compositions has a positive and a negative slope respectively.

The investigation of $TiH_{0.048}$ followed immediately its formation. An alternating current of one ampere was passed

through the ribbon for fourteen hours to achieve steady conditions prior to starting transport. A direct current of one ampere was then passed for 23 days, the direction being reversed after the passage of 202, 342, and 507 amp.-hr.

Sample D was then degassed, rehydrogenated to the composition $TiH_{0.54}$, and left to itself for twelve hours to allow the ribbon to approach steady conditions. A direct current of one ampere was passed for 45 hours. The measured resistances were erratic, probably because of internal heating; Hence, the current was reduced to one-half ampere and reversed after the passage of 104, 172, and 231 amp.-hr.

2. Results. (a) Resistance vs. Composition at 99° and 400°. Although the data at 99° in Figure 20 scatter considerably, one can conclude that the relative resistance increases sharply with hydrogen content at low concentrations, reaches a maximum of about 1.21 at about $TiH_{0.60}$, and then decreases.

Similar results for the series C-1, C-2, and D-1 at 400° are shown in Figure 21 up to $TiH_{1.5}$ and, on a larger scale up to $TiH_{0.06}$, in Figure 21a. There is good agreement among the three series up to about $TiH_{0.048}$, although the resistance is very sensitive to composition. The curve for series C-2 exhibits a flat maximum in the composition range $TiH_{0.08}$-$TiH_{0.16}$, where the relative resistance is 1.134; then the relative resistance decreases with increasing hydrogen concentration to 0.878 at $TiH_{1.46}$, with an inflection at about $TiH_{0.55}$.

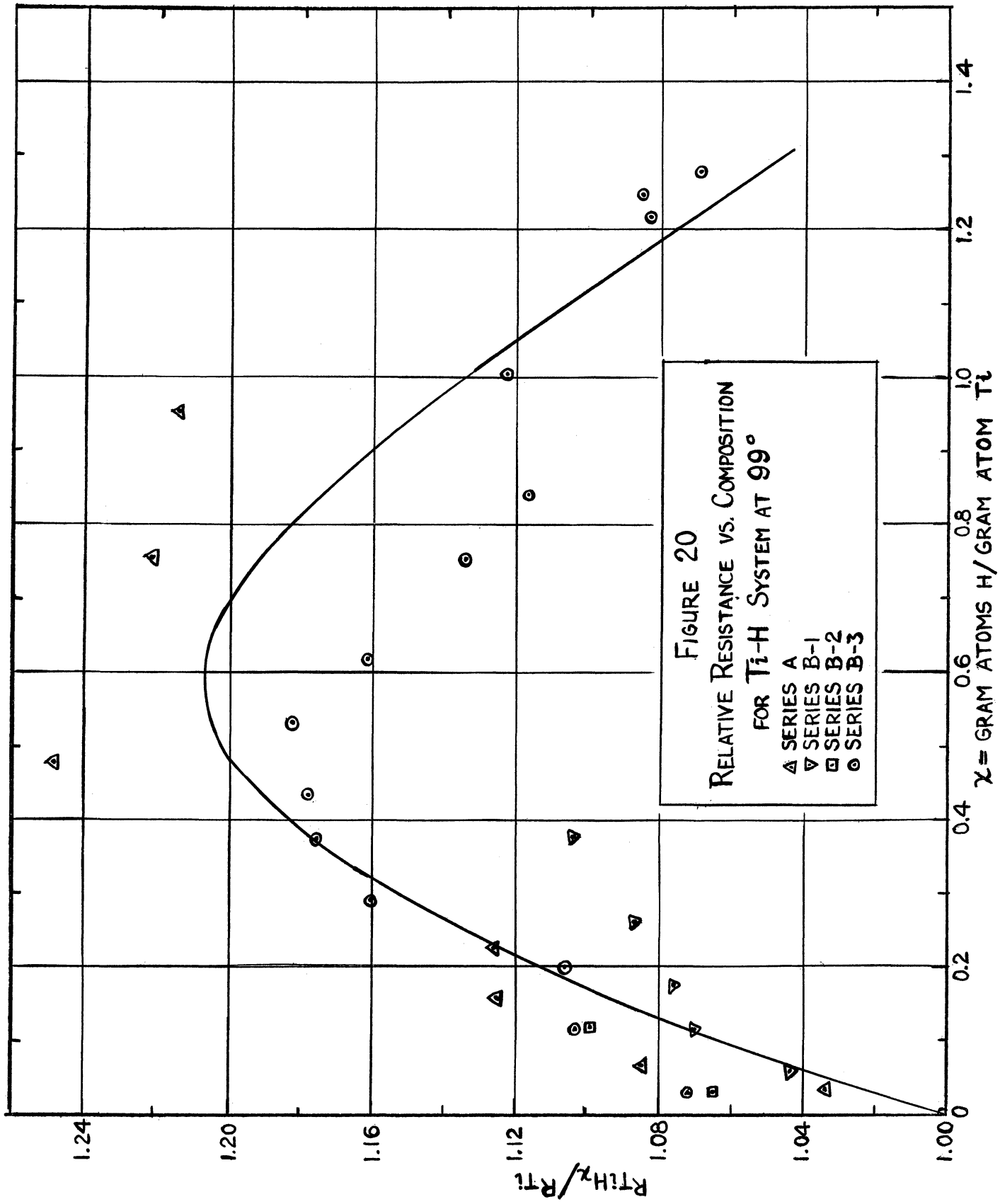
FIGURE 20
RELATIVE RESISTANCE VS. COMPOSITION
FOR Ti-H SYSTEM AT 99°
SERIES A
SERIES B-1
SERIES B-2
SERIES B-3
R_{TiH_x}/R_{Ti}
x = GRAM ATOMS H/GRAM ATOM Ti
1.00
1.04
1.08
1.12
1.16
1.20
1.24
0
0.2
0.4
0.6
0.8
1.0
1.2
1.4

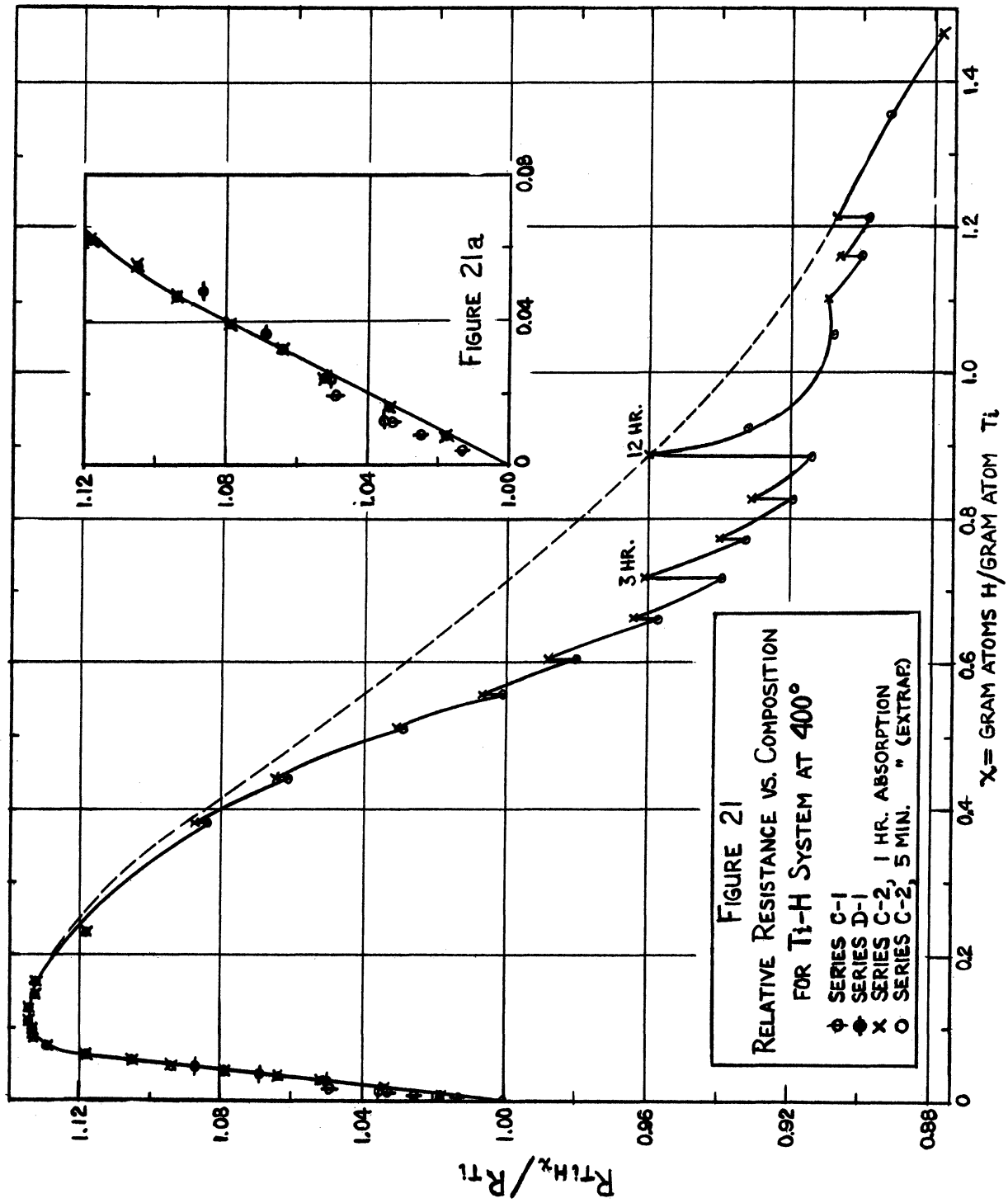
FIGURE 21
RELATIVE RESISTANCE VS. COMPOSITION
FOR Ti-H SYSTEM AT 400°
SERIES C-1
SERIES D-1
SERIES C-2, 1 HR. ABSORPTION
SERIES C-2, 5 MIN. " (EXTRAP.)
12 HR.
3 HR.
FIGURE 21a
R_{TiH_x}/R_{Ti}
X= GRAM ATOMS H/GRAM ATOM Ti

The time dependence of the resistance (series C-2) in the composition range $TiH_{0.38}$-$TiH_{1.35}$ is shown by the difference between the values (o) extrapolated to zero pressure, i.e., corresponding to complete absorption after about five minutes, and the resistance (×) measured about an hour later when absorption was actually complete (see section II, D, 1, b), the latter value always being higher. At each composition both resistances are given in Figure 21, and the drawn curve connects the timewise successive points. For compositions up to $TiH_{0.6}$, the differences between the two sets of values amounted to about 0.005 ohm, i.e., about 2% of the total resistance change (0.976-0.765 ohm) in series C-2. At compositions between $TiH_{0.6}$ and $TiH_{1.25}$, the differences were on the average 0.01 ohm. At the composition $TiH_{0.88}$, the extrapolated resistance was 0.040 ohm less than the resistance measured after twelve hours.

The time dependence of the resistance indicates that the redistribution of hydrogen and/or the attainment of the equilibrium state for some other process, e.g., rift formation (see section II, A, 1, b), which may follow the rapid absorption of hydrogen, occur slowly. Therefore, the values measured about an hour after absorption should be considered as the lower limit of the equilibrium resistance. The dashed line in Figure 21 represents the estimated "equilibrium" curve, obtained by interpolating between the time independent portions of the curve from the maximum to the region below $TiH_{1.21}$, through the point at $TiH_{0.88}$ which was presumably measured

near equilibrium (see above).

The R vs. C dependence observed in series D-2 is shown in Figure 22. Absolute rather than relative resistances are plotted, because of the uncertainty regarding the state of the metal at the start of the series*. The values given for the compositions are based on the weight of the metal before the loss by evaporation, and may be up to 10% low. The curve for series D-2 is similar to that for series C-2 (Figure 21) obtained at 400° and to that obtained at 99° (Figure 20). The resistance at the maximum is larger than the initial one by 9.5% for series D-2, but by 13.4% for series C-2. The difference may be due to the metal resistance being measured with the sample not at equilibrium. If the resistance for H/Ti = 0 for D-2 is adjusted so that the relative resistance at the maximum is 1.134 for both series, then the two curves coincide closely over the whole range of compositions. Comparison of the original resistance, 1.098 ohms, of the metal ribbon with this adjusted value indicates that 8.5% of the metal evaporated during the degassing process which preceeded series D-2. This result is in accordance with the upper limit of 10% determined by weighing.

(b) Transport at 400°. (i) $TiH_{0.048}$. The zero of the abscissa in Figure 23 corresponds to the previous passage of 85 amp.-hrs., since up to that time the variation of the total resistance of the sample was large in comparison with the variation of differences between the two ribbon segments.

---

*See Section II, D, 1,b.

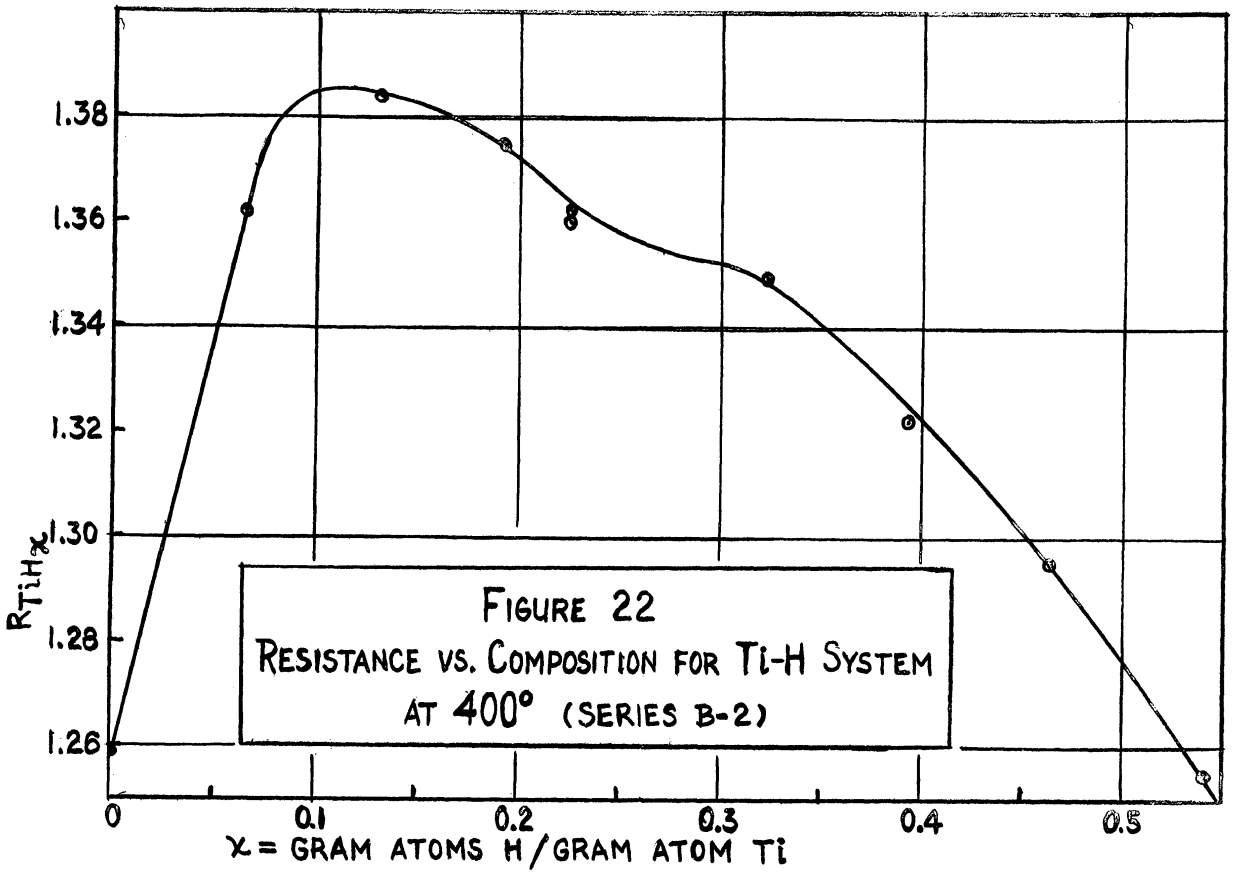

FIGURE 22
RESISTANCE VS. COMPOSITION FOR Ti-H SYSTEM AT 400° (SERIES B-2)

Except for the small scattering probably due mainly to hange in the condition of the ribbon caused by temperature fluctuations between resistance measurements, the total resistance (curve A) decreased monotonously with time, independently of the current direction, toward a constant value. This indicates that stresses and/or hysteresis were being overcome during transport, and that little polarization occurred (see section II, A, 2). The resistances of the individual segments (curves B and C) increased or decreased while they were cathodic or anodic respectively. The smoothness of the resistance ratio (curve D) shows that the scattering in curve A is due mainly to processes (e.g. thermal fluctuations) occurring uniformly throughout the ribbon. Since the R vs. C curve has a positive slope at the composition $TiH_{0.048}$, the results demonstrate that hydrogen was transported toward the cathode

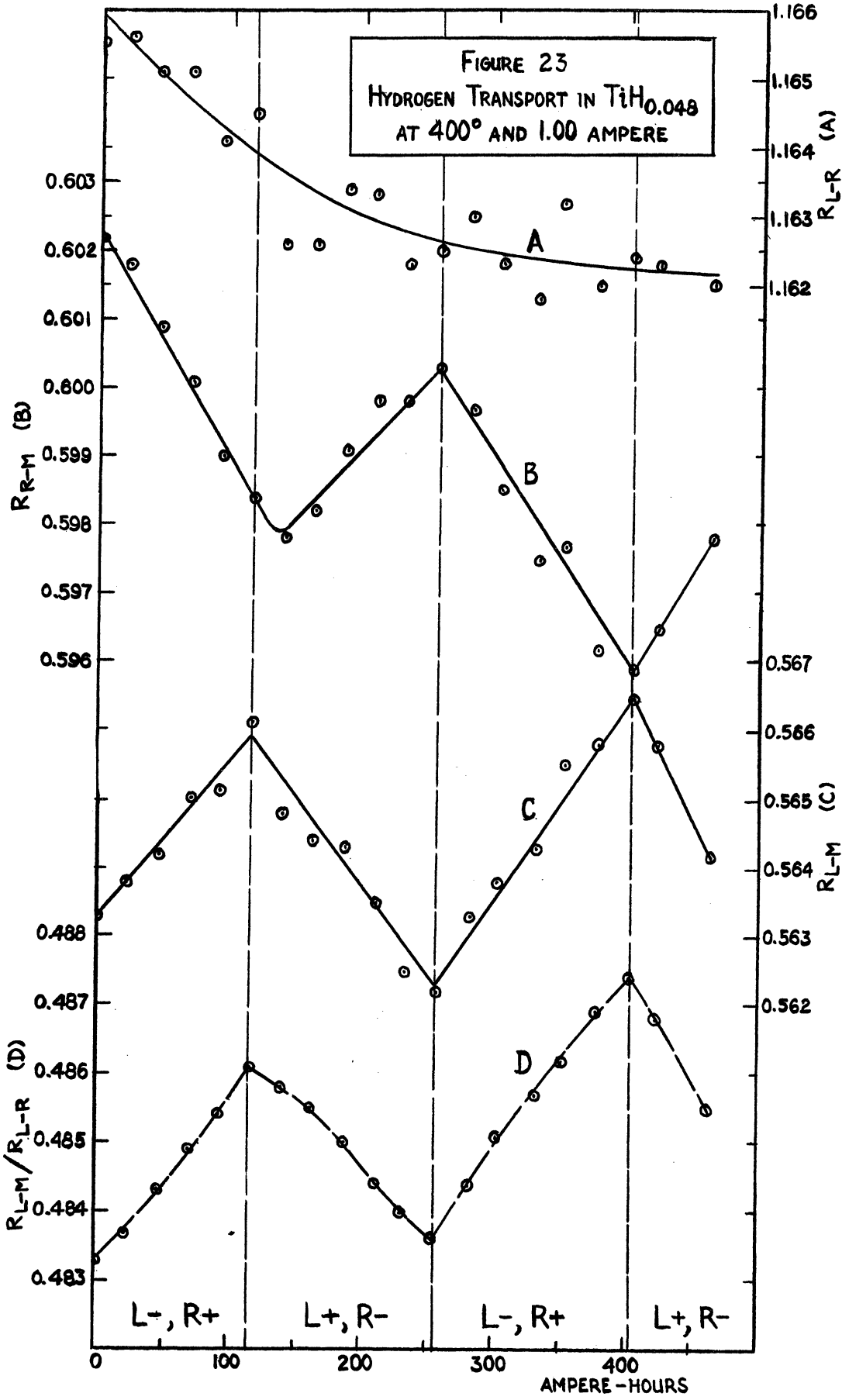
FIGURE 23
HYDROGEN TRANSPORT IN $TiH_{0.048}$
AT 400° AND 1.00 AMPERE
A
B
C
D
R_{L-R} (A)
R_{R-M} (B)
R_{L-M} (C)
R_{L-M}/R_{L-R} (D)
1.166
1.165
1.164
1.163
1.162
0.603
0.602
0.601
0.600
0.599
0.598
0.597
0.596
0.567
0.566
0.565
0.564
0.563
0.562
0.488
0.487
0.486
0.485
0.484
0.483
L-, R+
L+, R-
L-, R+
L+, R-
0
100
200
300
400
AMPERE-HOURS

and was therefore positively charged.

(ii) $TiH_{0.54}$. According to the data plotted in Figure 24, the total resistance (curve A) increased sharply for about fifteen amp.hrs. following each reversal, but not at the start, of the current, and then decreased until the next current reversal. This behavior was analogous to that observed in the Ta-H system at $TaH_{0.209}$ (section II, C, 2, b), and is indicative of polarization effects.

The resistance vs. amp.-hr. curves (B and C) for the individual segments, and even that (D) for the resistance ratio, show rather complicated behavior.

It is obvious that several factors were operating during transport. However, if one considers only the total change of resistance between two consecutive changes of the current direction, as shown by the dotted lines in Figure 24, the net result was that the resistance diminished in the cathodic segment and increased in the anodic one. Since the R vs. C curve has a negative slope at the composition involved, the result shows that hydrogen was again transported toward the cathode and was positively charged.

E. Secondary Results.

1. Transport Number and Mobility of Hydrogen. In Table III are given the transport numbers and mobilities calculated from the slopes of the transport and the R vs. C curves for the various systems as well as the measured weight, length, and resistance of each sample ribbon (see sections II, A, 6,

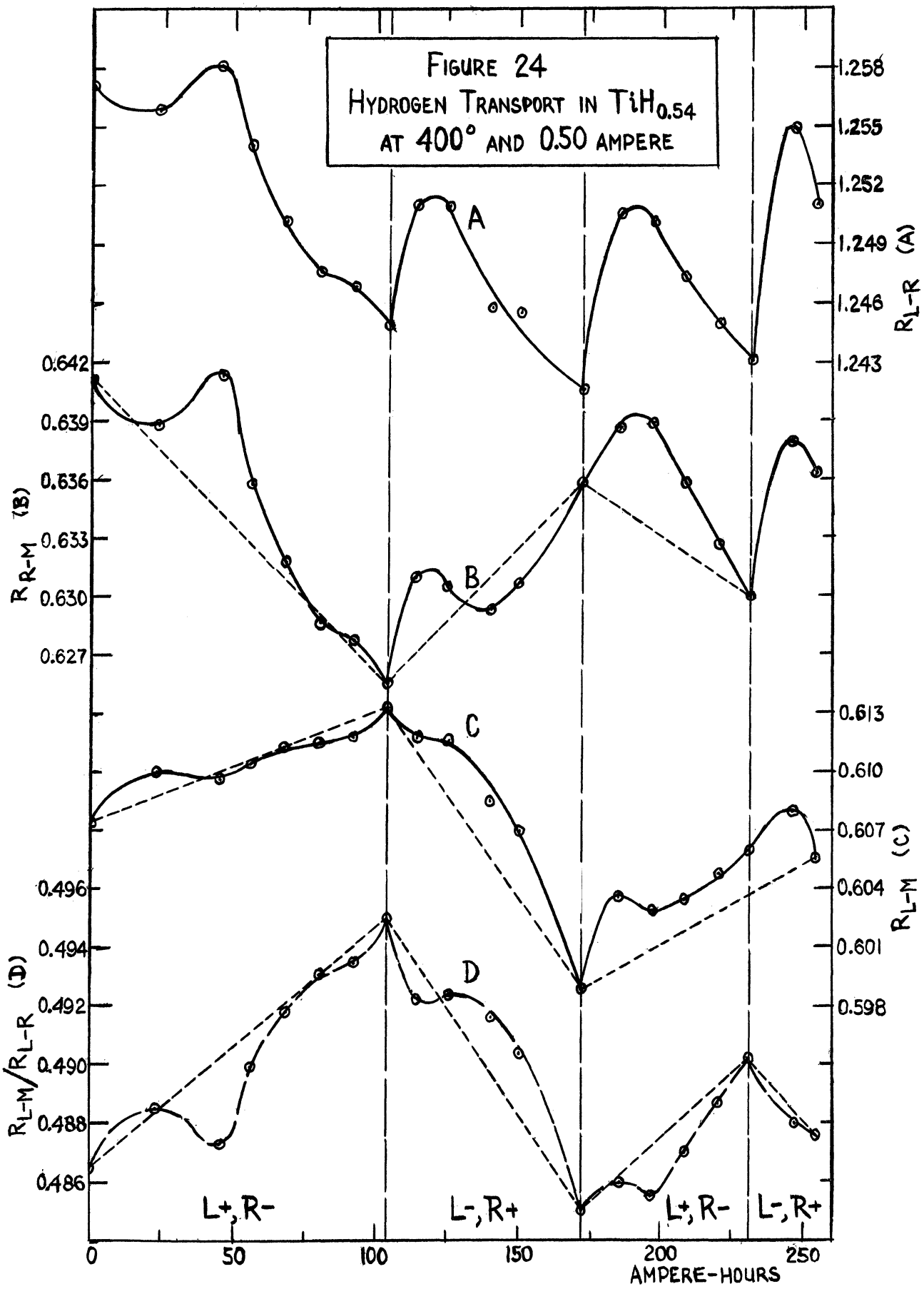
FIGURE 24
HYDROGEN TRANSPORT IN $TiH_{0.54}$
AT 400° AND 0.50 AMPERE
A
B
C
D
R_{L-R} (A)
R_{R-M} (B)
R_{L-M} (C)
R_{L-M}/R_{L-R} (D)
1.258
1.255
1.252
1.249
1.246
1.243
0.642
0.639
0.636
0.633
0.630
0.627
0.613
0.610
0.607
0.604
0.601
0.598
0.496
0.494
0.492
0.490
0.488
0.486
L+, R-
L-, R+
L+, R-
L-, R+
0
50
100
150
200
250
AMPERE-HOURS

Table III

Transport Number and Mobility of H^+ in the Pd-H, Ta-H, and Ti-H Systems

Composition	Temp. °C.	Transport No. $t \times 10^6$	Mobility (cm^2/sec volt) $m \times 10^5$	Investigator
$PdH_?$	20	-	0.76	Coehn (10)
"	33	-	1.04	"
"	49	-	1.96	"
"	60	-	2.41	"
"	72	-	2.73	"
$PdH_{0.46}$	72±4	3.5 ± 1.4	4 ± 2	Present
$PdH_{0.027}$	182	1.19	14.6	Wagner & Heller (16)
$PdH_{0.020}$	240	0.79	28.0	"
$TaH_{0.16}$	72±4	2.6 ± 0.4	6 ± 1	Present
$TiH_{0.048}$	400	3.0 ± 0.4	5.3 ± 0.6	Present
$TiH_{0.54}$	400	70 ± 35	10 ± 5	"

c, i and ii).

In computing the result for $PdH_{0.46}$, for which transport was performed at 72°, the slope of the R vs. C dependence was taken as the average of that of the previously reported[6] curve for 18°, 0.85 (g.-at. H/g.-at. Pd)$^{-1}$ given in Figure 2, and those of the two linear branches of the 160° curve of Brüning and Sieverts (see reference 5, Figure 5), corresponding to increasing and decreasing hydrogen concentration (0.65 and

1.06 respectively). This 160° curve is similar to that at 180° (Figure 3), except that the linear branches at 160° extend well beyond $PdH_{0.46}$.

The slopes used in deriving the result for $TaH_{0.16}$ were obtained from Figures 15 and 17, while those for $TiH_{0.048}$ come from Figures 21a and 23. No calculations were made from the transport data for $TaH_{0.209}$ at 99°, because of the uncertainty in the R vs. C slope.

Since the resistance ratio vs. amp.-hr. curve (Figure 24) for $TiH_{0.54}$ is so complex, the slopes of the dotted lines have been used in calculating t and m. These slopes usually differed by no more than 30% from those directly observed after transport had proceeded for 25-50 amp.-hr. following the start of the experiment as well as each current reversal. Furthermore, since the R vs. C relation (Figure 21) was found to be time dependent in this composition region (see section II, D, 2, a), the slope at $TiH_{0.54}$ was taken to be that of the dashed "equilibrium" curve. As a result of these approximations, the calculated values of t and m may be in error by about ±50%.

The values of t x 10^6 and m (cm^2/sec volt) x 10^5 for $PdH_{0.46}$ at 72°, namely 3.5 ± 1.4 and 4 ± 2 respectively, are consistent with the more precise previous values which were obtained using entirely different techniques. Within experimental error, the mobility agrees with the value 2.73 found by Coehn at the same temperature in a hydride of unspecified composition. It also fits the law, $m = m_o e^{-\frac{E}{RT}}$

(m_o = 9.9 cm^2/sec volt, E = 4.6 kcal/mole, and R = gas constant), also obeyed by the previous results which range from 20° to 240°. Thus, the reverse order of t, namely 3.5 at 72° and 1.19 at 182° is only "apparent", since the latter was obtained by Wagner and Heller at a considerably lower hydrogen concentration. Assuming that the transport number of an ionic species is proportional to its concentration, one should compare t/x_H, where x_H is the atom ratio of hydrogen to metal. This quotient times 10^6 at 72°, 182°, and 240° respectively is 8.0, 42.5, and 35.0. The present smaller value at the lower temperature is to some extent influenced also by the higher mobility of the electrons.

The mobilities x 10^5 at 72° for $TaH_{0.16}$ (6 ± 1) and $PdH_{0.46}$ (4 ± 2) do not differ by more than the experimental error. In order to compare these values with the value 5.3 ± 0.6 for $TiH_{0.048}$, one must take into account that the latter applies to 400°, at which temperature the extrapolated mobility (see above) for the Pd-H system is about 80. Therefore, the mobility for Ti-H is considerably smaller than for the two other systems.

The transport numbers are of the same order of magnitude in all cases. The large apparent difference between the two titanium values is mainly due to the difference in concentration, as is shown by the t/x_H ratios, 62 ± 8 and 130 ± 65 for $TiH_{0.048}$ and $TiH_{0.54}$ respectively, which do not differ within experimental error.

The resistivities of the fresh metal ribbons, given in Table IV, were calculated from the resistance R, weight w, length L, and density d of each according to $\rho = Rw/L^2d$ ohm cm. This relation assumes a uniform ribbon cross-section, the lack of which probably accounts for the fact that the observed values are 21% and 14% larger than the reported values for Pd and Ta respectively. However, the reproducible observed value, 59 ± 2, of the resistivity of Ti metal is 18 times larger than the value 3 given in the International Critical Tables[43], but only 28% smaller than the value 82 reported by Clausing and Moubis[44].

Table IV

Resistivity of Pd, Ta, and Ti Metal

Reported $\rho^{20°}$ (ohm cm x 10^6)	10.8	15	3 (Int. Crit. Tables) $82^{0°}$ (Clausing & Moubis)
Observed $\rho^{28°}$ (ohm cm x 10^6)	13.3 ± 0.8	17.7 ± 0.8	59 ± 2

2. Temperature Coefficients of Resistivity. Although no systematic studies were made to determine the dependence of resistance upon temperature in the various metal-hydrogen systems, some incidental data were obtained. The temperature coefficients of resistance, α, defined here as $\alpha = \frac{1}{R_{25°}} \frac{\Delta R}{\Delta T}$, were calculated to see how the positive coefficient for the metal is influenced by occluded hydrogen.

The sample assembly design and experimental conditions

used in the transport and R vs. C studies were not favorable for accurate determinations of α, because of the heat conduction away from the ribbon through the heavy silver lead wires. Since the heat loss is the larger, the higher the temperature, the observed ΔT is too large, so that the calculated values of α are estimated to be up to 20% low. For a given series and temperature, however, the heat conductivity of the ribbon would not vary appreciably so that these heat loss effects were approximately constant for all compositions. Therefore, the values of α, relative to one another, are reproducible to about ±1%.

For the Ta-H system in Figure 25 the lack of agreement among the results of Sieverts and Brüning[8], Holborn[45] and the present ones, and even between ribbons 1 and 2 indicates that the history of the sample is more important than the composition. No conclusion can be drawn even regarding the sign of the effect due to occluded hydrogen.

For the fresh Ti ribbon the average value of $\alpha \times 10^3$ obtained from four samples is 3.09 ± 0.05, as compared with 4.20 reported by Clausing and Moubis[44] for material of still higher purity. The coefficient for previously hydrogenated metal (3.00-1.87) was found here to be smaller than that for the parent ribbon. Since the fresh ribbons were degassed prior to measurement, under conditions approximating those subsequently used to expel absorbed hydrogen, this decrease must have resulted from non-reversible changes produced by hydrogenation.

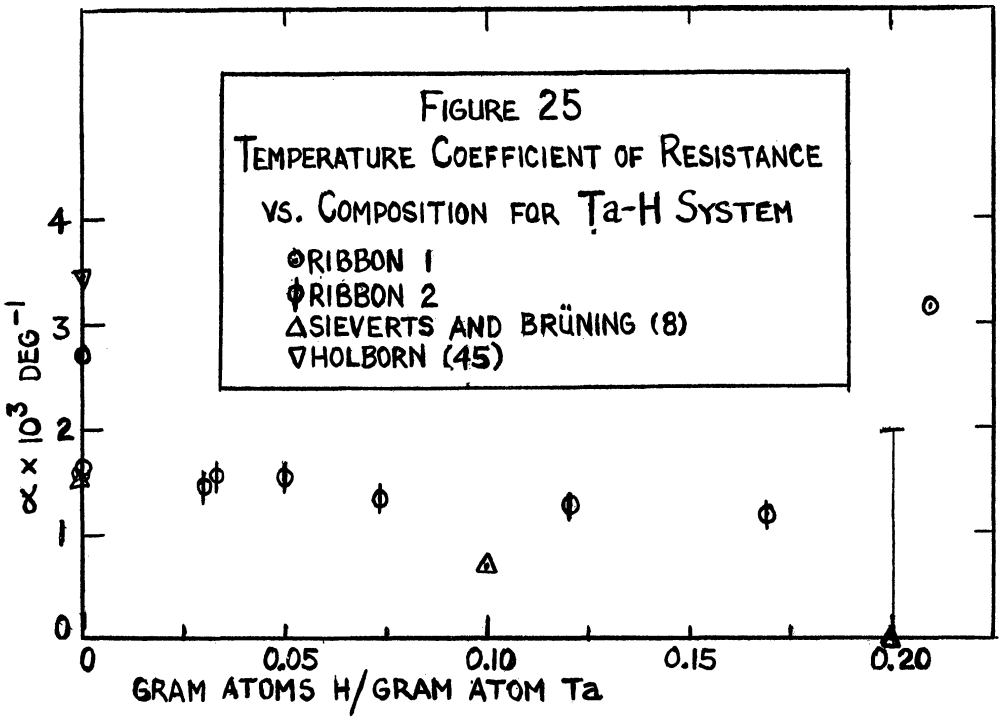
FIGURE 25
TEMPERATURE COEFFICIENT OF RESISTANCE
VS. COMPOSITION FOR Ta-H SYSTEM
⊙RIBBON 1
ϕRIBBON 2
ΔSIEVERTS AND BRÜNING (8)
▽HOLBORN (45)
α x 10³ DEG⁻¹
0
1
2
3
4
0
0.05
0.10
0.15
0.20
GRAM ATOMS H/GRAM ATOM Ta

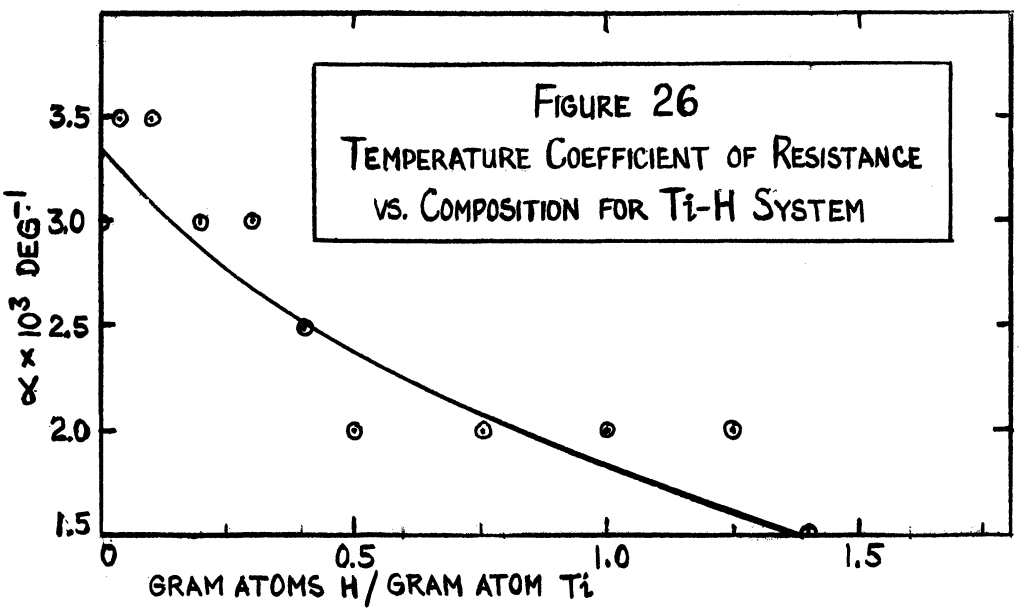
FIGURE 26
TEMPERATURE COEFFICIENT OF RESISTANCE
VS. COMPOSITION FOR Ti-H SYSTEM
α x 10³ DEG⁻¹
1.5
2.0
2.5
3.0
3.5
0
0.5
1.0
1.5
GRAM ATOMS H/GRAM ATOM Ti

For the Ti-H system the dependence of the temperature coefficient upon composition, given in Figure 26, was calculated from the data at 99° and 400° shown in Figures 20 and 21. The measurements at the two temperatures were not made on the same sample. The increase observed at low hydrogen concentrations may be due to experimental error, since the calculated coefficient is very sensitive to the position of the maximum in the R vs. C curve at 99° relative to that in the curve at 400°, and since the R vs. C results at 99° showed considerable scattering. However, the trend toward lower values of α at higher concentrations seems to be real.

III. Magnetic Susceptibilities for the Tantalum-Hydrogen and Titanium-Hydrogen Systems at 20°

A. Principles of the Method.

1. Definitions. A substance is termed diamagnetic or paramagnetic respectively, depending on whether it is repelled by or attracted into an inhomogenous magnetic field.

The orbits of electrons in any substance placed in a magnetic field, precess about the field direction with a frequency proportional to the field strength. This results in a magnetic moment which is aligned is opposition to the field of the magnet, thus reducing the magnetic flux density within the substance. While this diamagnetic component is a general property of matter, in a paramagnetic substance the field orders permanent moments along its direction, increasing the flux density in the material. This paramagnetic component usually overshadows the relatively small diamagnetic effect. In the absence of field, neither paramagnetic nor diamagnetic substances possess a net moment, which is present only in ferromagnetic materials.

In classical electromagnetic theory, the relation between the internal flux density B and the applied field H is given by

$$B = H + 4\pi J.$$

The magnetic dipole moment J induced in a unit volume is proportional to H, except for ferromagnetic materials, and one defines as the dimensionless volume susceptibility K:

$$K = J/H.$$

The various types of magnetic susceptibility can be characterized as follows:

Diamagnetic:	$B < H$	$K < 0$	$K \sim -10^{-6}$
Paramagnetic:	$B > H$	$K > 0$	$K \sim +10^{-3}$
Ferromagnetic:	$B \gg H$	$K \gg 0$	$K \sim +10^{2}$

Magnetic susceptibility is also expressed in terms of susceptibility per gram, χg, or per mole (or gram atom), χ_M.

2. Gouy Method. In this study the well-known Gouy method was used for the determination of magnetic susceptibility. In the magnetic balance schematically shown in Figure 27, the force exterted on the substance in an inhomogenous magnetic field is balance by weights. The substance is usually contained in the upper half of a cylindrical glass tube, the lower part of which is evacuated. The tube is suspended by a filament from one arm of the balance, and is so adjusted that the horizontal glass partition between the two halves of the tube is in the middle of the magnetic field. Because of the symmetrical position of the tube itself in the magnetic field, only a very small force is exerted on it, for which a correction will be applied in section III, B, 4,a.

The magnetic field is adjusted by measuring and controlling the current flowing through the coils of an electromagnet. The apparent change in weight of the substance due to the field is observed on the balance. For absolute determinations of susceptibility, the cross-section of the sample and the field intensities at the upper and lower ends of the

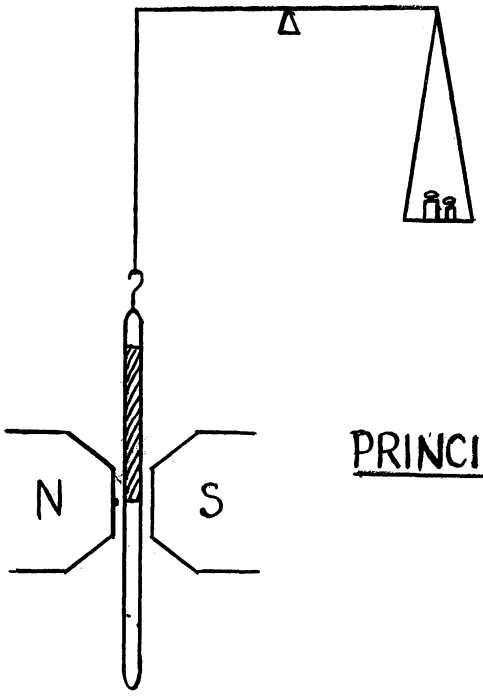

FIGURE 27
PRINCIPLE OF THE GOUY METHOD

sample must also be measured. More customary are relative measurements, in which the change of weight of a sample is compared with that of a standard of known susceptibility, measured under identical conditions.

3. Equations Related to the Gouy Method. The volume susceptibility of a homogenous substance can be calculated from its geometry, the spatial dependence of the field strength, and the force exerted on the substance, given here by the apparent change in weight.

Let the z-axis coincide with the suspension filament. Then the force, f_z, exerted in this direction on a magnetic dipole of moment μ, is

$$f_z = \mu \frac{\partial H}{\partial z} ,$$

and the force on the volume increment dV is

$$dF_z = JdV \cdot \frac{\partial H}{\partial z} = KH \cdot \frac{\partial H}{\partial z} \cdot dV = gdW ,$$

where g is the gravitational constant, and dW is the increment of apparent weight. Assuming K to be constant, the total force exerted on the sample of volume V which extends from z_1 to z_2 is

$$F_z = K \int_V H \cdot \frac{\partial H}{\partial z} \cdot dV = g\Delta W . \quad \text{Eq. (10)}$$

For absolute measurements, in general, the following assumptions are made:

(1) The sample has a uniform cross-section.

(2) The magnetic field is uniform over the cross-section A, so that

$$g\Delta W = KA \int_{z_1}^{z_2} H \frac{\partial H}{\partial z} \, dz$$

$$= KA \int_{H_1}^{H_2} H dH = \frac{KA}{2} (H_1^2 - H_2^2), \quad \text{Eq. (11)}$$

where $H_1 = H(z_1)$ and $H_2 = H(z_2)$. For measurements made in air, K is to be replaced by $(K - K_{air})$.

Relative measurements make assumptions (1) and (2) and measurement of cross-section and field intensities unnecessary. If the reference substance and the sample are measured under identical conditions, then using <u>e.g.</u>, water as reference,

$$\frac{\Delta W}{\Delta W_{H_2O}} = \frac{K - K_{air}}{K_{H_2O} - K_{air}} , \text{ or}$$

$$K = \frac{\Delta W}{\Delta W_{H_2O}} (K_{H_2O} - K_{air}) + K_{air} . \quad \text{Eq. (12)}$$

In the case of a non-uniformly packed powder, the calculated K is an average in which the susceptibility of each volume is weighted by the factor $H \frac{\partial H}{\partial z}$.

The molar susceptibility is given by $\chi_M = \frac{K \cdot M}{d}$. For a powder, d refers to its apparent density in the tube, including intergranular voids.

B. Experimental.

1. Materials. (a) Tantalum. Tantalum powder (finer than 400 mesh) obtained from the Fansteel Metallurgical Corporation, had a specified purity of > 99.9%. In order to remove any grease contamination, it was treated with reagent grade carbon tetrachloride for twelve hours in a Soxhlet extractor. Since the magnetic susceptibility of the powder showed a field dependence characteristic of ferromagnetic impurities, it was treated with boiling concentrated HCl for twelve hours. An α,α'-dipyridyl spot test[46] of the acid showed that 7 ± 2 ppm of iron was leached from the powder. After careful washing with distilled water and then with acetone, the powder was dried with filtered air. No HCl-soluble iron was found by the spot test (sensitivity, 0.5 ppm).

(b) Titanium. Titanium sponge was provided by the E. I. du Pont de Nemours Company, Inc. No analysis of this particular sample was available. However, a reported nominal analysis of the commercial product[42] is as follows: > 99.5% Ti; 0.05-0.25% Fe; 0.01-0.05% Mg; 0.05-0.10% Cl; 0.06-0.10% O; 0.01-0.05% C; 0.01-0.02% N; 0.006-0.009% H.

In order to comminute the 1/4-1/2" pieces of sponge, they were converted to the friable hydride. Approximately 6-g batches of metal were treated with "extra pure" hydrogen

(see section II, A, 3, b) in a Vycor tube at 500°. The resulting material was ground in a glass mortar until it passed through a carefully cleaned 350 mesh sieve. This powder was reconverted to metal by heating in a Vycor tube at 500° under high vacuum for four hours. The somewhat sintered material was removed from the tube and repulverized. A second degassing at temperatures increasing slowly up to about 500° was again followed by pulverizing.

During each degassing, a brown transparent film appeared on the surface of the reaction tube, and a silvery mirror formed above the hot zone of the tube. When air was admitted to the cooled tube, most of the mirror changed to a dull light gray material, the water solution of which felt slippery, had a pH>10, and gave a strong sodium flame test. Furthermore, the Vycor appeared to be attacked and became very fragile where it was in contact with the hydride.

The evidence indicates that sodium metal distilled onto the cool portions of the reaction tube. It seems unlikely that Ti, although it is a powerful reducing agent at high temperatures, could have reduced the small amount of Na_2O in the Vycor. It is more probably that sodium had become alloyed with the Ti sponge during the manufacturing process. The attack on the Vycor suggests that SiO_2 was reduced to Si.

Since α,α'-dipyridyl indicated the presence of iron, the Ti was leached for 24 hours with cold 5N HCl, filtered off, washed first with 5N HCl to prevent hydrolysis and then with

ethanol, and was finally dried at room temperature by a stream of air.

(c) Hydrogen. "Extra pure" hydrogen (section II, A, 3, b) was used in the hydrogenation of the metal powders.

2. Sample Tube. The magnetic susceptibility sample tube A, shown in Figure 28, was constructed of Vycor so that the metal could be hydrogenated at 400° in situ without distorting the glass. The 25 cm long tube, having outside and inside diameters of about 7 and 4 mm respectively, was partitioned 10 cm from the end, which after evacuation was sealed off. The other end was ground to conform to a standard 7/25 taper. A fiducial mark was etched around the tube 100.0 ± 0.2 mm from the partition, and five secondary marks were spaced at 1 mm intervals on either side of this mark.

The tube cap B consisted of a micro stopcock, to opposite arms of which were sealed a male and a female T 7/25 joint. The stopcock bore, initially 1 mm , was enlarged to 2 mm by grinding with carborundum. The core of the stopcock was carefully lapped into the shell using 600 mesh carborundum and kerosene. The stopcock could be connected through the upper joint to the hydrogenation and water purification trains, and permitted the sample tube to be removed from either system for magnetic measurements without exposing its contents to the atmosphere. The position of cap B was controlled by lining up reference marks on it and the tube.

The hook on the cap C pointed always at the stopcock handle, and served for suspending the tube on the balance.

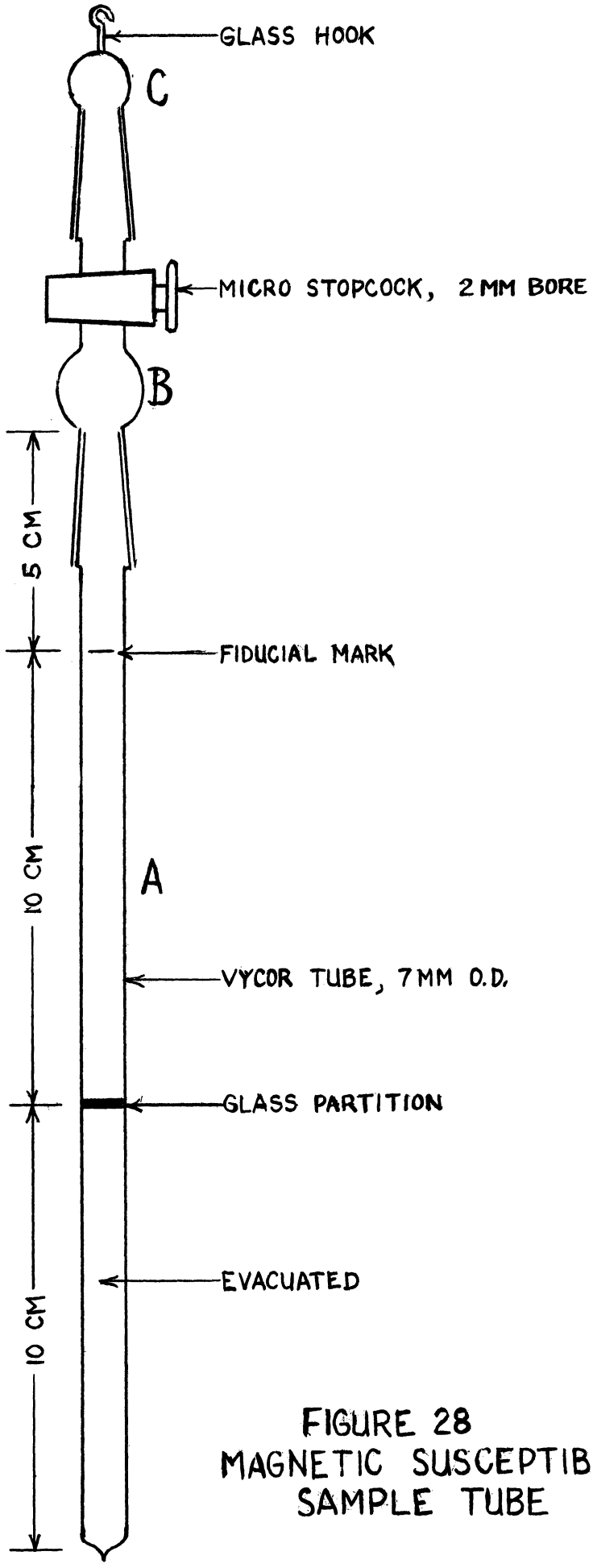

FIGURE 28
MAGNETIC SUSCEPTIBILITY
SAMPLE TUBE

3. General Procedure. (a) Treatment of Sample Tube. The sample tube and cap were immersed in hot, concentrated nitric-sulfuric acid for at least an hour, rinsed with distilled water, and dried with filter paper. Filtered air was used to dry the interior. After cleaning, the tube was handled with filter paper, chamois, or a nylon stocking.

Cap B was sealed to the tube with Apiezon W wax. The stopcock was lightly greased with Dow-Corning High Vacuum Silicone Grease. Following each hydrogenation, traces of grease were removed from the tube cap with carbon tetrachloride.

When the tube was not in use, it was protected from dust by a glass case.

(b) Filling of the Sample Tube. (i) Argon. The sample tube was attached by means of cap B to the vacuum system (Figure 28), evacuated, and filled with argon at atmospheric pressure. The stopcock in the cap was closed, and the tube transferred to the magnetic balance. An argon atmosphere was maintained also over the water and powder samples during the magnetic measurements.

(ii) Water. The water used for the calibration of the sample tube was carefully freed of dissolved air and of non-volatile impurities by means of the purification train shown in Figure 29. It consisted of a 50 ml glass-stoppered flask, to which was connected a cold trap followed by a stopcock and the vacuum system. A T 7/25 joint for connection to the sample tube was located between the cold trap and the

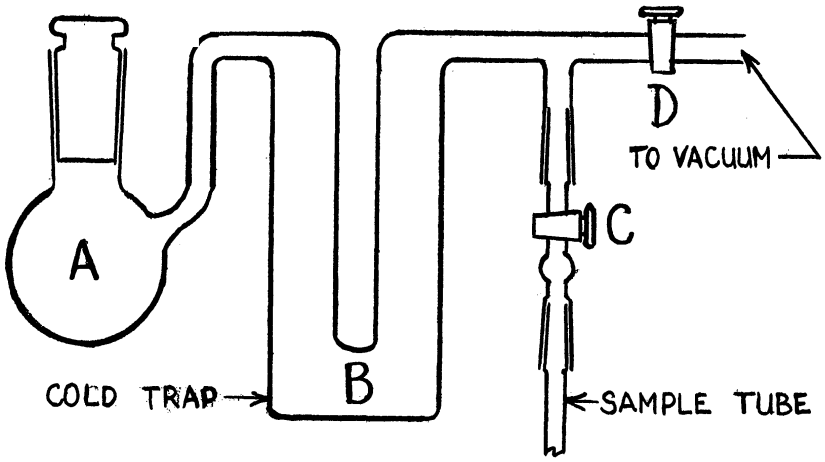

FIGURE 29. WATER PURIFICATION TRAIN

stopcock.

With about 5 ml of distilled water in the flask, stopcock A was opened to the vacuum system, keeping stopcock B closed. After boiling the water for a few minutes, it was frozen with dry ice to further expel dissolved air. The train was then evacuated to 10^{-3} mm , the stopcock to the vacuum system closed, a propanol-dry-ice mixture applied to the cold trap C, and the flask warmed. When all the water had condensed as ice in the cold trap, stopcock B was opened to the previously evacuated sample tube, and the cold trap was warmed. By cooling the sample tube, water was condensed in it to the 10 cm mark. The sample tube was then removed from the train for magnetic calibration.

(iii) Powders. With cap B on the sample tube, the calibration water was removed by draining and evacuating. A micro funnel was inserted through the stopcock in cap B, and the metal powder was poured in to the mark. During the filling the tube was agitated by a small massage-type vibrator to compact the powder as homogenously and effectively as possible.

The tube was then slowly evacuated, avoiding sweeping out the powder. Argon was admitted, and the tube was closed and transferred to the magnetic balance.

(c) Hydrogenation. Following magnetic measurements on the metal, the sample tube was connected to the hydrogenation train, and the powder was degassed overnight under high vacuum at 200-400°. After admitting argon and vibrating the cooled tube to compact the powder to the level it had prior to degassing, the susceptibility of the degassed sample was measured. A small amount of powder was then withdrawn for X-ray analysis by inserting a capillary through the bore of the stopcock into the mass of the powder, and gently sucking on the capillary. The weight of the powder removed was determined.

The sample tube was again connected to the hydrogenation train and evacuated to 10^{-6} mm. A measured volume of hydrogen was delivered to the sample from the burette, as described in sections II, A, 4, b, ii and iii. The temperature of the sample was gradually raised by means of a cylindrical resistance furnace until absorption occurred. In the case of tantalum hydride temperatures up to 400° were used. The Ti powder absorbed hydrogen readily without any heating up to the composition $TiH_{0.9}$. For further hydrogenation the titanium hydride was heated up to 200°. A hydrogen pressure of one atmosphere was maintained until the volume corresponding to the desired hydride composition had been delivered from the

burette. As the sample was allowed to cool slowly, it continued to absorb hydrogen until the equilibrium pressure at room temperature was reached. Any unabsorbed hydrogen was returned to the gas burette by means of the Toepler pump, and the sample tube was filled with argon. After vibrating the tube to break up lumps and recompact the powder, magnetic measurements were made on the material. A sample was removed for X-ray analysis, and the above procedure was repeated.

(d) Magnetic Measurements. The sample tube, suspended by a thin wire from the balance, was allowed to come to equilibrium overnight at 20.0° Then currents of 2.00, 6.00, 8.00 and 10.50 amperes were passed through the magnet, and the apparent change in weight was determined. At least six measurements were made at each field strength, the current direction being reversed for successive readings. The weight without current was checked before and after each measurement with the field.

The current through the magnet was manually controlled by means of a rheostat to ±0.2% and was measured by a Weston 0 - 15 ampere D.C. ammeter, observed through a thirty power microscope.

4. Calculation of Results. (a) Volume Susceptibility. According to Klemm[47], for water and air at 20°, K = -0.720 x 10^{-6} and +0.0294 x 10^{-6} respectively. Therefore, Eq. (12) in section III, A, 3 becomes

$$K \cdot 10^6 = -\frac{0.691 \Delta W}{\Delta W_{H_2O}} + 0.0294 ,$$

for given calibration conditions. The observed apparent changes in weight include the small contribution of the sample tube itself, for which a correction has to be made. If ΔW_e, ΔW_s and ΔW_w are the apparent changes in weight of the tube when it is empty, contains the sample or water, then

$$K \cdot 10^6 = \frac{\Delta W_s - \Delta W_e}{\Delta W_w - \Delta W_e} 0.691 + 0.0294 \quad \text{Eq. (13)}$$

where all terms on the right are experimentally observable.

Since the powder volume increased during hydrogenation, and since some was removed for X-ray analysis, the level of the hydride usually did not coincide with the 10 cm mark. Hence, the height of the powder level above the partition was measured with a ruler to ± 0.2 mm. Corrections for the variation in level are calculated from Eq. (11) (section III, A, 3) and the dependence of magnetic field on distance (Appendix C, 2, b). The variation in apparent change in weight due to variation in powder level is given by

$$\frac{\partial \Delta W}{\partial z_2} = \frac{A(K - K_{air})}{g} \cdot H(z_2) \frac{\partial H}{\partial z}\Big]_{z_2} = -4 \times 10^{-4} \; \Delta W/\text{mm. change in height of the powder level.}$$

Therefore, the correction is negligible in most cases.

(b) Powder Density. The apparent density, used for the evaluation of the molar susceptibility, is obtained from the weights of the water contained in the sample tube up to the 10.00 cm mark, and of the powder up to the height h, according to:

$$d_{app.}^{20°} = \frac{W_{sample}}{W_{H_2O}} \times \frac{10.00 \text{ cm.}}{h \text{ cm.}} \times 0.998 \text{ g./cc.}$$

C. Results.

1. Ta-H System. The magnetic susceptibility of Ta-H was determined at five compositions. The metal used for determination (det.) 1 was degassed overnight at 450° under high vacuum before the start of det. 2. For dets. 3-7, a new metal sample was used which had been degassed for three days and gradually hydrogenated.

The results are given in Table V. The uncertainty, 0.02 g./cc., in the apparent density is based on an estimated

Table V

Magnetic Susceptibility of the Ta-H System at 20°

Det.	Material	$d_{app.}$ ±.02 (g./cc.)	K x 10^6 (cc./cc.)	χ_M x 10^6 (cc./formula wt.)	π No. of unpaired electrons per Ta atom
1	Ta (before degassing)	8.63	6.936 ± .011	145.4 ± .6	.115
2	Ta (partially degassed)	8.50	6.952 ± .015	147.2 ± .7	.116
3	Ta (thoroughly degassed)	8.48	6.449 ± .019	137.8 ± .7	.108
Ta, weighted Ave. = $[1\cdot(1)+3\cdot(2)+3\cdot(3)]/7$				= 143 ± 4	.113
4	$TaH_{0.1175}$	8.33	6.347 ± .016	137.8 ± .7	.108
5	$TaH_{0.2284}$	8.37	5.758 ± .008	124.6 ± .5	.098
6	$TaH_{0.3464}$	7.92	4.873 ± .008	111.4 ± .5	.088
7	$TaH_{0.5078}$	7.58	4.431 ± .021	105.8 ± .8	.083

error of 0.2 mm in reading the powder height. The uncertainty

in K is the standard deviation of the mean of the susceptibilities determined at four field strengths. However, it does not include the systematic error in the calibration quantity ($\Delta W_w - \Delta W_e$) because, once determined, the latter is taken to be a known quantity. This latter error is taken into account in Table VI.

The difference between the susceptibility (x 10^6) of the paramagnetic tantalum resulting from det. 3 (137.8) and the average from dets. 1 and 2 (146.3 ± 1.1) is well beyond experimental errors. Since the samples for dets. 2 and 3 were degassed, they have been given triple weight in computing the average of the three determinations, 143 ± 4. Within the given mean deviation from the mean, this value agrees with that of Selwood[48,145].

As Figure 30 shows, the magnetic susceptibility per g.-at. Ta decreases monotonously with increasing hydrogen content to a value which for the composition $TaH_{0.5}$ is 26% smaller than that of the metal. The susceptibility vs. composition curve shows an inflection at a composition of about $TaH_{0.2}$.

The number of unpaired electrons at 20° per Ta atom (Π) was calculated, neglecting diamagnetic contributions, according to

$$\chi_M = \Pi \frac{N\beta^2}{3KT} \cdot 4S(S+1) \quad , \qquad \text{Eq. (14)}$$

in which the designations are: N, Avagadro's number; ß, Bohr magneton; K, the Boltzmann constant; T, °Kelvin; and S = 1/2, the electron spin.

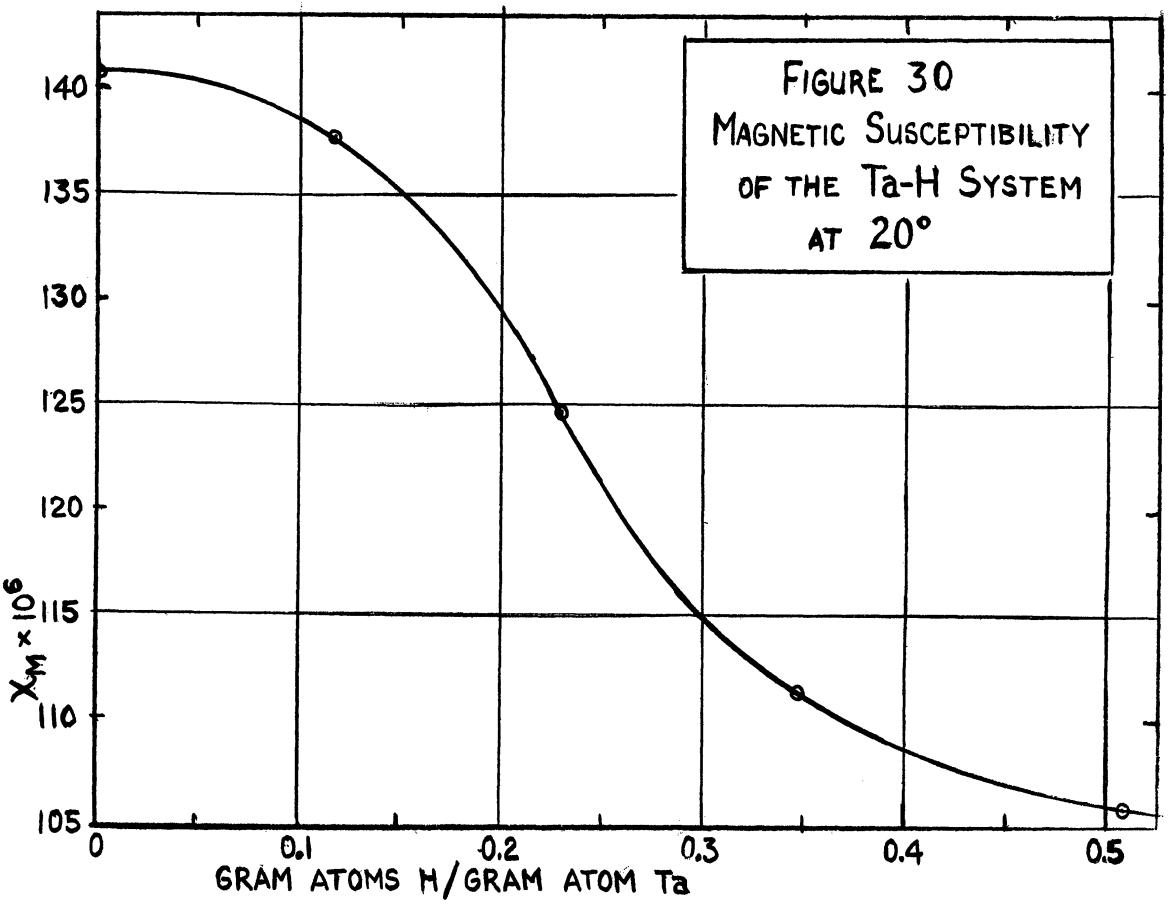

The volume susceptibilities at the various field strengths for each extreme of the composition range are given in Table VI. The uncertainties given for the results at each field are the standard deviations and include the uncertainty in the calibration. For the weakest field (2.00 amp.), K is distinctly larger than the average for the higher fields. This deviation is only slightly larger than the experimental error at 2.00 amp. in det. 2, but is 2.5 times larger in det. 7. This may indicate the presence of a trace of ferromagnetic impurity not removed by the treatment with HCl. If so, the absence of a systematic variation at the larger fields indicates that saturation of the impurity occurs already at 6.00 amp., so that the values above 2.00 amp. give the correct K value. The maximum error in the average due to including the value at 2.00 amp. is only 0.5%.

Table VI

Field Dependence of Volume Susceptibility,

$K \times 10^6$, for Ta and $TaH_{0.5}$

Amperes		Ta (Det. 2)		$TaH_{0.5}$ (Det. 7)
2.00		6.994 ± .045		4.483 ± .033
6.00	Ave. 6.938	6.928 ± .033	Ave. 4.400	4.409 ± .019
8.00		6.952 ± .033		4.400 ± .020
10.50		6.933 ± .042		4.391 ± .025
		6.952 ± .015		4.421 ± .021

2. Ti-H System. The magnetic susceptibilities in the Ti-H system were studied at eight compositions up to $TiH_{1.73}$. The Ti powder used for det. 1 was degassed overnight at 350° under high vacuum and gradually hydrogenated for dets. 2-9. The results are given in Table VII. The uncertainties given have the same meaning as in Table V.

The difference of 4.0 in units of 10^{-6} cc/g.-at. between the susceptibilities of the paramagnetic titanium in dets. 1 and 2 is beyond the experimental error. Since considerable gas was evolved from the Ti used in det. 1, det. 2 has been given triple weight in computing the average susceptibility, 147.9 ± 1.5. This result agrees with Selwood's[49] value, 150.

According to Figure 31, χ_M (and also T) of the metal decreases as the hydrogen content increases up to about $TiH_{0.2}$, to a minimum about 4% smaller. Then χ_M increases, becoming 21% larger than the metal value at $TiH_{1.73}$. The

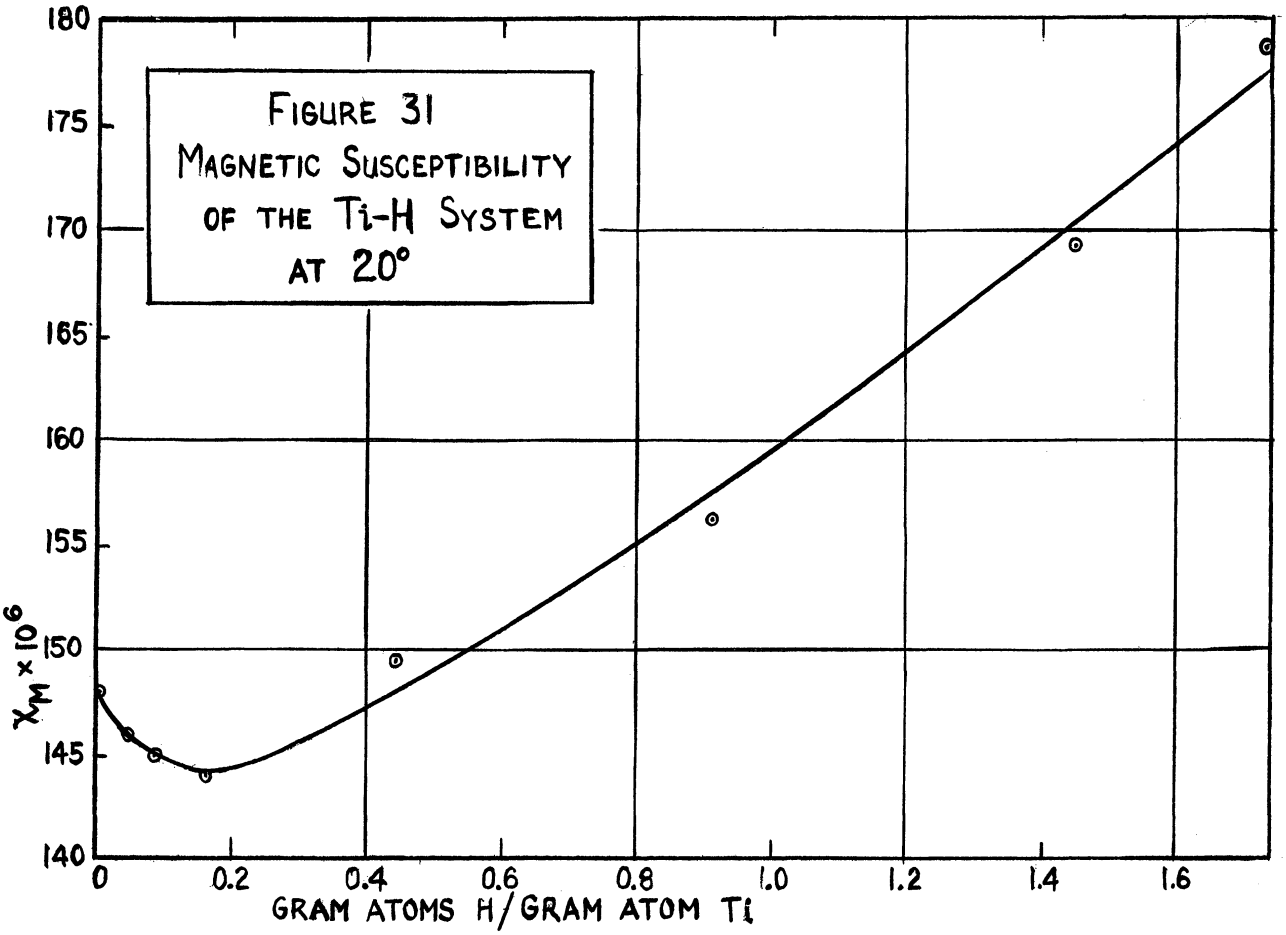

Table VIII

Magnetic Susceptibility of the Ti-H System at 20°

Det.	Material	$d_{app.}$ ±.004 (g./cc.)	K x 10^6 (cc./cc.)	χ_M x 10^6 (cc./formula wt.)	π No. of unpaired electrons per Ti atom
1	Ti (before degassing)	1.799	5.441 ± .008	144.9 ± .6	.114
2	Ti (degassed)	1.762	5.355 ± .014	148.9 ± .8	.117
Ti, weighted Ave. = $[1\cdot(1)+3\cdot(2)]/4$				= 147.9 ± 1.5	.116
3	$TiH_{0.0442}$	1.716	5.219 ± .010	145.9 ± .6	.115
4	$TiH_{0.0869}$	1.692	5.102 ± .017	144.8 ± .9	.114
5	$TiH_{0.1634}$	1.675	5.015 ± .012	143.9 ± .8	.113
6	$TiH_{0.4455}$	1.677	5.175 ± .009	149.3 ± .7	.118
7	$TiH_{0.9120}$	1.655	5.293 ± .012	156.1 ± .8	.123
8	$TiH_{1.4463}$	1.507	5.166 ± .005	169.2 ± .6	.133
9	$TiH_{1.7318}$	1.475	5.309 ± .008	178.6 ± .8	.141

minimum is believed to be real, since χ_M decreased systematically. Fitzwilliam, Kaufmann, and Squire[21] give the value 186 for $TiH_{1.2}$, while the value 165 is obtained by interpolation from the present results.

The volume susceptibility does not show any systematic dependence on field strength, as is shown in Table VIII for the two extreme compositions. This proves the absence of ferromagnetic contaminants.

Table VIII

Field Dependence of Volume Susceptibility, K x 10^6 , for Ti and $TiH_{1.73}$

Amperes	Ti (Det. 2)	$TiH_{1.73}$ (Det. 9)
2.00	5.369 ± 0.035	5.315 ± 0.035
6.00	5.318 ± 0.014	5.287 ± 0.015
8.00	5.381 ± 0.010	5.326 ± 0.008
10.50	5.352 ± 0.008	5.308 ± 0.007
	Ave. = 5.355 ± 0.016	Ave. = 5.309 ± 0.008

IV. X-Ray Diffraction Investigations of the Tantalum-Hydrogen and Titanium-Hydrogen Systems

A. Principle of Method. When X-rays strike a crystal, diffraction occurs only when the Bragg condition is satisfied, i.e., when

$$n\lambda = 2d\sin\theta ,$$

where λ is the wave length of the radiation, θ is the angle between the beam and a given crystal plane, d is the spacing between two nearest equivalent parallel planes of atoms, and n is an integer.

In the conventional crystal powder analysis, a collimated monochromatic pencil of X-rays impinges on a sample consisting of randomly oriented crystal grains. For each characteristic plane, some grains are positioned so that diffraction occurs. By determining the angle between the primary and diffracted beams and the relative intensities of the latter, the geometry of the crystal can be determined in principle. Details of this method may be found in the book by Barrett[50].

B. Experimental.

1. X-Ray Equipment. Two standard cylindrical X-ray cameras having circumferences of 450 mm and 360 mm were used to investigate the Ta-H and Ti-H systems respectively. The samples were mounted on a rotating shaft so that they were concentric with the film. Nickel-filtered copper K_α radiation impinged on the samples after passing through two 0.01" dia. collimating pinholes.

2. Materials. Powder samples for the systematic investigation of the Ta-H and Ti-H systems were prepared incidentally to magnetic susceptibility studies (section III, B, 3, c). A sample was also prepared from fragments of the $TaH_{0.173}$ ribbon described in section II, C, 1, d, in order to determine the reason for its sudden disintegration during a resistance vs. composition study.

An incidental investigation was made on a sample of titanium hydride of unknown composition, which had been prepared about two years previously by the reaction of $TiCl_4$ and AlH_3 in anhydrous ether solution under an atmosphere of dry nitrogen. The fine black precipitate had been washed with anhydrous ether, dried under nitrogen, and bottled. Prior to the diffraction investigation it was found to contain NH_4Cl; hence it was washed with a water-alcohol mixture and dried.

3. Preparation of Samples. Each powder sample was mixed with a small amount of cellulose nitrate cement and rolled into a strand of less than 0.01" diameter. As a means of calibrating the X-ray films, reagent grade NaCl was mixed with each powder except the precipitated titanium hydride.

4. Procedure. In the Ta-H studies with the 450 mm camera, an 18 hour exposure at 20 milliamperes was required for satisfactory film intensities. A 6-10 hour exposure at 15 milliamperes was sufficient when the 360 mm camera was used.

From films exposed in the 450 mm camera, the Bragg angles θ were computed from the diameters of the diffraction rings, measured to ± 0.1 mm with a steel ruler. The corresponding error in θ is ± 0.03°.

The design of the 360 mm camera did not permit convenient measurement of the diameters of the diffraction rings. Hence, the values of θ ± .025° were computed from the radii of the rings as measured to ±0.05 mm on a vernier-equipped scale. The position of the undiffracted beam was determined by extrapolating the center of the diffraction rings to θ = 0.

A correction curve was obtained for each film by comparing the observed θ values for NaCl with those calculated assuming a to be 5.627 Å[51].

Intensities were estimated visually. The numerical scale of intensities used for the Ta-H films was based on the value 100 for the most dense line on a given film. For the Ti-H films, a modified scale ranged from 10 for a completely opaque line to 1 for a line at the limit of detectability.

5. Evaluation of Results. The corrected θ values were used to calculate corresponding d values by means of the Bragg equation, using as λ the average for the copper K(α_1) and K(α_2) lines, since in general these two components were unresolvable.

The lines were indexed using the Hull-Davey charts[52]. For the cubic phases, the unit cell length a was calculated for each line and these results extrapolated to θ = 90°, thus

eliminating most systematic errors. The a, b and c parameters for the orthorhombic phase (II) of tantalum hydride were derived from the nOO, OnO and OOn (n = 2 or 4) spacings respectively. For the hexagonal titanium hydride phases, the reported a parameter is the average computed from the observed 100, 110, 200, 120 and 300 spacings; the c parameter is taken to be twice the 002 spacing.

To compensate for the change in number of metal atoms per unit cell when a phase change occurs, the cell volumes divided by the number of metal atoms per cell were calculated from the lattice constants.

C. Results.

1. Ta-H System. The X-ray analysis results of the Ta-H system are summarized in Table IX. In deriving the average, 3.300 ± .002Å, for a of the body centered cubic (b.c.c.) metal, the result for sample (1) was given half weight, since a better experimental technique was applied to (2) and (3). This average agrees with previous measurements and corresponds to the density 16.71 g./cc. As hydrogen was absorbed at room temperature, a increased monotonously up to the composition $TaH_{0.35}$, for which it was 1% larger than for the metal. However, at the composition $TaH_{0.51}$ obtained at 200-400°, and in the sample (8) hydrogenated at 400° to the composition $TaH_{0.173}$; the hydride was present as the orthorhombic phase (II). The uncertainties in the reported parameters for this phase are estimated to be ± .01 Å.

Table IX

Composition Dependence of Lattice Parameters and Volumes for Ta-H

Sample	Material	Lattice Parameters in Å	V_A (Volume Å^3 per Ta atom)
		Phase I	
		a	
(1)	Ta, as received	3.305 ± .003	
(2)	Ta, HCl extracted	3.300 ± .001	
(3)	Ta, degassed at 400°	3.298 ± .001	
	Ta, average 1+2·(2)+2·(3)	3.300 ± .002	17.97
(4)	$TaH_{0.1175}$	3.318 ± .001	18.27
(5)	$TaH_{0.2284}$	3.327 ± .007	18.41
(6)	$TaH_{0.3464}$	3.333 ± .003	18.51
		Phase II	
(7)	$TaH_{0.5078}$	a = 4.80 b = 4.72 c = 3.41	19.4
(8)	$TaH_{0.173}$	a = 4.82 b = 4.78 c = 3.43	19.8
	γ-Tantalum Hydride (Hagg[24])	a = 4.821 b = 4.791 c = 3.340	19.26

Previous results for tantulum metal: a = 3.298[24], 3.297[25], 3.2959[53].

V_A, the volume of the unit cell divided by the number of Ta atoms per unit cell, i.e., the volume per atom Ta, increased only from 18.0 to 18.5 $\mathring{A}^3$ as phase I was hydrogenated to the composition $TaH_{0.35}$. With the relatively small further increase in composition to $TaH_{0.51}$, V_A increased to 19.4 $\mathring{A}^3$, indicating a discontinuous volume change. This value agrees with Hägg's[24] result, but is smaller than that for sample 8.

Sample 6, which has the highest hydrogen content for the b.c.c. phase (I), is compared in Table X with the samples of phase II. Line intensities (Int.), and interplanar spacings (d_{hkl}), are given in each case. The Miller indices for Phase I refer to a cubic lattice; those for Phase II are the line assignments given by Hägg for a face centered orthorhombic (f.c. rhombic) lattice. Thus, the transformation I $\longrightarrow$ II consists of a 2.8% expansion (relative to the original metal) along two directions, and a 4.1% expansion along the third direction, as well as a distortion of the angle between the two equal edges from 90° to 89.65°. As the cubic symmetry is destroyed, the single lines observed for sample 6 split into groups of two or three lines in Phase II. Except for a few unidentified extra lines in sample 8, marked by * in Table X, the results for samples 7 and 8 are in agreement with those given by Hägg for his γ phase.

However, with regard to the stability of the various phases as a function of composition, there is a complete lack of agreement among the results of Hägg, Horn and Ziegler[25],

Table X

X-Ray Diffraction Patterns of Phases I and II for Ta-H

Phase I			Phase II							
Sample 6 $TaH_{0.3464}$			Sample 7 $TaH_{0.5078}$		Sample 8 $TaH_{0.173}$		"γ - TaH_x" (Hägg)		Hägg 24	
Int.	d_{hkl}	hkl	Int.	d_{hkl}	Int.	d_{hkl}	Int.	d_{hkl}	hkl	
					0.5	2.743*				
					10	2.667*				
100	2.359d	110	50 50	2.401 2.358	100	2.437- 2.380	100 70	2.415 2.383	111,200 020	
					2	1.875*				
10	1.665	200	10 10 10	1.706 1.687 1.664	20 30	1.714 1.689	70 100	1.711 1.692	002 220	
					5	1.536d*				
50	1.3578d	211	25 25 25	1.3888 1.3783 1.3625	50	1.391- 1.376	100 100 100	1.3938 1.3880 1.3820	202,022 311 131	
					0.5	1.334*				
20	1.1782d	220	8 6	1.2004 1.1818	30 5	1.205 1.195	100 100	1.2040 1.1936	222,400 040	
5	1.0822*									
20	1.0533d	310	8 8 8	1.0782 1.0674 1.0567	30 50	1.082 1.070	100 100	1.0833 1.0723	113 420,331	
5	0.9629	222	1 1 1	0.9754 0.9637 0.9499	10 2	0.9826 0.9788	100 100	0.9849 0.9804	402 420	
			5	0.9100- .9027	20 70	0.9131-.9010 0.9080				
10	0.8961*									
20	0.8928	321	1 2 5	0.8993 0.8932 0.8874						
			0.5 0.5 2	0.860 0.857 0.846	5 10	0.8559 0.8458				
					10 20 20 20	0.8080 0.8042 0.8017 0.7993				

* unidentified line
"d" diffuse line
(re Intensity (Int.)
see section IV, B, 4

FIGURE 32
COMPOSITION RANGES OF Ta-H PHASES
ACCORDING TO VARIOUS INVESTIGATORS

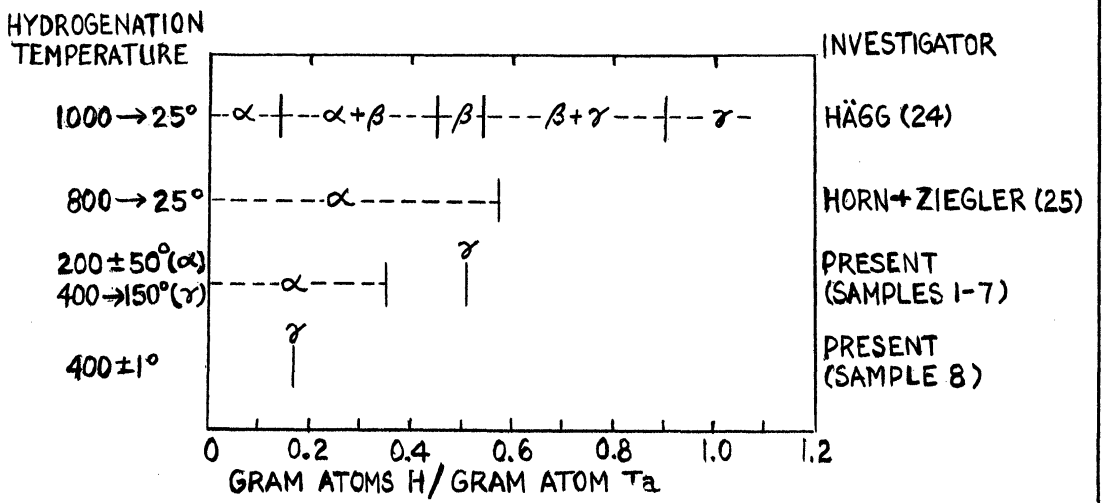

and the present ones, as shown diagrammatically in Figure 32. Hägg reports the following phases:

α (b.c.c.)	from Ta	to $TaH_{0.14}$
α + β	" $TaH_{0.14}$	" $TaH_{0.45}$
β (h.c.p.)	" $TaH_{0.45}$	" $TaH_{0.54}$
β + γ	" $TaH_{0.54}$	" $TaH_{0.90}$
γ (f.c. rhombic)	" $TaH_{0.90}$	" $TaH_{?}$.

On the other hand, Horn and Ziegler found only the b.c.c. phase up to $TaH_{0.572}$. In the present study on powder, only the b.c.c. phase was observed at compositions up to $TaH_{0.35}$, and only the f.c. rhombic phase was found at $TaH_{0.51}$. However, only the latter phase was present at $TaH_{0.17}$ in the ribbon (sample 8) which spontaneously disintegrated during a R vs. C study at 400°. No evidence for the existence of Hägg's hexagonal phase has been found. This lack of agreement shows that at least some of the investigated samples did not represent the phase which is stable at room temperature.

Hägg's hydrides were prepared by heating the metal to 1000° or higher and allowing it to cool in the presence of hydrogen. Horn and Ziegler absorbed hydrogen in 99.9% Ta by cooling the metal from 800° under purified hydrogen. The state of the hydrides was thus largely dependent upon the unspecified rate of cooling. In the present study on Ta powder, purified hydrogen was absorbed at 150-200° up to $TaH_{0.23}$, and at 150-400° above this composition, while the ribbon was hydrogenated isothermally at 400°. The much higher concentration at which phase II appeared in the powder as compared with the ribbon may be due to the lower hydrogenation temperature for the powder. The rate of formation of phase II was probably much slower in the powder, and supersaturation of phase I occurred instead.

While Horn and Ziegler report that the b.c.c. phase extends up to $TaH_{0.572}$, a new phase appeared (at $TaH_{0.51}$ in sample 7 and at $TaH_{0.17}$ in sample 8) in this study. This difference may be a matter of interpretation. In both investigations the diffraction lines became increasingly diffuse with increasing hydrogen concentration, as shown by the lines marked "d" in Table X. It is possible that this broadening is caused by a splitting of the individual lines, due to a continuous distortion of the shape of the unit cells, and that Horn and Ziegler were unable to resolve the lines. On the other hand, in this study the sudden appearance of resolvable groups of lines in going from samples 6 to 7, and the

large increase of V_A, suggest that a discontinuous change does occur. The data of Horn and Ziegler seem to show a discontinuity in the dependence of lattice parameter upon composition at about $TaH_{0.1}$.

The results of the present and previous observations concerning the dependence of the parameter of Phase I on composition are summarized in Figure 33. According to the present results, the parameters are less sensitive to changes of composition than was found previously. This may again be due to the differences in the thermal histories of the various samples.

2. Ti-H System. In the Ti-H system, a phase of the hexagonal close packed type and a face centered cubic one were found. The lattice parameters for the hexagonal form were found to be independent of the composition up to $TiH_{1.446}$, and are given in Table XI: a = 2.945 ± .004 Å; c = 4.693 ± .005 Å= c/a = 1.593 ± .005 Å. Between $TiH_{1.446}$ and $TiH_{1.732}$ a transformation to the cubic phase occurs. In Table XII data for the compositions on either side of the transformation are given, as well as the results of Hägg[24] for the cubic phase, and those for the precipitated titanium hydride. The observed diffraction pattern for $TiH_{1.732}$ corresponds closely to that of the hexagonal $TiH_{1.446}$ and only the presence of the 220 cubic line and the absence of a few other lines expected for a hexagonal lattice indicate that $TiH_{1.732}$ is not hexagonal. The lines produced from the precipitated hydrides

Table XI

Powder Patterns for Hexagonal Phase of Ti-H System up to Composition $TiH_{1.446}$

	Ti, non-degassed		Ti, degassed		$TiH_{0.0442}$		$TiH_{0.1634}$		$TiH_{0.9120}$		$TiH_{1.446}$		
hkl	I	d_{hkl}	I	d_{hkl}	I	d_{hkl}	I	d_{hkl}	I	d_{hkl}	I	d_{hkl}	(I = Intensity)
100	4	2.552	4	2.557	10	2.548	4	2.550	3	2.552	4	2.559d	
002	4	2.348	4	2.349	3	2.348	4	2.344	3	2.347	3	2.343	
101	5	2.240	7	2.233	6	2.241	7	2.238	5	2.241	4	2.247	
102	3	1.726	4	1.724	3	1.726	2	1.727	2	1.724	3	1.731	
110	3	1.472	3	1.472	3	1.474	4	1.473	2	1.472	3	1.475	
103	3	1.3360	4	1.3338	5	1.332	3	1.334	2	1.332	3	1.333	
200	1	1.2742	-	--	-	--	-	--	-	--	1	1.275	
112	3	1.2476	4	1.2482	3	1.248	3	1.247	2	1.246	3	1.247	
201	3	1.2325	4	1.2314	3	1.232	3	1.230	2	1.230	3	1.230	
202	1	1.1202	-	--	1	1.120	1	1.120	1	1.122	1	1.120	
203	-	--	2	0.9882	-	--	2	0.9870	1	0.9849	2	0.9817	
120	-	--	-	--	-	--	1	0.9650	-	--	-	--	
121	2	0.9450	2	0.9438	2	0.9448	2	0.9453d	2	0.9447	2	0.9443	
114	2	0.9180	2	0.9180	2	0.9174	1	0.9173d	1	0.9166	2	0.9171	
122	2	0.8882	-	--	-	--	-	--	-	--	-	--	
105	-	--	2	0.8812	2	0.8804d	1	0.8808	1	0.8805	2	0.8808d	
204	-	--	-	--	-	--	-	--	-	--	-	--	
300	3	0.8463	-	--	-	--	-	--	-	--	-	--	
123	2	0.8231-	-	--	2	0.8204d	2	0.8208d	1	0.8213	3	0.8193d	
302	-	.8188	2	0.7994	2	0.8003d	2	0.8008	1	0.7994	3	0.7986d	

("d" indicates diffuse line)

a	2.941	2.946	2.944	2.946	2.944	2.949	Ave. 2.945±.004
c	4.696	4.698	4.696	4.688	4.694	4.686	4.693±.005
c/a	1.599	1.597	1.593	1.590	1.591	1.589	1.593±.003

Ave. for Ti metal: a ,2.944; c , 4.697; c/a, 1.596 (re intensity, see section IV, B, 4)

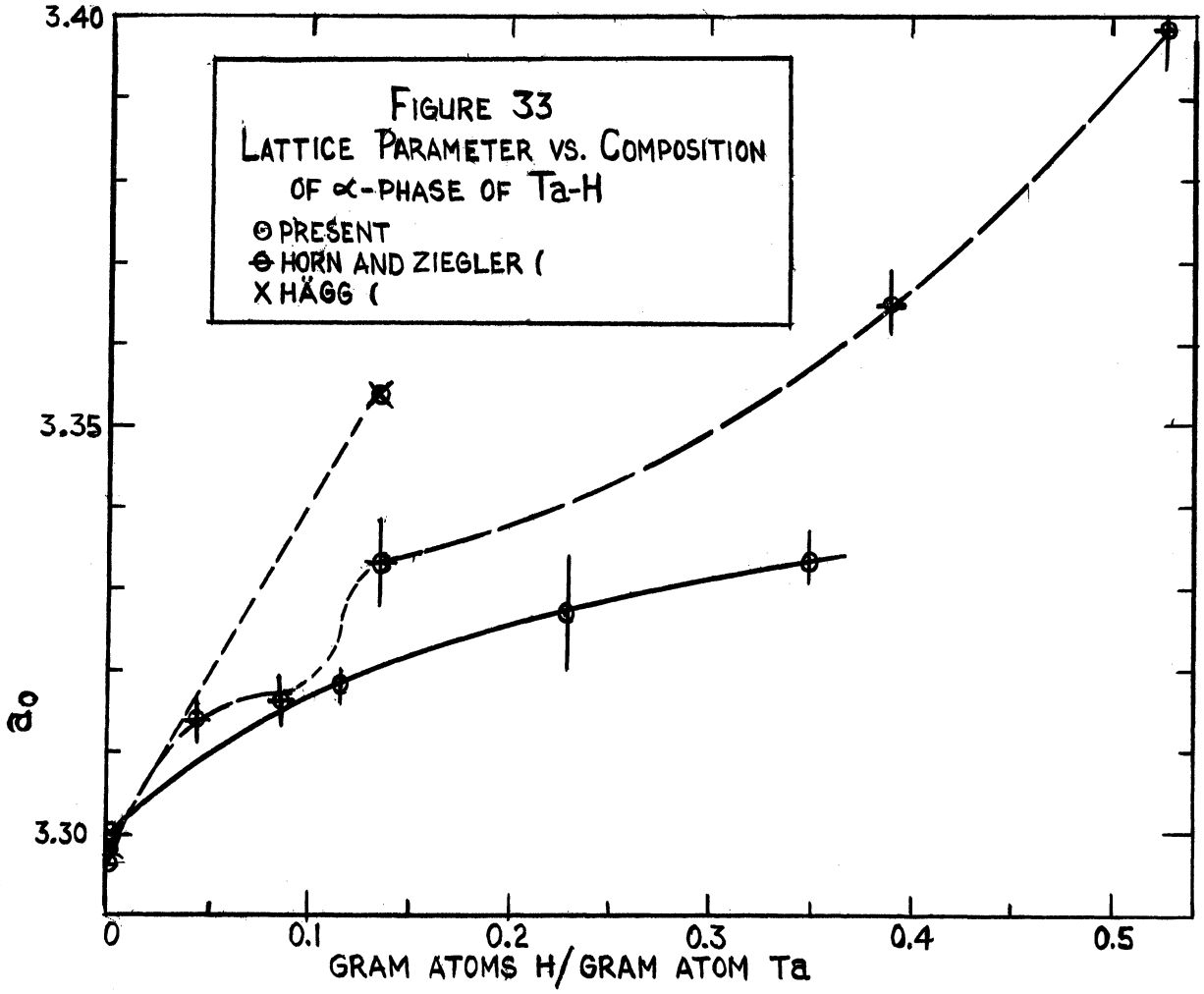

were so diffuse and faint that no reliable assignment of crystal system was possible.

Table XII

Comparison of Powder Patterns for the Hexagonal and Cubic Phases of Ti-H System

Hexagonal			Cubic						System Not Known	
$TiH_{1.446}$ $V_A = 17.65$			$TiH_{1.732}$ $V_A = 22.12$			$TiH_{0.90}$ (Hagg[24]) $V_A = 21.25$			TiH_x (pptd.)	
$a = 2.949, c = 4.686$			$a = 4.456 \pm .005$			$a = 4.397$				
hkl	I	d_{hkl}	hkl	I	d_{hkl}	I	d_{hkl}		I	d_{hkl}
100	4	2.559d	111	6	2.569d	8	2.539		2	3.94dd
002	3	2.343	200	5	2.233d	6	2.199		6	2.29dd
101	4	2.247							3	1.975dd
102	3	1.731								
			220	4	1.5750d	8	1.554			
110	3	1.475							2	1.455dd
103	3	1.333	311	4	1.3420d	8	1.326		2	1.396dd
200	1	1.275	222	3	1.2840d	6	1.269		1	1.195dd
112	3	1.247							1	1.141dd
			400			3	1.099			

(For notation see previous table)

The calculated V_A of the cubic phase is 25.3% larger than that of the hexagonal form. The fact that a two-phase region was not observed indicates either that the two-phase region is narrow, or that the hexagonal phase was supersaturated.

As shown in Table XIII, the present value, $\underline{a}$ = 4.456, for the cubic $TiH_{1.73}$ is in agreement with those of the previous investigations on $TiH_{1.66}$ and TiH_2. However, the present results for the hexagonal phase do not agree with the previous ones, regarding either the composition range of stability, or the dependence of lattice parameter upon hydrogen concentration. These differences can only be reconciled if the temperature of hydrogenation is a major factor. Both Hägg and Fitzwilliam, Kaufmann, and Squire[21] prepared their samples by cooling the metal from 1000° in a hydrogen atmosphere, whereas in the present investigation hydrogenations were effected at room temperature over most of the hexagonal range. No information regarding preparation of the X-ray samples was reported by Gibb and Kruschwitz[2].

Table XIII

Composition Dependence of Lattice Parameters for Ti-H System

Composition	Lattice Parameter Hexagonal a	Hexagonal c	Cubic a		Investigator
Ti	2.953	4.729		(1)	Hägg (24)
Ti	2.95	4.69			Patterson (54)
Ti	2.944	4.697			Present
$TiH_{0-1.446}$	2.945±.004	4.693±.005			Present
$TiH_{0.67}$	3.11	5.02		(1)	
$TiH_{0.86}$	2.95	4.68	4.395	(2)	Gibb and Kruschwitz (2)
$TiH_{0.90}$			4.397	(1)	
$TiH_{1.2}$			4.45		Fitzwilliam, Kaufmann, Squire (21)
$TiH_{1.55}$			4.40	(2)	
$TiH_{1.66}$			4.460	(1)	
$TiH_{1.73}$			4.456		Present
TiH_2			4.45	(2)	

V. State of Hydrogen in Palladium, Tantalum, and Titanium; Electric and Magnetic Properties

A. Evidence for Mono-nuclear Condition of Occluded Hydrogen.

The usual assumption that hydrogen occluded in the transition metals is not molecular is based upon the space requirements of the molecule, as well as on heats of occlusion, and Sievert's law (see section I, A, 2, a and b).

The internuclear distance in the hydrogen molecule is 0.74 Å, and its effective diameter in solid hydrogen is 3.75 Å [55]. Therefore, molecular H_2 cannot enter a b.c.c., f.c.c., or h.c.p. lattice, without severe distortion of the lattice. The strong energy required for this process would have to be provided by the relatively weak electrical interaction between the metal cores and di- or higher poles induced in the slightly polarizable molecule. However, once intragranular rifts are formed in the solid, H_2 can easily enter them.

The exothermic heats of occlusion for Pd[56], Ta, and Ti[57] hydrides, 9.28, -9.2*, and -36 kcal/mole of H_2 respectively, further demonstrate the improbability of the mere solution of molecular H_2 in the metal.

Sieverts' law, stating that the concentration of absorbed hydrogen is proportional to the square root of the hydrogen

---

*This value has been calculated from the temperature dependence of the equilibrium constants measured by Sieverts et al.[8,58], and is more reliable than the values -9 and +3.6 derived from heats of combustion[59].

pressure, indicates any of the following equilibria:

1) $H_2\ (g) \rightleftharpoons 2H^\circ$ (occluded) , $K_1 = [H^\circ]^2/[H_2]$

2) $H_2\ (g) \rightleftharpoons 2H^+$ (occl.) $+ 2e^-$, $K_2 = [H^+]^2\ [e^-]^2/[H_2]$

3) $H_2\ (g) \rightleftharpoons 2H^-$ (occl.) $- 2e^-$, $K_3 = [H^-]^2/[H_2]\ [e^-]^2$,

in which [ ] indicates the concentration of the designated species and $\pm 2e^-$ indicates that electrons are being added to or supplied by the electrons of the metal. If the concentration of hydrogen is small, then $[e^-]$, the original concentration of the "electron gas" of the metal remains nearly constant, and the expressions for the equilibrium constants K_1, K_2 and K_3 assume the form of Sieverts' law.

Palladium hydride obeys Sieverts' law at 160° and above, up to the appearance of the ß phase[5] (see Figure 1), strongly supporting the view that the absorbed hydrogen is dissociated. For Ta-H at 500° and above, the law has been verified up to one atmosphere pressure[8,58]. For Ti-H the law has been tested and confirmed for compositions below about $TiH_{0.2}$ at temperatures of 1000° and above, while marked deviations from the law occur at concentrations above $TiH_{0.2}$.

Nuclear magnetic resonance studies have been made recently on several hydrides, including those of Ta and Ti. It is claimed that the state of the hydrogen can be determined from the width of the absorption lines. According to Garstens[60], the very narrow absorption line observed for Ta hydride indicates a rapid internal motion of the protons between the various lattice positions. On the other hand,

he interprets the broad lines for several hydrides in the range $TiH_{0.38}$-$TiH_{1.57}$ as indicating that the hydrogen nuclei occupy more or less definite positions and that ". . . the hydrogen atoms are sufficiently close, probably in molecular form, to allow the strong interaction necessary to produce the broad line". However, the fixed positions could be attributed as well to the strong binding of the hydrogen "atom" to the metal indicated by the large heat of occlusion.

B. Electronic Structure of Occluded Hydrogen.

A transport of hydrogen toward the cathode was found in all reliable measurements on the Pd-H, Ta-H and Ti-H systems. This is understandable if at least part of the hydrogen present does not have the quantum configuration H or H^-, but the protons are dissolved in the "electron gas" which is common to the whole structure, i.e., which is quantized with respect to all positive cores involved. The view that hydrogen is present as protons has been criticized[61] because the effective charge per absorbed hydrogen atom has been concluded to be less than one elemental charge (see section I, B). This criticism was anticipated by Herzfeld and Goeppert-Mayer[40], who considered the apparent decrease of the charge of the proton to be due to screening of the latter by the conduction electrons.

As hydrogen is added to the paramagnetic Ta-H system, the magnetic susceptibility decreases and χ_M (in units of

10^{-6} cc/formula wt) = 106 at $TaH_{0.51}$ (see Figure 34b). According to Eq. (14), the susceptibility for atomic hydrogen χ_A = +1270 at 20°. Therefore, even if the susceptibility of $TaH_{0.51}$ were completely due to hydrogen, not more than 16% of the occluded amount can be present as ground-state hydrogen atoms. For $TiH_{1.73}$, χ_M = 179, so that not more than 8% of the occluded gas can be present in this state. Therefore, most of the electrons introduced with the hydrogen are paired after absorption. In principle one must consider also the equilibrium $H^+ + (e^-)_2 \rightleftharpoons H^-$. However, no evidence is known for the presence of H^-.

C. Electrical Properties.

When hydrogen is first absorbed in Pd, Ta or Ti, the resistance increases as in other cases when a foreign atom is introduced into the lattice of a metallic conductor. As more hydrogen is absorbed, the resistance of the Pd-H and Ti-H systems (Figures, 3, 34a and 34c) displays a maximum, while in the Ta-H system it increases monotonously up to $TaH_{0.28}$ (Figure 34b).

The change in the resistance of the metal upon hydrogenation depends on various factors. (1) The presence of protons in the metal lattice destroys the periodicity of the potential barrier between equivalent lattice sites, increasing the resistivity approximately proportionally to the number of protons added[62]. (2) The electrons from the hydrogen contribute to the conduction. (3) Expansion of the lattice may

occur. The change in resistance due to a change in volume has been calculated[63] for various metals, including Pd and Ta, from the compressibilities and pressure coefficients of resistivity. The resistance of Pd and Ta decreases upon compression as in most other cases, and it can be expected that a small expansion would produce an increase of resistance. However, for an expansion up to 25% due to hydrogenation, such extrapolation is not permissible. (4) The resistance of the samples will be changed by the opening and closing of intra-granular rifts.

Smith (p. 120 ff.) attributes the resistance decrease, both temporary and permanent (see section II, A, 1, b and Figures 1-3) in the ß phase region of Pd-H to co-conduction by protons located in the rifts. This view would be plausible only if surface conduction were appreciable. However, the transport numbers of the protons in the Pd, Ta, and Ti hydrides are about 10^{-6}, and the mobilities are of the order of 10^{-5} to 10^{-4} cm^2/sec volt. The mobility of the conduction electrons in the parent metals, assuming about one conducting electron per metal atom, is about 10^5 times larger. Since it does not appear probable that the proton mobilities at the surface and in the interior of the hydride could differ by 10^5, no appreciable decrease in resistance can be attributed to proton conduction.

Therefore, the smaller resistance of titanium hydride as compared with the metal can be explained only in terms of

an increase in electronic conductivity. Further investigation is necessary to ascertain whether this is due to an increase in electronic mobility, or to the increase in the number of conducting electrons, or both.

D. Relation between Magnetic Susceptibility and Electrical Resistance.

Figures 34 a-c show that in the Pd-H, Ta-H and Ti-H systems a change in the magnetic susceptibility, due to an increase in hydrogen concentration, is nearly generally accompanied by an opposite behavior of the electrical resistance. In the case of Pd-H, the resistance continues to increase after the susceptibility has reached its constant limiting value. The Ti-H system displays a minimum in susceptibility at about $TiH_{0.2}$, whereas the more precise R vs. C measurements show a flat maximum extending from $TiH_{0.08}$ to $TiH_{0.16}$.

Because of the many factors influencing the resistance (see previous section), it is not possible to determine which are dominant in each case, or which also influence the magnetic susceptibility.

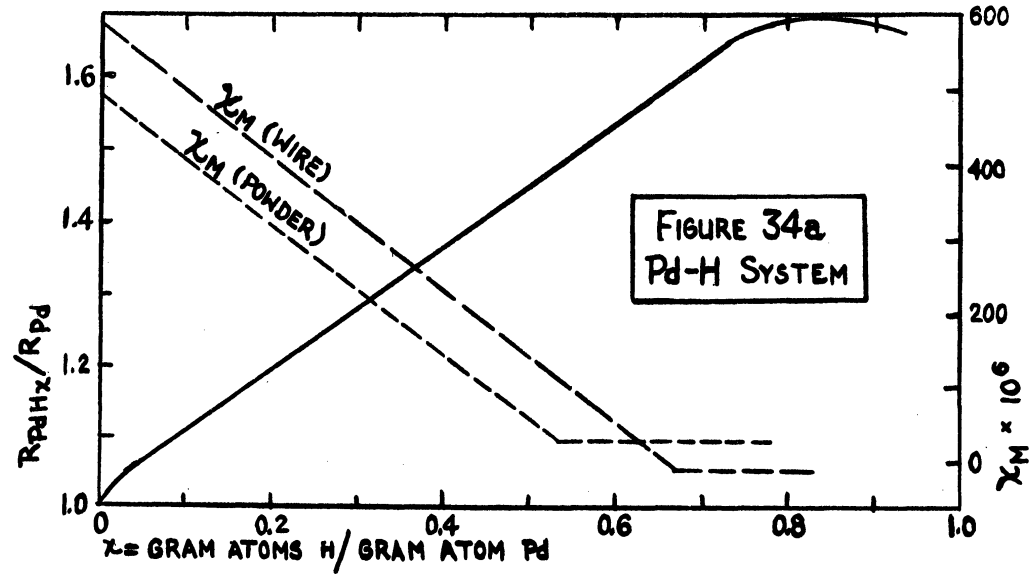

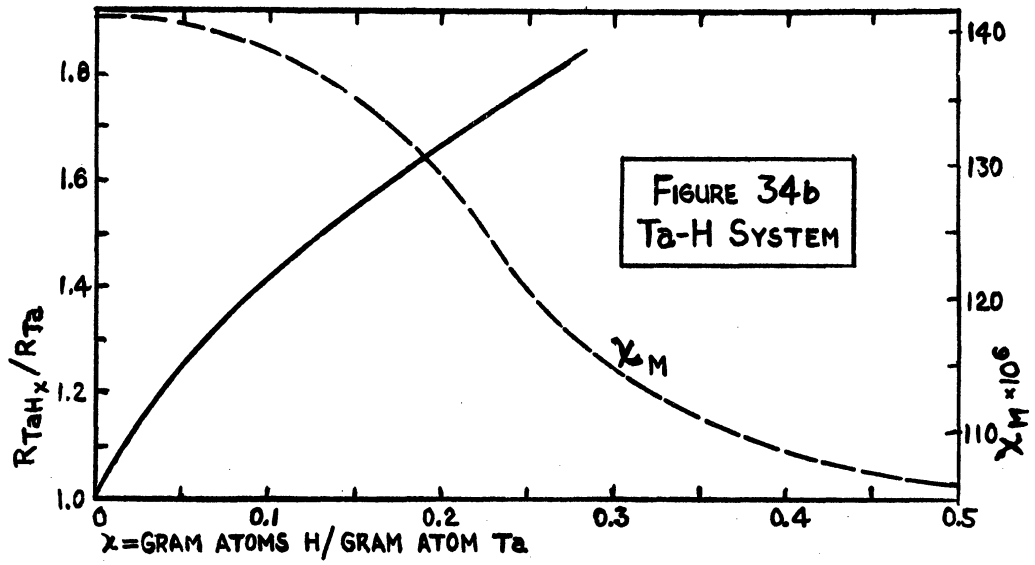

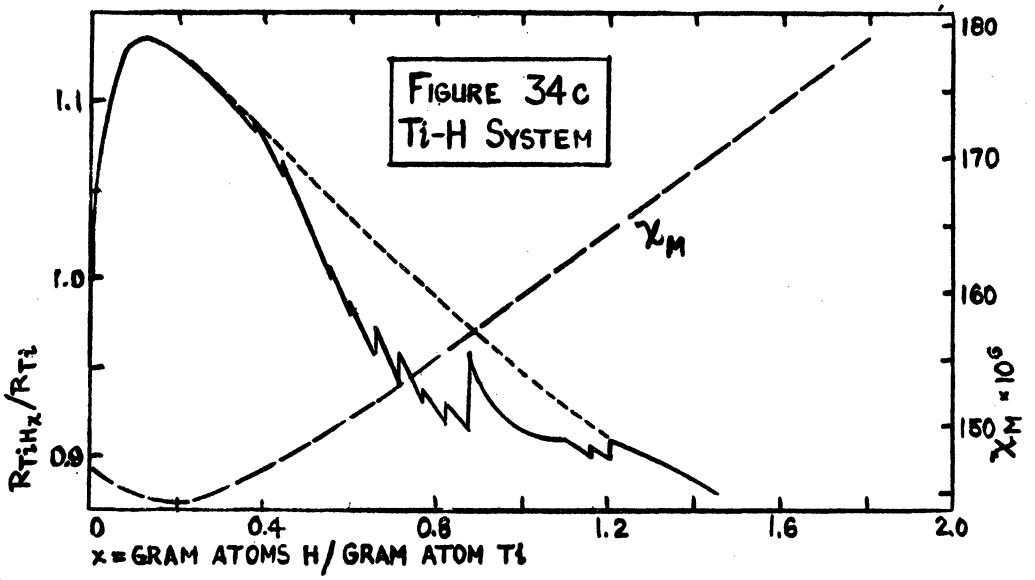

DEPENDENCE OF MAGNETIC SUSCEPTIBILITY AND ELECTRICAL RESISTANCE ON COMPOSITION IN Pd-H, Ta-H, AND Ti-H SYSTEMS

VI. Summary

1. Non-stoichiometric hydrides of Pd, Ta, and Ti have been prepared by direct combination of the elements at temperatures ranging from 25° to 400°. Higher temperatures were frequently required to initiate absorption.

2. The dependence of resistance on hydrogen content for compositions between Ta and $TaH_{0.28}$ was observed to have a positive slope at 76°, 99° and 400°.

3. As hydrogen dissolved in Ti at 99°, the resistance increased to a maximum value, 21% larger than that of the metal, at the composition $TiH_{0.6}$. At 400°, the resistance increased up to 13.4% at the maximum, which extends over the range $TiH_{0.08}$-$TiH_{0.16}$. At higher concentrations, the resistance decreases to its original value at about $TiH_{0.55}$ and to 88% of this value at $TiH_{1.46}$.

4. The temperature coefficient of resistivity in the Ti-H system was found to decrease with increasing hydrogen concentration.

5. Electrical transport was investigated in the Pd-H, Ta-H, and Ti-H systems by measuring changes of resistance of two segments of a ribbon upon passage of a direct current. The sign of the resistance change was opposite for the two segments and reversed upon each current reversal. The interpretation of these resistance changes in terms of the transport direction of hydrogen in $PdH_{0.46}$ confirms Coehn's finding that hydrogen migrates toward the cathode. All other reliable

measurements on $TaH_{0.16}$ at 72° and $TaH_{0.209}$ at 99°, as well as on $TiH_{0.048}$ and $TiH_{0.54}$ at 400° also show that hydrogen is transported toward the cathode.

6. The calculated mobilities of the protons in these transition metal hydrides are of the order 10^{-5} to 10^{-4} cm^2/sec volt, and the transport numbers are 10^{-6} to 10^{-5}. No significant difference was found between the proton mobilities in Pd and Ta at 72°, but in Ti the mobility at 400° was less than 0.1 of that in Pd.

7. The magnetic susceptibility χ (in 10^{-6} cc/formula weight) of Ta metal at 20°, 143, decreased monotonously with increasing hydrogen content to 106 for $TaH_{0.51}$. That of Ti metal, 148, decreased to a minimum, 144, for $TiH_{0.2}$, and then increased to 179 for $TiH_{1.73}$.

8. X-ray diffraction powder diagrams showed that as Ta absorbs hydrogen, the body centered cubic lattice of the metal expands from $\underline{a}$ = 3.300 Å up to $\underline{a}$ = 3.333 for $TaH_{0.35}$. Only a face centered orthorhombic phase, $\underline{a}$ = 4.80, $\underline{b}$ = 4.72, $\underline{c}$ = 3.41, was observed at the compositions $TaH_{0.51}$ and $TaH_{0.173}$. The latter powder was made from a ribbon which had disintegrated during a resistance $\underline{vs}$. composition study at 400°.

The atomic arrangement of the hexagonal "close packed" titanium, a = 2.944, c = 4.697, c/a = 1.596, was found to undergo no change within the experimental errors up to the composition $TiH_{1.45}$. At $TiH_{1.73}$ only a face centered cubic phase, $\underline{a}$ = 4.463, was found.

9. From a consideration of previous data and the observed magnetic susceptibility and direction of electrical transport, it is concluded that in Ta and Ti the absorbed hydrogen is present neither as H_2 molecules nor, to an extent greater than 16%, as ground state H atoms. Since there is no evidence for the existence of H^-, the hydrogen is considered to be present predominantly as protons dissolved in an electronic system quantized with respect to all positive cores involved.

10. The changes of electrical resistivity and of magnetic susceptibility as functions of hydrogen content in Pd, Ta, and Ti have in general opposite sign. In Ti a maximum for the resistivity occurred at about the same composition as the minimum for the susceptibility.

VII. Appendix: The Magnetic Balance

The apparatus required for magnetic measurements by the Gouy method consists of three main parts: (1) A balance; (2) A sample tube, together with its suspension and jacketing assemblies; and (3) An electromagnet.

A. The Balance.

1. General Description. A Christian Becker (Model 6410) magnetically damped microbalance equipped with an optically projected pointer scale, was used in the present investigation. The support of the balance has been previously described by Curet[64].

In preliminary work with the microbalance, the apparent weight of an object was found to vary with time, usually systematically but sometimes very erratically. In order to improve the reproducibility of the weighing operation, it was necessary to make several mechanical modifications of the balance and to control its environment more closely.

2. Mechanical Modifications. (a) Rider. Five mg U-shaped riders of 0.3 mm dia. aluminum wire were supplied with the balance. It was very difficult to ascertain a vertical position of these riders to better than ± 2°, corresponding to an error of ± 5 μg. A dumbbell-shaped rider made from a straight piece of No. 36 platinum wire eliminated this error. The weight of this rider was made equal within ± 3 μg to that of one calibrated by the N. B. S.

(b) Pan Arrest Mechanism. The rest point of the

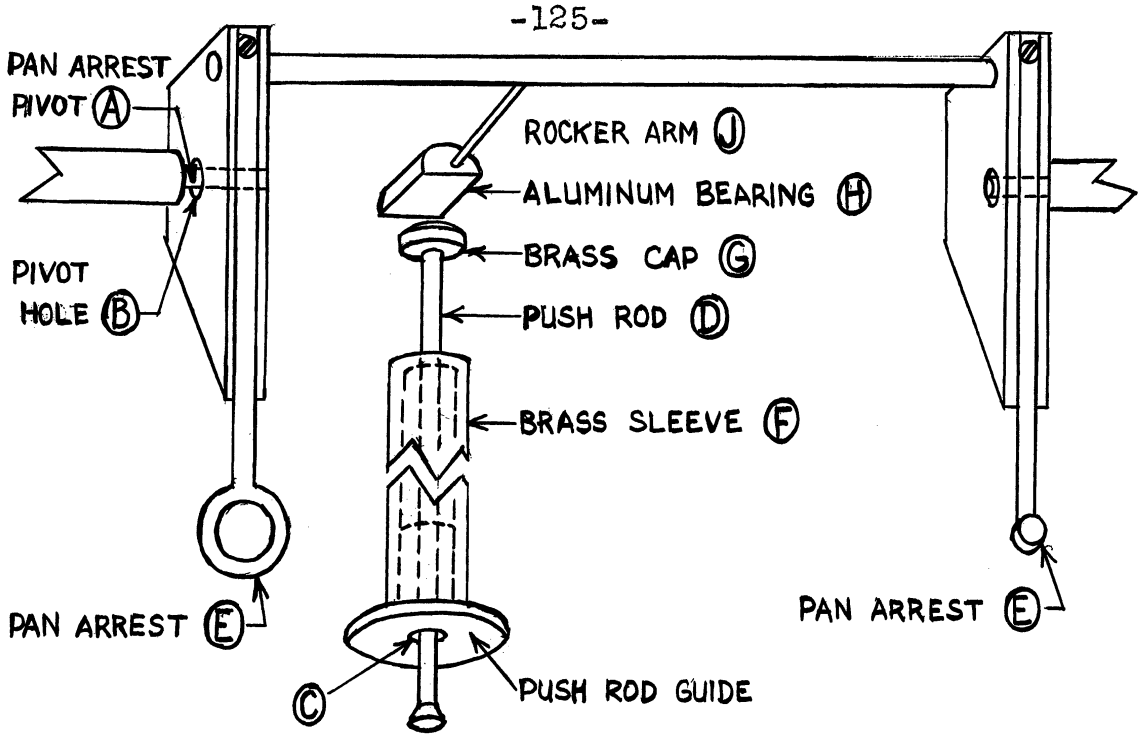

FIGURE 35. PAN ARREST MECHANISM

balance is affected by the manner of loading the knife edges and releasing the beam. These operations could not be carried out reproducibly with the original construction of the balance. This defect was traced to two causes: (1) The pan arrest mechanism (Figure 35) was not constructed to close enough tolerances. The pan arrest pivots, A, were about 1/64" smaller in diameter than the pivot holes B. The hole C in the push rod guide, which accomodates the 1/8" dia. push rod D, had sufficient clearance to allow a play of approximately 1/16" at the end of the push rod. (2) Some fibers extended above the apparent surface of the wool felt which covered the pan arrests. By means of a cathetometer it was observed that these fibers were compressed when the arrests were raised to support the pans, and upon subsequent release of the arrests imparted their energy to the pans.

Polished brass pan arrests replaced the felt covered ones,

and new pan arrest pivots, 0.001" in diameter smaller than the pivot holes, were fabricated. A bushing was inserted in the hole at the front of the push rod guide, clearing the push rod by 0.001". The motion of the rod was further defined by press fitting a brass sleeve, F, over the push rod guide. The hole in the sleeve cleared the push rod by 0.001", and the sleeve served as a housing for the push rod spring (not shown).

If the axes of the push rod and the rocker arm do not lie in the same plane, the push rod will exert a side thrust on the rocker arm. To eliminate this, a brass cap, G, having a radius of curvature of about 5 cm, was placed on the end of the push rod, and a flat polished aluminum bearing surface, H, was mounted on the rocker arm. A small spring fastened to the rocker arm, J, and to the balance case kept the arm always in contact with the push rod.

3. Control of Environmental Factors. (a) Temperature. A change in the temperature of the balance affects the geometry of the beam and therefore the sensibility of the balance, the effect being more serious the less uniform the temperature change over the whole beam. A non-uniform temperature within the balance case also causes convection currents. Sources of temperature inhomogeneity were: (1) variation in ambient room temperature; (2) heat from the operator's body; and (3) heat from the intermittently operated balance light.

(i) Room Temperature. The apparatus was

transferred from a laboratory which received sunshine in the afternoon to a windowless constant temperature room maintained at 20 ± 0.5°. The temperature varied within these limits every four to six minutes. Since the heat of the room lights affected room temperature, the lights were burned permanently.

(ii) Thermal Shielding of the Balance. To avoid drafts and convection currents during measurements, a large celluloid window replaced the door of the protection case which surrounds the balance case. The window was fitted with a small door to permit access to the balance, and with control extensions for operating the balance from the outside. The control extensions minimized the amount of body heat transferred to the balance. The temperature of the air between the outer protection case and the balance was constant to ± 0.1°.

(iii) Balance Light. Originally, the 10 watt light bulb, which serves to project the pointer scale, turned on only when the beam support was released. To achieve steady heating, the lamp was rewired to operate independently of the balance controls, and was turned on at least two hours prior to weighing. The heating effect was greatly reduced by a water-cooled housing around the bulb, a heat absorption cell containing $CuSO_4$ solution, and an increase in the distance between the bulb and balance. The light was concentrated with a condensing lens.

(b) Humidity. Corwin[65] observed that differences in the hygroscopicities of the agate parts may lead to

considerable drifting of zero points and sensibilities. In order to determine the magnitude of this effect, the rest points and sensibility of the balance were measured isothermally at relative humidities of 15, 35, and 72%. The rest points varied within 300 μg, and the sensibilities within 3%. Both were found to be dependent not only on humidity but also on time, as expected for an adsorption process. The agate bearings were cleaned with silicone-impregnated lens tissue. Since the relative humidity in the balance case does not vary by more than 1-2% per day, weighing errors due to this factor are negligible.

(c) Static Charge. When a charged polystyrene rod was brought near the balance controls, an apparent change in weight of as much as 0.1 mg resulted, explaining the erratic behavior occasionally observed when the controls or the celluloid window were touched. In order to eliminate static charge, ground connections were made to the pan arrest, beam arrest, and rider transport mechanisms, and to the beam support column, the arrested beam, and the dumping magnets. In addition, two small polonium sources were located inside the balance case to leak off charges accumulating on the balance pans.

4. Cleaning the Balance. It was necessary to clean the balance from time to time. After it had been dis-assembled in a draft-free and dust-free place, the parts were carefully dusted with a camels hair brush equipped with a polonium strip

to eliminate static charge. Any fibrous material found on the pointer, damping vanes, or damping magnets was removed.

Any oxide layer on the beam supports was polished off with talc on chamois, and the talc was carefully removed. Silicone-impregnated lens tissue was used to polish the end bearings and knife edges, and the latter were then wiped with clean chamois and with a wooden splint wrapped in silk lens tissue. The bearings and knife edges were finally examined for dirt particles under a 60 power microscope. Dirt in beam crevices, particularly in the rider notches, was removed by means of a glass capillary connected to a suction line.

5. Factors in Balance Operation. (a) Rest Point "Hysteresis". The rest position of the pointer was found to vary with the length and the direction of the pointer swing. With equal load on each pan, the pointer was made to approach its rest position from various distances in either direction: the pointer was allowed to come to rest with an auxiliary 1 mg rider in various notches, and then the auxiliary rider was removed. The maximum difrerence, 11μg, in the rest point resulted when the 1 mg rider had been placed in the end notches. The rest point depended also on the previous history of a weighing, and was shifted toward previous rest points if the weight was changed by less than about 0.6 mg.

(b) Non-Linearity of Pointer Scale. Among the symbols used in this discussion are:

a = scale reading
a_o = zero point reading
w = excess weight on load pan when total load is W
S_{app} = apparent sensibility = $\frac{\Delta a}{\Delta w}$ when Δw = 1 mg
S = $\frac{da}{dw}$ = true sensibility

Weighings with the microbalance are made by the sensibility method[66]. Weights of less than 1 mg, which are required to return the pointer to the zero point, are usually obtained by interpolation according to

$$w_{calc} = \frac{a - a_o}{S_{app}} . \qquad \text{Eq. (15)}$$

Equation (15) is exact if the scale is linear, i.e., if S_{app} is constant over the entire scale. Preliminary investigation revealed that S_{app} is 4-5% larger at either end of the scale than at the middle, so that w_{calc} is only a first approximation. The actual weight, w, which produces the scale reading, a, is given by

$$w = \int_{a_o}^{a} \frac{da}{S} = f(a). \qquad \text{Eq. (16)}$$

Although S, which is a function of a, cannot be measured directly, f(a) was determined as follows.

The 5 mg rider was replaced by a 1 mg rider made of No. 40 enameled copper wire, the difference between successive notch positions corresponding to 0.200 mg and about 200 scale divisions. With the 1 mg rider in the central notch 5, a load was chosen which gave a reading with ± 50 divisions from 0. Using the technique of the actual weighings (see next section), readings were taken every two minutes, with rider

positions scanned in various orders. As a control, notch 5 was used for at least every fifth reading. For loads of 0, 10, 15, 20 and 30 g, at least four weighings were made with the main rider in each notch position; the mean deviation of the readings from the mean corresponded to about ±3 μg.

In this way, $\Delta a/\Delta w$ (for w = 0.200 mg) was found to be nearly constant within about 300 divisions of the center of the scale, and was taken as the "standard sensibility", S°. The deviation, y, of an observed scale reading from that calculated on the basis of s° is defined by

$$y = a - S^{\circ}w. \qquad \text{Eq. (17)}$$

The plot of y vs. a for a load of 15 g is shown in Figure 36. The error in y is estimated to be <2.5 scale divisions. The readings at the ends of the scale are about 3% larger than the values calculated assuming a constant sensibility. This deviation from linearity can be neglected in the scale interval -500 to +500. since here it amounts to less than the error of an individual weighing (3 μg).

By differentiating Eq. (17) with respect to w, and rearranging,

$$S = \frac{da}{dw} = S^{\circ} + \frac{dy}{dw} .$$

S is given as a function of a in Figure 37 for 0-30 g loads, and is seen to be 7-9% [e.g. at 0 load, (1062 - 970)/970 = 0.09] greater at the ends of the scale than at the center.

It must be concluded that this non-linearity of scale is caused by non-uniformity of the engraved reticle or by its distortion upon projection. The non-linearity cannot be

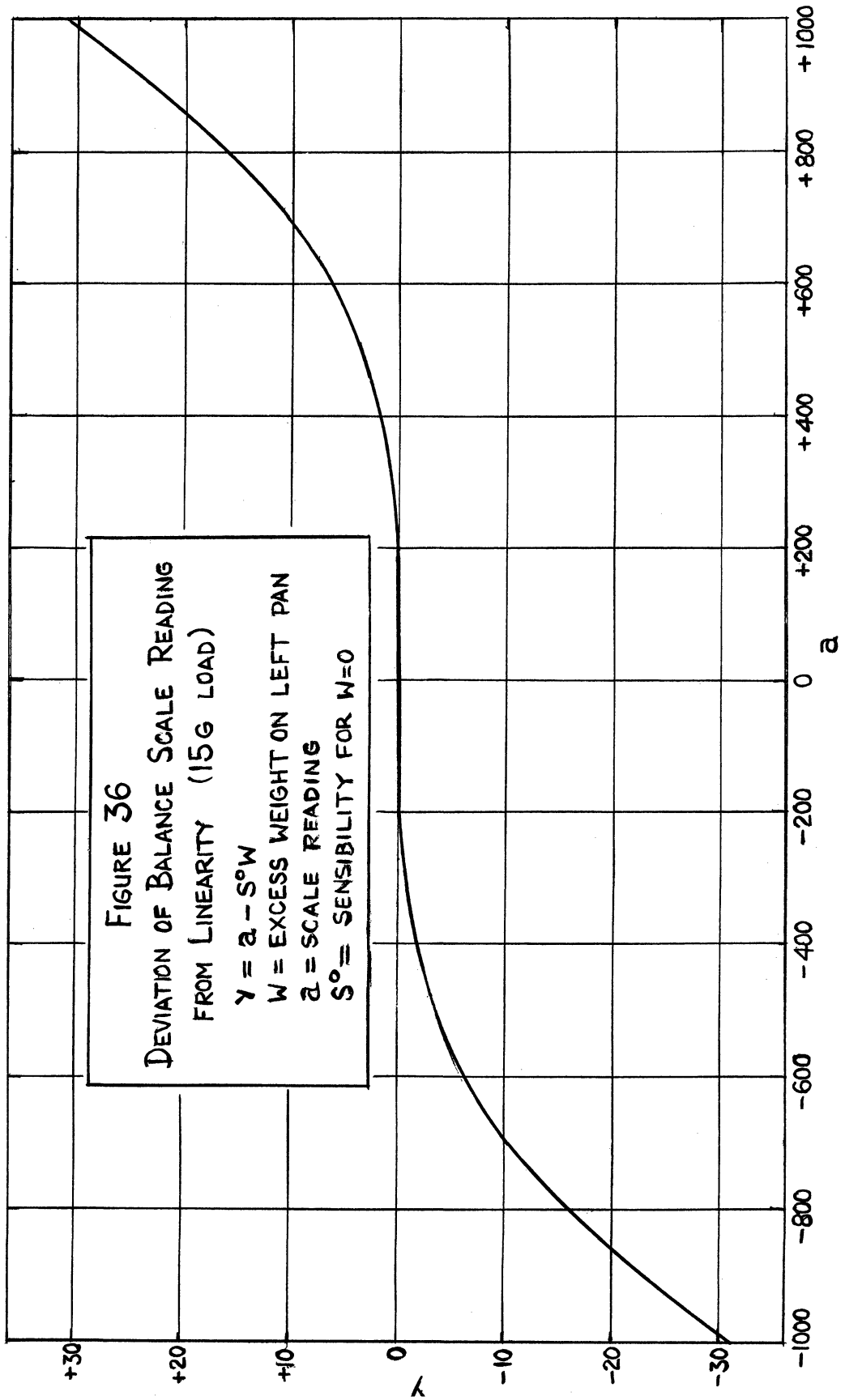

FIGURE 36
DEVIATION OF BALANCE SCALE READING FROM LINEARITY (15G LOAD)
$y = a - S^{\circ}W$
W = EXCESS WEIGHT ON LEFT PAN
a = SCALE READING
S° = SENSIBILITY FOR W=0

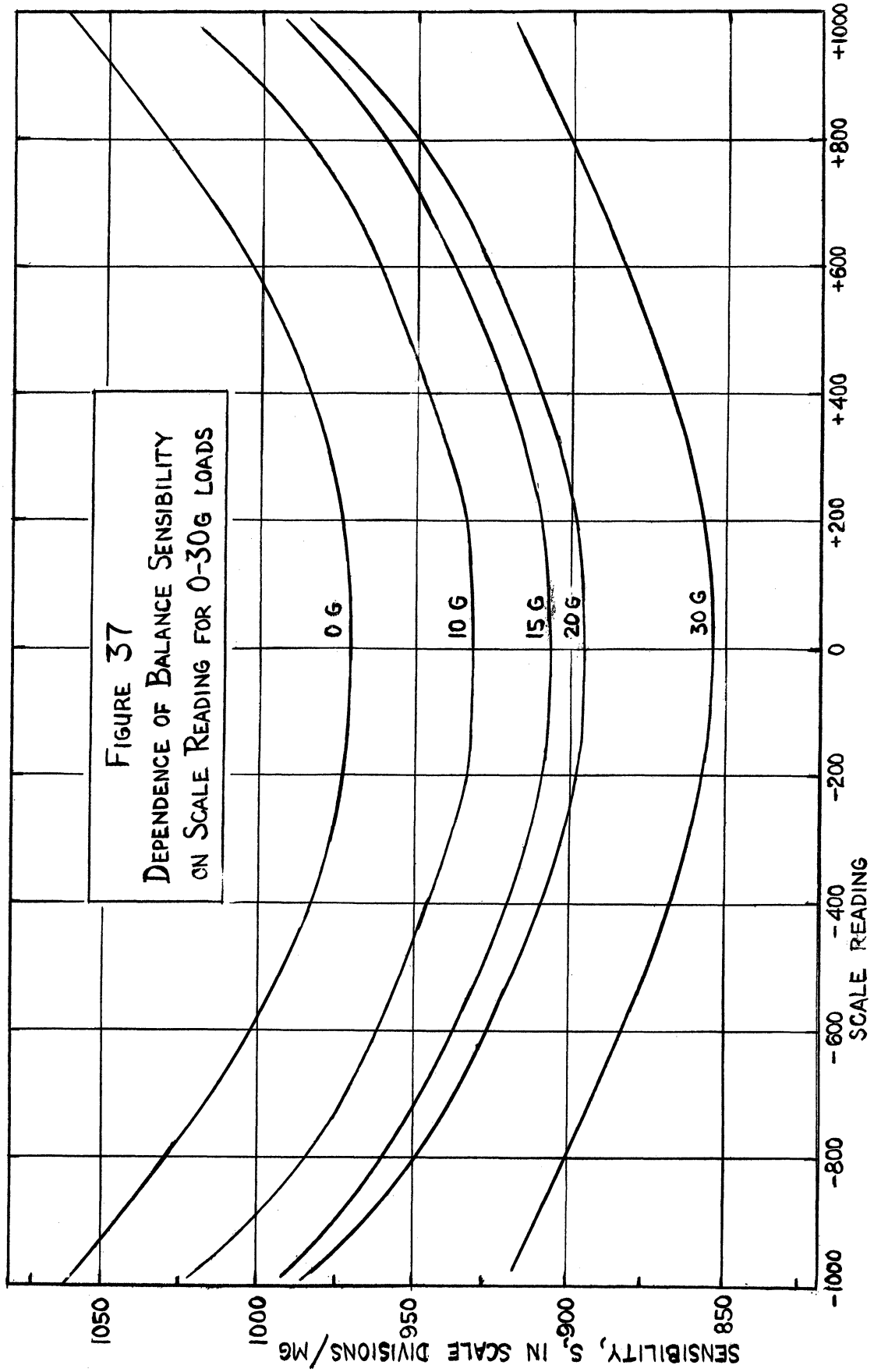

FIGURE 37
DEPENDENCE OF BALANCE SENSIBILITY ON SCALE READING FOR 0-30G LOADS

due to the substitution of the angular displacement of the pointer, measured in arbitrary units by the scale reading,

the glass thread is hygroscopic.

2. In order to eliminate static charge, a thin copper gauze (100 mesh) liner was fitted snugly inside the protection jacket surrounding the sample tube and grounded. Grounded aluminum foil was wrapped around the tube which protects the suspension filament from drafts. The glassware was sprayed inside and outside with "Staticlean", a preparation used to eliminate static charge on phonograph records.

3. Water at constant temperature was circulated around the protection jacket in which the sample tube is suspended.

C. The Electromagnet.

1. Description of Magnet and of Field Measuring Device. The electromagnet and its controls are those described by Curet.

A field measuring device was constructed in order to test the reproducibility of the field strength at a given energizing current, as well as its dependence on the distance from the center of the magnet, and on the current at the distance zero. The device is essentially an A.C. potentiometer[67], in which the standard potential is supplied by a coil rotating in the field of a permanent magnet, and the test potential is provided by a second coil rotating in the field of the electromagnet. A 10,000 ohm potential divider across the reference coil balances the potential from the test coil, the phases being balanced by orienting the permanent magnet through the proper angle. An oscilloscope detects the null point. A

synchronous motor rotates the 1 cm x 1 cm test coil and the 1 cm x 2 cm reference coil at 1800 r.p.m. Three volts were induced in the reference coil by the 5 kilogauss field of the permanent magnet. The voltage of the test coil, given in terms of the potential divider setting, measures the field strength in arbitrary units and could be determined to about 1 part in 2000.

2. Characteristics of Electromagnet. (a) Magnetic Field Dependence on Current. The magnetic field dependence upon current, given in Table XIV and Figure 38, shows that the measured values (A) are proportional to those (B) calculated by Curet from magnetic susceptibility measurements on a standard substance. The uncertainties indicated in the measured values are due to hysteresis. The residual magnetic field in the absence of current amounted to 50 ± 15 gauss, the field direction and strength depending upon the path by which the current was reduced to zero. At high amperages the hysteresis effect is smaller.

Table XIV

Dependence of Magnetic Field Strength on Current

Amperes	Field Strength (A) Measured Potentiometrically (Arbitrary units)	Field Strength (B) Given by Curet[64] (Kilogauss)	$\frac{(A)}{(B)} \times 10^3$
0	0 ± 50	0	-
1.10	2225 ± 10	-	-
2.00	3530 ± 15	3.6	0.98
6.00	5790 ± 10	5.7	1.01
8.00	6560 ± 5	6.5	1.01
10.50	7430 ± 5	7.4	1.00

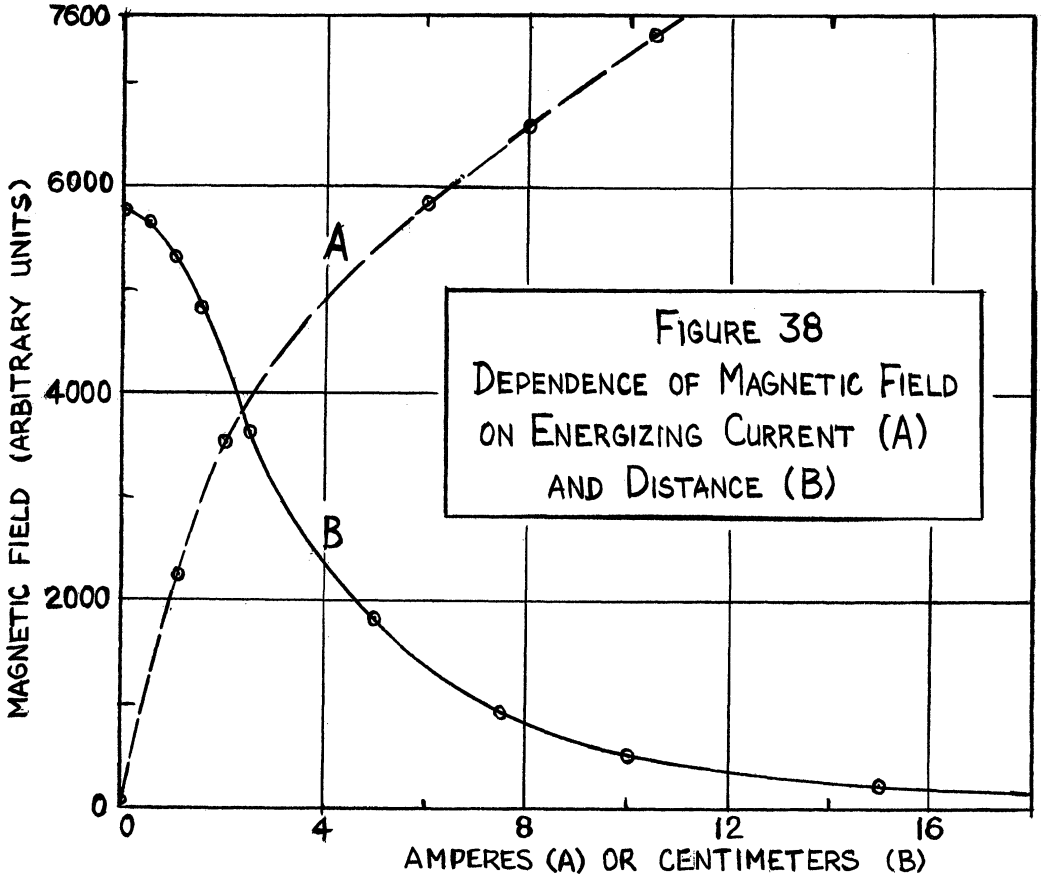

FIGURE 38
DEPENDENCE OF MAGNETIC FIELD ON ENERGIZING CURRENT (A) AND DISTANCE (B)

(b) Magnetic Field Dependence on Distance. The dependence of the field upon distance from the center of the magnet at 6 amperes is given in Table XV and Figure 38. The field, 523, at the top of a 10 cm. long sample is 9% of the maximum field, 5776.

Table XV

Magnetic Field Strength Dependence on Distance

Distance from Center of Magnet, cm	Field (Arbitrary Units)
0	5776
0.5	5625
1.0	5286
1.5	4761
2.5	3630
5.0	1788
7.0	934
10.0	523
15.0	194

BIBLIOGRAPHY

1. Hurd, D. T., "An Introduction to the Chemistry of the Hydrides", John Wiley and Sons, Inc., New York, 1952.

2. Gibb, T. R. P., Jr., and Kruschwitz, H. W., Jr., J. Am. Chem. Soc., 72, 5365 (1950).

3. Rundle, R. E., Shull, C. G., and Wollan, E. O., Acta Cryst., 5, 22 (1952).

4. Hoitsema, C., Z. physik. Chem., 17, 1 (1895).

5. Brüning, H., and Sieverts, A., ibid., 163A, 409 (1933).

6. Fischer, F., Ann. Physik., [4], 20, 503 (1906).

7. Krüger, F., and Gehm, G., ibid., [5], 16, 174 (1933).

8. Sieverts, A., and Brüning, H., Z. physik. Chem., A174, 365 (1935).

9. Coehn, A., Naturwissensch., 16, 183 (1928).

10. Coehn, A., Z. Elektrochem., 35, 676 (1929).

11. Coehn, A., and Specht, W., Z. Physik., 62, 1 (1930).

12. Coehn, A., and Jürgens, H., ibid., 71, 179 (1931).

13. Coehn, A., and Sperling, K., ibid., 83, 291 (1933).

14. Duhm, B., ibid., 94, 434 (1935).

15. Duhm, B., ibid., 95, 801 (1935).

16. Wagner, C., and Heller, G., Z. physik. Chem., B46, 242 (1940).

17. Aharoni, J., and Simon, F., ibid., B4, 175 (1929).

18. Biggs, H. G., Phil. Mag., [6], 32, 131 (1916).

19. Sieverts, A., and Danz, W., Z. anorg. u. allgem. Chem., 247, 141 (1941).

20. Svensson, B., Ann. Physik., [5], 18, 299 (1933).

21. Fitzwilliam, J., Kaufmann, A., and Squire, C., J. Chem. Phys., 9, 678 (1941).

22. Rundle, R. E., J. Am. Chem. Soc., 73, 4172 (1951).

23. Smith, D. P., "Hydrogen in Metals", The University of Chicago Press, Chicago, 1948.

24. Hägg, G., Z. physik. Chem., B11, 433 (1931).

25. Horn, F. H., and Ziegler, W. T., J. Am. Chem. Soc., 69, 2762 (1947).

26. Dreyfus-Alain, B., Compt. rend., 235, 540 (1952).

27. Dreyfus-Alain, B., ibid., 235, 1295 (1952).

28. Rossi, A., Nature, 133, 174 (1934).

29. Kirschfeld, L., and Sieverts, A., Z. physik. Chem., 145, 227 (1929).

30. Sieverts, A., and Roell, E., Z. anorg. u. allgem. Chem., 153, 289 (1926).

31. Hall, M. N. A., Martin, S. L., and Rees, A. L. G., Trans. Faraday Soc., 41, 306 (1945).

32. Fajans, K., Am. Mineralogist, 32, 100 (1947).

33. Fajans, K., and Bauer, N., J. Chem. Phys., 10, 410 (1942).

34. Hägg, G., Z. physik. Chem., B12, 33 (1931).

35. Oxley, A. E., Proc. Roy. Soc. (London), A101, 264 (1922).

36. Oxley, A. E., Nature, 111, 54 (1923).

37. Vogt, E., Z. Elektrochem., 37, 460 (1931).

38. Vogt, E., Ann. Physik., [5], 14, 1 (1932).

39. Mott, N. F., and Jones, H., "The Theory of the Properties of Metals and Alloys", Clarendon Press, Oxford, 1936.

40. Herzfeld, K. F., and Goeppert-Mayer, M., Z. physik. Chem., B26, 203 (1934).

41. Harding, E. A., and Smith, D. P., J. Am. Chem. Soc., 40, 1508 (1918).

42. Gee, E. A., Sutton, J. B., and Barth, W. J., Ind. Eng. Chem., 42, 243 (1950).

43. "International Critical Tables of Numerical Data, Physics, Chemistry, and Technology", McGraw-Hill Book Co., New York, 1926-33. Vol. I, p. 104.

44. Clausing, P., and Moubis, G., Physica, 7, 245 (1927).

45. Holborn, L., Z. Physik., 8, 58 (1921).

46. Feigl, F., "Laboratory Manual of Spot Tests", Academic Press, Inc., New York, 1943 (p. 120).

47. Klemm, W., "Magnetochemie", Akademische Verlagsgesellschaft M. B. H., Leipzig, 1936 (p. 45).

48. Selwood, P. W., "Magnetochemistry", Interscience Publishers, Inc., New York, 1943 (p. 200).

49. Selwood, P. W., ibid., (p. 197).

50. Barrett, C. S., "Structure of Metals", McGraw-Hill Book Company, Inc., New York, and London, 1943. (p. 115 ff.).

51. "Handbook of Chemistry and Physics", Chemical Rubber Publishing Company, Cleveland, 1943. (p. 1948).

52. Hull, A. W., and Davey, W. P., Phys. Rev., 17, 549 (1921).

53. Barrett, C. S., op. cit.[50]. (p. 554).

54. Patterson, R., Phys. Rev., 26, 56 (1925).

55. "Strukturbericht", Band II, Akademische Verlagsgesellschaft M. B. H., Leipzig, 1937. (p. 166).

56. Gillespie, L. J., and Ambrose, H. A., J. Phys. Chem., 35, 3105 (1931).

57. Hurd, D. T., op. cit.[1]. (p. 181).

58. Sieverts, A., and Bergner, E., Ber., 44, 2394 (1911).

59. Sieverts, A., and Gotta, A., Z. anorg. u. allgem. Chem., 187, 155 (1930).

60. Garstens, M. A., Phys. Rev., 79, 397 (1950).

61. Barrer, R. M., Discussion Faraday Soc., No. 4, 68 (1948).

62. Mott, N. F., and Jones, H., op. cit.[39]. (p. 296 ff.).

63. Mott, N. F., and Jones, H., ibid. (p. 272).

64. Curet Cuevas, J. D., Dissertation, University of Michigan, 1948. (p. 31 ff.).

65. Corwin, A. H., Ind. Eng. Chem., Anal. Ed., 16, 258 (1944).

66. Willard, H. H., and Furman, N. H., "Elementary Quantitative Analysis", D. Van Nostrand Company, Inc., New York, 3rd Ed., 1940. (p. 51).

67. Vigoreau, P., and Webb, C. E., "Principles of Electric and Magnetic Measurements", Prentice-Hall, New York, 1936.